REPUBLIC OF TURKEY
ACIBADEM MEHMET ALİ AYDINLAR UNIVERSITY
INSTITUTE OF HEALTH SCIENCES

IN VITRO DEVELOPMENT of MULTILAYERED CONSTRUCT FOR BLOOD VESSEL TISSUE ENGINEERING

GÖZDE ERVİN KÖLE

MASTER THESIS

DEPARTMENT of MEDICAL BIOTECHNOLOGY

SUPERVISOR
Asst. Prof. Dr. Deniz YÜCEL

Co-Supervisor
Prof. Dr. Vasıf HASIRCI

ISTANBUL, 2020

REPUBLIC OF TURKEY
ACIBADEM MEHMET ALİ AYDINLAR UNIVERSITY
INSTITUTE OF HEALTH SCIENCES

IN VITRO DEVELOPMENT of MULTILAYERED CONSTRUCT FOR BLOOD VESSEL TISSUE ENGINEERING

GÖZDE ERVİN KÖLE

MASTER THESIS

DEPARTMENT of MEDICAL BIOTECHNOLOGY

SUPERVISOR
Asst. Prof. Dr. Deniz YÜCEL

Co-Supervisor
Prof. Dr. Vasıf HASIRCI

ISTANBUL, 2020

DECLARATION

I hereby declare that this thesis has been written by me based on the information and data obtained in accordance with academic and scientific rules and ethical conduct. All information, data, comments, analyses have been collected and processed through scientific, academic writing style, and literature used have been duly shown by giving reference to the original sources in accordance with the publication ethics. I also announce and emphasize that I have not violated any rules secured by patent and copyrights whilst and writing of this research.

02/07/2020

Gözde Ervin Köle

ACKNOWLEDGEMENTS

I wish to express my sincere appreciation to my advisor Asst. Prof. Deniz YÜCEL for convincing guidance, encouragement and her support during the all stages of my study. I also appreciate her valuable advice, comments, suggestions and useful critiques that improve the quality of the work. I would especially like to thank her for the kind attitude, physical and mental support she has shown since the first day.

I would like to express my deepest respect and gratitude to my co-advisor Prof. Dr. Vasıf HASIRCI for his valuable and constructive suggestions during the planning and development of this study.

I am especially grateful to Assoc. Prof. Dr. Halime KENAR for her guidance and support in the cell isolation experiments.

I would like to express my appreciation to Prof. Dr. Gamze Torun KÖSE for her support.

I would like to extend my thanks to Hazal Gezmiş for transferring her knowledge and experience to me since the beginning of my work.

I am also indebted to Nesteren MANSUR ÖZEN for continuous support and guidance at both academic and personal level.

I would like to express my thanks to Dr. Tuğba DURSUN USAL for training scanning electron microscopy technique and I like to thank Funda CAN for helping me in the mechanical testing study.

I would also like to extend my thanks to Selçuk BİRDOĞAN who is the responsible personnel of the electron microscopy, and to Görkem GÜN who is the technician of the research laboratory.

I would like to express my gratitude to Tuğçe DEVECİ and Aslıhan AKALINLI for their invaluable support and help in my study, and also their friendship.

I would like to thank Mustafa TİTİZ, Tayyip KARAMAN, and Sümeyye AKÇELİK for their friendship, kindness, and help both professionally and personally.

I wish to show my gratitude to Elif BİÇER who stay by me from the day we met for her invaluable friendship and for the contribution to my study.

I also express my thanks to my friends, Beyza GÜRLER, Selen YAPMIŞ, Özgür Evrim TURSUN, Salva Asma ALGILANI, Cemre KEFELİ, Kübra KOÇAK for their continuous support and motivation whenever I need.

This study was supported by TÜBİTAK SBAG 118S587 and TÜBİTAK-BİDEB 2210-C program, and these grants are gratefully acknowledged. This study was also supported by Acıbadem Mehmet Ali Aydınlar University, and its facilities are gratefully acknowledged. I would like to thank METU-BIOMATEN for its physical and technical contribution during my thesis.

Finally, I would like to present my deepest gratitude and thanks to my family. I wish to thank my father Basri KÖLE and mother Emine KÖLE for always being so supportive and understanding during the study and throughout my life. I also whole-heartedly appreciate to my sisters Atty. Elif Naz KÖLE and Damla Dilek KÖLE for their incredible encouragement, understanding, and support under all circumstances. I would like to extend my special thanks to my uncle Atty. Nazmi KÖLE, who inspires me by winning the biggest debate of his life. Without their support and trust, this study could not be achieved.

TABLE OF CONTENTS

LIST OF ABBREVIATIONS \ SYMBOLS

ALP	Alkaline Phosphatase
bFGF	Basic Fibroblast like Growth Factor
BSA	Bovine Serum Albumin
CHL	Chloroform
CVDs	Cardiovascular Diseases
DAPI	4',6-Diamidino-2-Phenylindole, Dihydrochloride
DCM	Dichloromethane
DMEM	Dulbecco's Modified Eagle Medium
DMF	Dimethylformamide
DMSO	Dimethyl Sulfoxide
ECM	Extracellular Matrix
ESC	Embryonic Stem Cells
ECs	Endothelial Cells
EGF	Epidermal Growth Facor
EGM	Endothelial Growth Medium
FBS	Fetal Bovine Serum
FITC	Fluorescein Isothiocyanate
GAGs	Glycosoaminoglycans
HBSS	Hank's Balanced Salt Solution
HUVEC	Human Umbilical Vein Endothelial Cell
IGF	Insulin Like Growth Factor
IMA	Internal Mammary Artery
L-Asc	L-Ascorbic Acid
MSCs	Mesenchymal Stem Cells
P-D,L-LA	Poly(D,L-Lactic Acid)
P(L-D,L)LA	Poly(L-lactide-co-D,L-lactide)
PAD	Periphery Artery Disease
PCL	Polycaprolactone
PECAM	Platelet Endothelial Adhesion Molecule

PFA	Paraformaldehyde
PGA	Polyglycolic Acid
PGS	Polyglycerol sebacate
PLA	Polylactic Acid
PLGA	Poly(lactide-co-glycolide)
PLLA	Poly(L-Lactic Acid)
PU	Polyurethanes
SE	Synthetic Elastin
SEM	Scanning Electron Microscope
SMC	Smooth Muscle Cell
TGFβ	Transforming Growth Factor β
Try-EDTA	Trypsin-Ethylenediamine tetraacetic acid
VE- Cad	Vascular Endothelial Cadherine
VEGF	Vascular Endothelial Growth Factor
vWF	von Willebrand Factor
WJ	Wharton's Jelly

LIST OF FIGURES

LIST OF TABLES

SUMMARY

The challenge in vascular tissue engineering is to obtain functional blood vessel by imitating layers of arterial wall. The aim of this study is to develop a small-medium sized multilayered arterial substitute to mimic layers of artery, and to evaluate this tissue-engineered blood vessel by *in vitro* studies. In this study, the multilayered tubular arterial substitute was composed of porous film with endothelial cells as innermost layer, circumferentially aligned fibers with smooth muscle cells as intermediate layer, and random fibrous mat as outermost layer. The inner side of porous film seeded with human umbilical vein endothelial cells (HUVECs), while intermediate layer seeded with human mesenchymal stem cells (MSCs), which were differentiated into smooth muscle cells (SMCs). The multilayered vascular substitute containing MSC-derived SMCs and HUVECs was investigated in terms of proliferation, organization and expression of cell specific markers. The tubular scaffold with a lumen diameter of ~3 mm was obtained successfully. The circumferentially aligned and random fibrous mats were properly deposited over porous tubular film. HUVECs evenly distributed on inner side of the porous film, while MSCs were oriented on the circumferentially aligned fibrous mat. Differentiation of MSCs into SMCs was shown with the expression of SMC markers. It was revealed that MSC-derived SMCs and HUVEC preserved their cell morpholgy and cell specific protein expression on the multilayered, scaffolds. The results indicates that the multilayer blood vessel substitute developed via tissue engineering has a potential to be tested in *in vivo* studies and could be a promising therapeutic approach for vascular disease.

Key Words: Blood Vessel Tissue Engineering, Circumferentially Aligned Fibrous Mat, Mesenchymal Stem Cell, Multilayered Tubular Scaffold, Smooth Muscle Cell Differentiation

ÖZET

Damar Doku Mühendisliği için İn Vitro Ölçekte Çok Katmanlı Damar Eşleniği Geliştirilmesi

Damar doku doku mühendisliğindeki zorluk, doğal arter duvarının katmanlarını taklit ederek fonksiyonel kan damarı elde etmektir. Bu çalışmanın amacı, arter duvarı katmanlarını taklit etmek için çok katmanlı, küçük-orta büyüklükte bir arteriyel damar eşleniği geliştirmek ve bu doku mühendisliği ile oluşturulan kan damarını *in vitro* çalışmalar ile değerlendirmektir.Bu çalışmada, çok katmanlı tübüler arteriyel damar eşleniği, en iç tabaka olarak endotel hücreleri içeren gözenekli film, ara tabaka olarak düz kas hücreleri ile çevresel olarak hizalanmış lifler ve en dış tabaka olarak düzensiz lifli yapıdan oluşmuştur. Gözenekli filmin iç tarafına insan göbek veni endotel hücreleri (HUVEC) ekilirken, orta tabakaya düz kas hücrelerine farklılaşan insan mezenkimal kök hücreleri (MSC) ekildi. MSC'den farklılaştırılan düz kas hücreleri ve HUVEC içeren çok katmanlı damar eşleniği, hücre proliferasyonu, organizasyonu ve hücre spesifik protein ekspresyonu açısından incelendi. Lümen çapı yaklaşık 3 mm olan çok katmanlı doku iskelesi başarıyla elde edildi. Çevresel olarak yönlenmiş lifli ve düzensiz lifli yapı gözenekli film tabakasının üzerine düzgün bir şekilde toplandı. HUVEC hücrelerinin tübüler filmin iç tarafına tutunduğu ve zamanla yayıldığı gözlendi. Öte yandan, MSC'lerinin çevresel olarak yönlendiği görüldü. MSC'lerin düz kas hücrelerine farklılaşması, düz kas hücrelerine özgü markerların ekspresyonu ile gösterildi. MSC'den farklılaştırılmış düz kas hücrelerinin ve HUVEC hücrelerinin çok katmanlı doku iskeleleri üzerinde yaşadığı ve hücre morfolojisini ve hücreye özgü protein ekspresyonunu koruduğu gösterildi. Elde edilen sonuçlar, doku mühendisliği yoluyla geliştirilen çok katmanlı damar eşleniğinin *in vivo* çalışmalarda test edilme potansiyeline sahip olduğunu ve vasküler hastalıklar için umut verici bir terapötik yaklaşım olabileceğini göstermektedir.

Anahtar Kelimeler: Çevresel Olarak Yönlü Lifli Yapı, Çok Katmanlı Doku İskelesi, Damar Doku Mühendisliği, Düz Kas Hücresi Farklılaşması, Mezenkimal Kök Hücre.

1. BACKGROUND and AIM OF THE STUDY

Cardiovascular diseases, one of the leading causes of death worldwide, and related diseases are often developed due to some problems in blood vessels like coronary artery, peripheral artery and carotid artery (1). There are different types of blood vessels depend on its type, size and location (2). In general, wall of blood vessel is composed of three layers, tunica intima, tunica media and tunica adventitia. The innermost layer, tunica intima, is composed of a single layer of endothelial cells and subendothelial connective tissue. The intermediate layer, tunica media, is composed of circumferentially arranged smooth muscle cells (SMC). The outermost layer, tunica adventitia is composed of fibroelastic connective tissue. In surgical treatments of vascular disease, autografts are extensively used. However, there are some limitations of autografts such as performance and limited availability of veins, and donor site morbidity. Synthetic grafts can be used as an alternative to autografts. But their patency especially in the small-diameter arteries is low and can cause thrombosis and hyperplasia (3).

Tissue engineering and regenerative medicine are rapidly growing, promising approaches to solve these problems. Tissue engineering aims to develop biological substitutes to restore, maintain, or improve the structure and function of the damaged tissue (4). Tissue engineered constructs are composed of cells, preferably the patient's own cells, and scaffolds which mimic the extracellular matrix. The chemical and physical properties of the scaffolds are crucial to provide the needed support for cells to attach and proliferate. In vascular tissue engineering, it is important to develop a multilayered, tubular and cell containing construct by mimicking the layers of the native blood vessels. Stem cells are promising candidates to be used in tissue engineering with their self-renewal and differentiation potential. Tissue engineered constructs prepared under *in vitro* conditions using preferably the patient's own stem cells and a biodegradable scaffold could be a promising therapeutic approach for treatment of damaged blood vessels.

The aim of this study was to develop multilayered, tubular tissue engineered blood vessel substitute and to investigate its performance via *in vitro* studies. For this purpose, the multilayered tubular arterial substitute, composed of porous film with endothelial cells (HUVEC) as the innermost layer, circumferentially aligned fibers with WJ MSC-derived smooth muscle cells as the intermediate layer, and random fibrous mat as the outermost layer, was constructed. The architecture and cellular composition of this construct, which was inspired by the histological features of the arteries, would be effective to achieve functional small-medium sized arteries in blood vessel tissue engineering.

2. INTRODUCTION

2.1 Cardiovascular Disease

Cardiovascular diseases (CVDs) are described as a group of diseases that affect blood vessels and heart. According to World Health Organization (WHO) cardiovascular diseases are responsible to 31% of all death in the world. The most common forms of the vascular disease are seen in the small-medium sized arteries such as coronary artery, peripheral artery and carotid artery (1). According to heart disease and stroke statistics, 2020 report, coronary heart disease, or coronary artery disease, is the most prevalent vascular disease accounting for 42.6% of all CVDs death in 2017 (5). Peripheral artery diseases (PAD) are responsible to 0.47% death of all CVDs in all age in 2017, and also prevalence of PAD is higher than 10% in the patient who their 60s or 70s (5, 6). Stroke, which is the cause of 17% of all CVDs, is associated with 20-30% extracranial carotid artery disease and 5-10% intracranial artery disease (5, 7). The underlying cause of these diseases is the narrowing of the blood vessels due to plaque deposition on the vessel wall, and it is known as arteriosclerosis (8). The endothelium of the arteries is damaged in the patients who suffer from high blood pressure or who have a sedentary lifestyle or a genetic preposition. Some lipid molecules, low-density lipoprotein (LDL) named as bad cholesterol, are carried with blood and start lipid accumulation beneath the endothelium at different locations in the arteries throughout the body. When the lipid accumulation gradually increases by time, lipid molecules start to above epithelium and deposit on the lumen of the blood vessel. This case called as arteriosclerosis can cause partial or complete occlusion of the blood vessels, especially in the coronary arteries (Figure 1). Coronary arteries are the vessels which carry oxygen and nutrient to the heart muscle (Figure 2). When arteriosclerosis progresses in the coronary arteries, called coronary artery disease, the heart muscles are not properly supplied with adequate blood and a decrease in the heart pumping process is progressed. Therefore, coronary artery disease is the most common

reason of myocardial infarction and stroke (9). Thus, permanent treatment approaches are urgently needed in clinic to save thousands of lives.

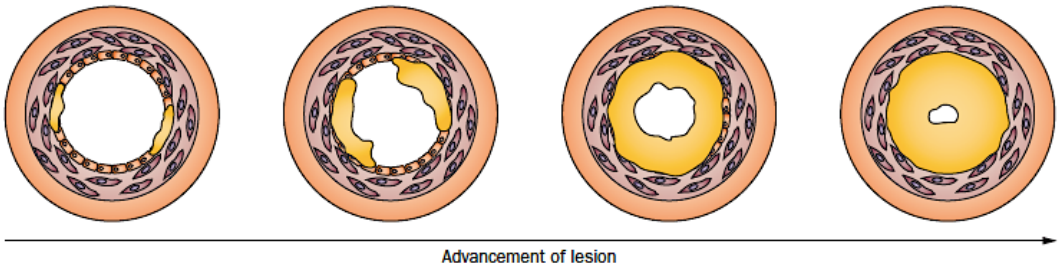

Figure 1. Illustration of progressive stages of the arteriosclerosis.

Reference: Seifu DG, Purnama A, Mequanint K, Mantovani D. Small-diameter vascular tissue engineering. Nat Rev Cardiol. 2013;10(7):410-21.

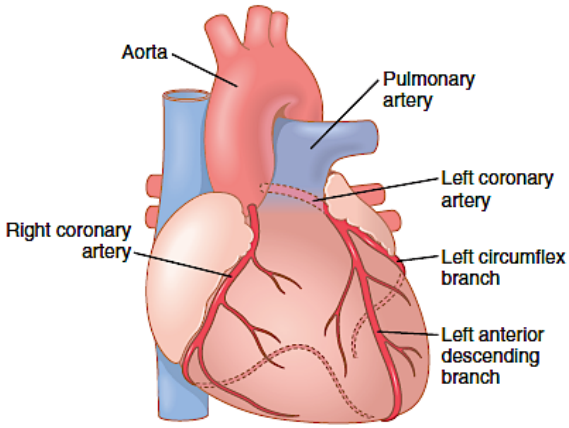

Figure 2. Illustration of the coronary arteries.

Reference: Hall JE. Guyton and Hall Textbook of Medical Physiology. 13th Edition ed. USA: Elsevier. p. 248-70.

2.2 Histology of Blood Vessels

The wall of both arteries and veins is composed of three layers also called as tunics. Layers of the vascular wall, from lumen to outermost side, are tunica intima, tunica media, and tunica adventitia (2). In general, arteries are subdivided into three categories according to their size and tunica media characteristics (Figure 3). Large arteries also named elastic arteries contain smooth muscle cells and fenestrated elastic

lamella in their tunica media (Figure 3a). Elastic arteries are the largest arteries having a lumen diameter larger than 10 mm and give rise to medium-sized, muscular arteries. The muscular arteries have a lumen diameter ranged between 3 and 10 mm and draw blood from elastic arteries. The tunica media of muscular arteries contains less elastic fibers and less smooth muscle cells compared to tunica media of elastic arteries (Figure 3b) (10). Small arteries contain less smooth muscle cells like eight layers of the smooth muscle cells, and their lumen size generally less than 2 mm. The smallest artery, arteriol, contains one or two layer of smooth muscle cells (Figure 3c) (2, 10).

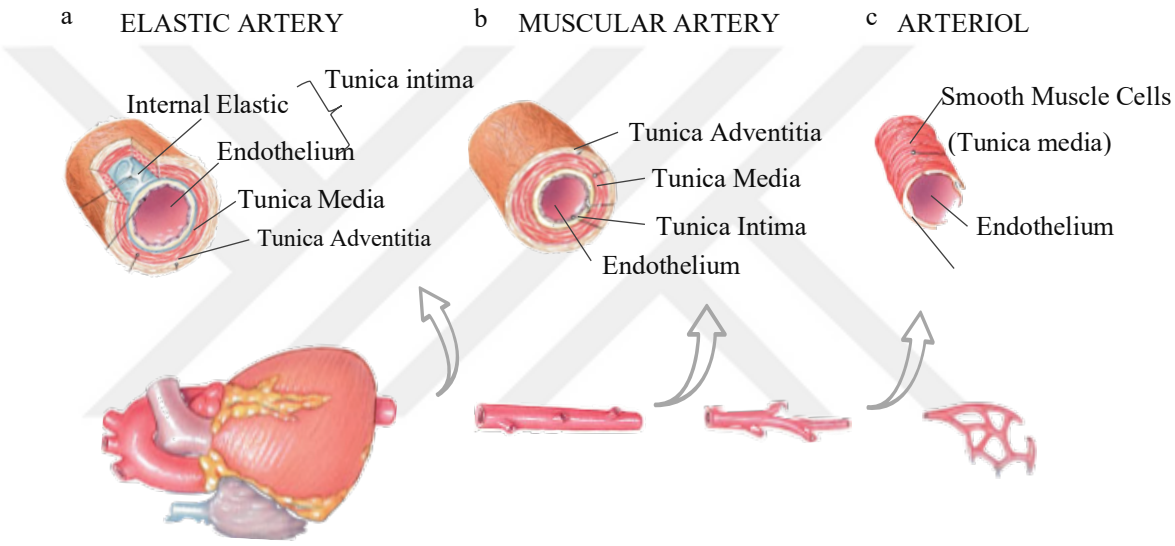

Figure 3. Classification of arteries according to their size and structure. (a) Large (elastic) arteries, (b) medium (muscular) arteries and (c) arterioles.

Reference: adapted from
http://websupport1.citytech.cuny.edu/Faculty/ibarjis/Teaching/Anatomy%20and%20Physiology/lecture21/Lecture/Lecture1.htm/ accessed date 03/05/2020

2.2.1 Muscular Arteries

2.2.1.1 Tunica intima

Tunica intima is the innermost layer of the vascular wall. In most of arteries, tunica intima is composed of by the following structures; 1) a single layer of endothelial cell lining, 2) a thin basal lamina with a thickness of 80 nm, 3) subendothelial layer, and 4) prominent internal elastic lamina (10). A continuous monolayer of elongated, polygonal endothelial cells lines the lumen and is called as endothelium. The characteristic appearance of endothelial cells is known as cobblestone morphology (Figure 4a, b). The endothelial cells with 0.2-0.5 μm thickness are aligned along the blood flow direction (2). Integrated endothelial cells form a steady organized endothelium, and thus serve as a selective barrier between blood and underlying tissue (10, 11).

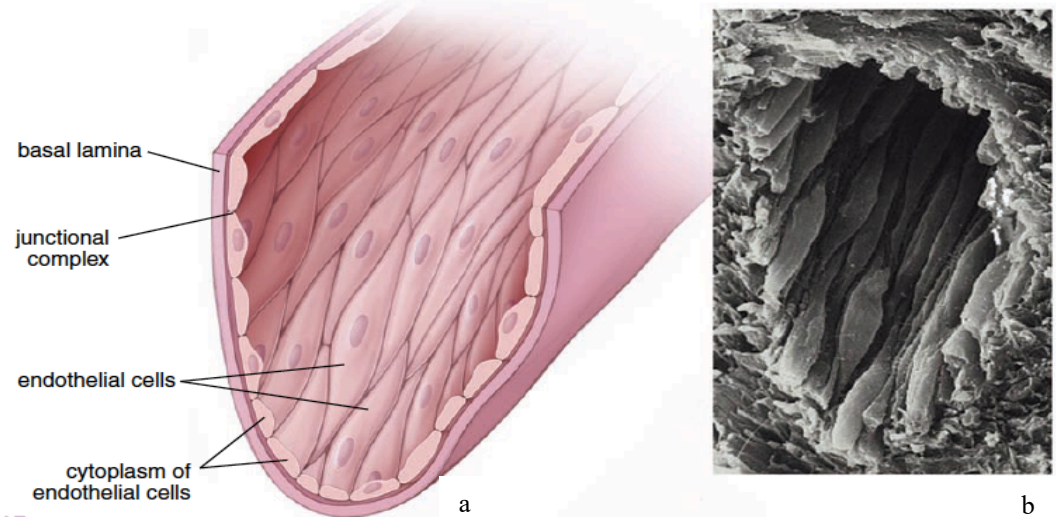

Figure 4. (a) Illustration of cobblestone morphology of the endothelial cells and junctional structure. (b) SEM image of the endothelial cells.

Reference: Michael H. Ross WP. Cardiovascular System. In: Taylor C, editor. Histology A Text and Atlas. Sixth Edition ed: Lippincott Williams & Wilkins, a Wolters Kluwer business. p. 400-39.

The integrity of endothelium is maintained by the junctional structures such as adherens and tight junctions. These junctions not only provide cell-cell communication but also take role in cell signaling, modulation of vascular hemostasis and apoptosis (Figure 5). One of the proteins, a component of cell-to-cell adherens junctions, is endothelial-specific calcium-dependent cadherin called vascular endothelial cadherin (VE-Cad). Restricted specificity of VE-Cad may be related to cell-cell communication and/or distinctive function of endothelial cells. The other junctional protein is platelet endothelial adhesion molecule (PECAM or CD31) which is important to protect endothelial cells from apoptosis (11). Besides these characteristic membrane proteins, endothelial cells have specific organelle in their cytoplasm called Weibel-Palade bodies. These organelles contain the von-Willebrand factor (vWf) which is a glycoprotein. This factor is secreted by arterial endothelial cells to the blood during endothelial injury to provide platelet adhesion (2). The antibodies against VE-Cad, CD31, and vWf are commonly used immunohistochemical markers for the characterization of the endothelial cells.

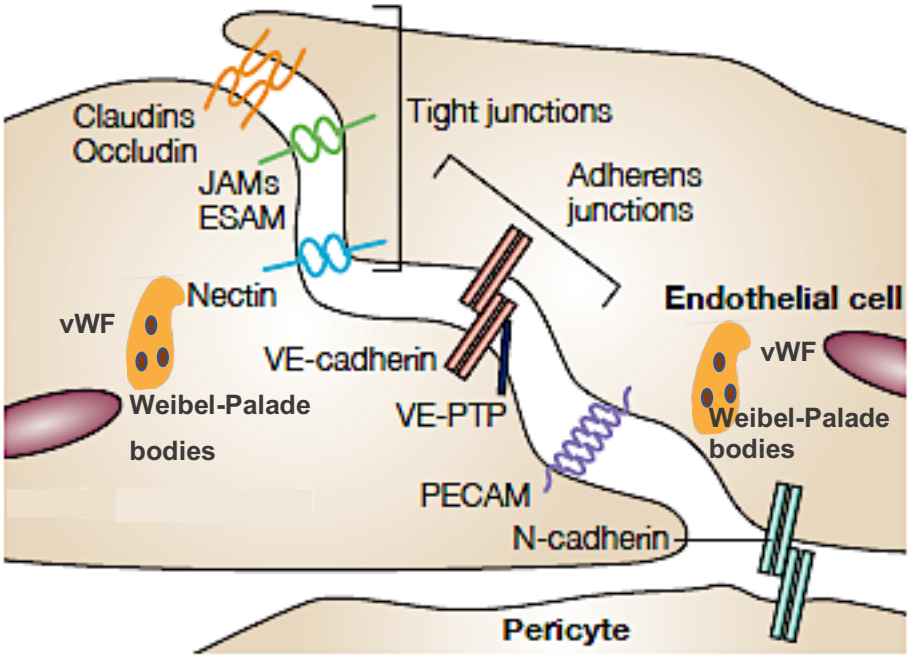

Figure 5. Illustration of the characteristic endothelial structures.

Reference: adapted from Dejana E. Endothelial cell-cell junctions: happy together. Nat Rev Mol Cell Biol. 2004;5(4):261-70.

The endothelial cells attach to basal lamina which is located between endothelium and subendothelial connective tissue (12). The subendothelial layer of the tunica intima is composed of collagen and elastic fibers and basal lamina fragments which are loosely arranged near the endothelium and become denser toward the tunica media border (10).

Muscular arteries contain a prominent internal elastic lamina which is found between subendothelial connective tissue and tunica media. The thickness of the muscular arteries changes related to age, physical and other factors. In young people generally, one-sixth of the wall is tunica intima; however, the tunica intima thickness may increase in relation to arteriosclerosis and aging (2).

2.2.1.2 Tunica media

The tunica media is the middle layer of the vascular wall. Tunica media of elastic arteries is composed of fenestrated elastic lamellae alternating with circumferentially oriented smooth muscle cell (SMC) layers (2, 10). Tunica media of muscular arteries also contains SMCs that are circumferentially aligned on collagen fibrils. However, in tunica media of muscular arteries there are few elastic fibers and it is devoid of organized, fenestrated elastic lamellae. SMCs not only help regulate blood pressure by contraction, but also synthesize the connective tissue content around them. The organization of SMCs as fiber bundles or sheets is called unitary smooth muscle or syntactical smooth muscle. In unitary smooth muscle cells, cells contact each other via adherence to their cell membranes, therefore contraction is transported to the next and causes synchronous contraction of muscle fibers together (Figure 6).

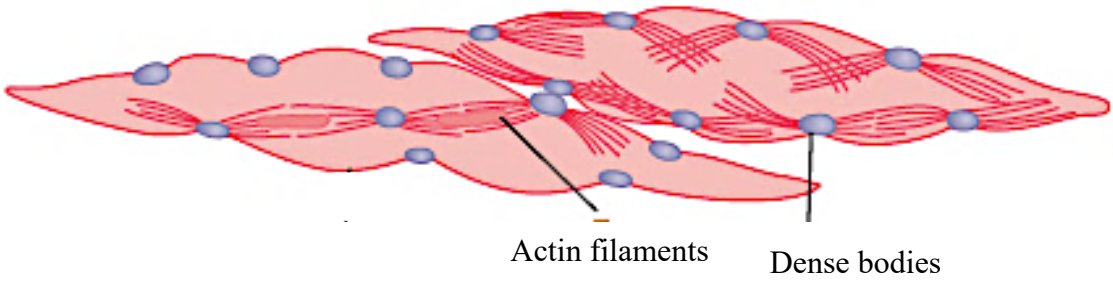

Figure 6. Syntactic organization of smooth muscle cells which provides vasodilation and vasoconstriction. Actin filaments, which are attached to the dense body, provide transmittance of the contraction from one cell to another.

Reference: Hall JE. Guyton and Hall Textbook of Medical Physiology. 13th edition ed: Elsevier; 2016. p. 97-105.

Endothelial cells and SMCs work together during contraction and relaxation of the arteries. When the endothelial cells are exposed to shear stress that is generated by the blood flow, they synthesize some regulatory molecules. These molecules diffuse to the underlying tunica media via the basement membrane. Since the SMCs have a great feedback control mechanism when the regulatory molecules reach the SMCs, cells are relaxed or contract. This process results in a change in vessel diameter which is called vasodilation or vasocontraction (2, 13). Contraction and the relaxation mechanisms give arteries to their mechanical properties (Figure 7).

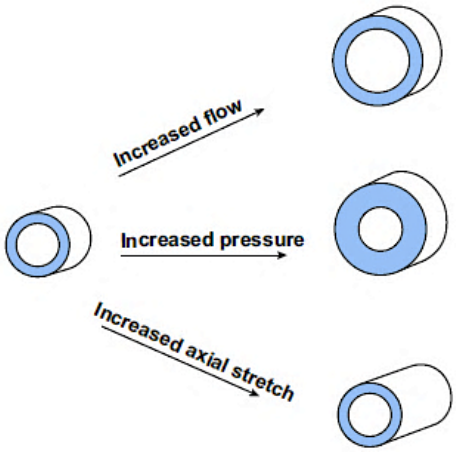

Figure 7. Mechanical response of the arteries to the changed conditions.

Reference: Schutter S. and Nerem R. Blood vessel tissue engineering. In: Buddy D. Ratner ASH, Frederick J. Schoen,Jack E. Lemons,editor. Biomaterials Science. Third edition. Canada: Elsevier. p. 1237-46.

The arrangement of the smooth muscle layer is changed depending on the contraction or relaxation state of the arteries. In the relaxation position, all SMCs are perpendicular to the lumen. On the other hand, in contraction SMCs in the outer region exhibit 30^{o} position to the lumen, while the cells in the middle region remain perpendicular to the lumen. These forms of the cells are called helices arrangement (Figure 8). The thickness of the tunica media differs due to the number of concentric layers the range in the number of 25-35 (10). For instance, Waller B.F. et al. determined the average tunica media thickness as 200 µm within 125-350 µm range (14).

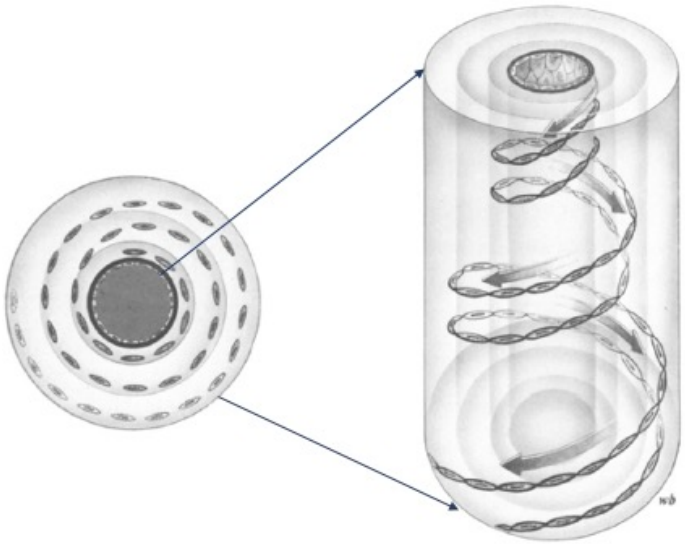

Figure 8. Helical arrangement of smooth muscle cells in muscular arteries.

Reference: Rhodin JAG. Architecture of the Vessel Wall. Comprehensive Physiology1980. p. 1-31.

2.2.1.3 Tunica adventitia

The tunica adventitia is the outermost layer of the blood vessels (Figure 9). Tunica adventitia of the elastic arteries contains loosely arranged collagen fibers and elastic fibers as well as vasa vasorum which provides nutrients and oxygen to vessel wall and removes the waste products (10). Tunica adventitia separated from tunica media with very distinct external elastic lamina in large muscular arteries, but external elastic lamina becomes less distinct in small-sized muscular arteries. The tunica adventitia is composed of connective tissue containing collagen fibers, fibroblasts, elastic fibers, and some blood vessels (2). Although fibroblasts are found in the tunica adventitia, the total cellular content of the adventitia is lower than tunica media or intima (15). Since the elastic fibers mostly represent in the external elastic lamina, the main extracellular component of adventitia is the loosely arranged collagen fibers. Collagen fibrils are longitudinally arranged in the inner side of the tunica adventitia, whereas the collagen fibers at the periphery exhibit circumferential alignment (10, 15). The nerves and small blood vessels are found in the large muscular arteries (Figure 9). The nerves also

named vasomotor nerves are responsible for the neurotransmitter secretion to regulate vascular contraction. In small arteries nutrients and oxygen can be provided to the cells of tunica media from lumen via diffusion through tunica intima. However, in larger arteries it is difficult to supply nutrients to the depth of thick tissue wall from the lumen. The small blood vessels found within tunica adventitia are called vasa vasorum which are defined as "vessels of the vessels" (15). The adventitia layer not only provides the nourishment to the cells but also gives stability to the vessel wall and connects the vessels to the other tissues. Tunica adventitia is thicker in muscular arteries compared to the elastic arteries (10). The thickness of the tunica adventitia is in the range of 300 to 500 µm (15).

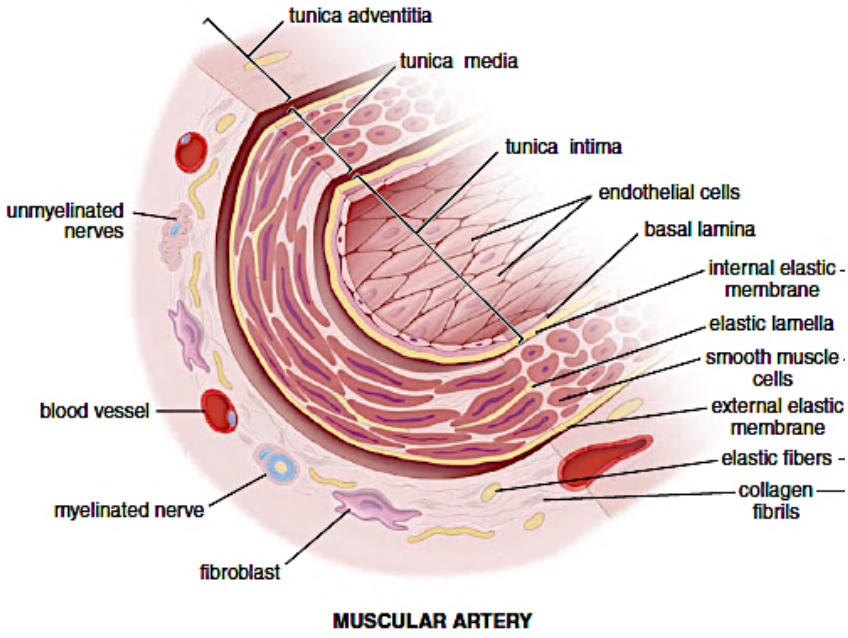

Figure 9. The vessel wall of the muscular artery.

Reference: Michael H. Ross WP. Cardiovascular System. In: Taylor C, editor. Histology A Text and Atlas. Sixth Edition ed: Lippincott Williams & Wilkins, a Wolters Kluwer business. p. 400-39.

2.3 Treatment Approaches for Vascular Diseases

In USA millions of CVDs operations performed in 2014 (Table 1). The average cost of direct or indirect CVDs was $ 351.2 billion between 2014 and 2015 and it is expected to increase up to $ 1.1 trillion by 2035. Among them, coronary heart disease costs $ 9 billion which is one of the 10 most expensive healthcare in the USA (5).

Table 1. Cardiovascular procedures performed in USA.

Indication	Number of Procedures
Angioplasty	480 000
Angioplasty with stents	430 000
Coronary artery bypass graft (CABG)	371 000
Valve replacement	156 000
Heart transplantation	3 408
Cardiac catheterization	1 016 000
Total cardiovascular procedures	7 971 000

Reference: adapted from Virani SS, Alonso A, Benjamin EJ, Bittencourt MS, Callaway CW, Carson AP, et al. Heart Disease and Stroke Statistics-2020 Update: A Report From the American Heart Association. Circulation. 2020;141(9): e139-e596.

Several treatment options for cardiovascular disease are available in the clinic like change in diet and lifestyle, medication and surgery (16). To make progress in the treatment of vascular disease three factors should be considered: 1) prevention of the plaque deposition even before lifestyle changes such as diet, tobacco use, etc.; 2) advancements in the conventional treatment methods of arteriosclerosis and 3) prevention of the recurrence of disease (17). However, healing of end-stage organ failure or tissue loss cannot be achieved with any of these options in the long term. Therefore, alternative treatment options urgently needed in the clinic (18).

Majority of the vascular disease occurs as a result of progression of arteriosclerosis. The main locations where arteriosclerosis develops first are abdominal aorta, coronary arteries, and internal carotid arteries. In small arteries, since arteriosclerosis expands rapidly and causes occlusion of the lumen, blood cannot be supplied efficiently to the organs, leading to ischemia and subsequent tissue damage or even loss (17). To overcome arteriosclerosis related vascular disease, different treatment options are applied according to plaque deposition level (Figure 10) (3).

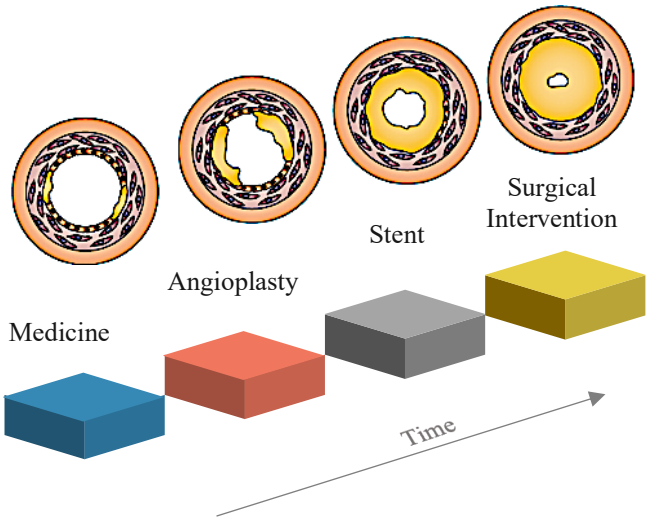

Figure 10. Progressive stages of the arteriosclerosis and treatment options according to plaque deposition level.

Reference: Seifu DG, Purnama A, Mequanint K, Mantovani D. Small-diameter vascular tissue engineering. Nat Rev Cardiol. 2013;10(7):410-21.

The people who genetically predisposition is advised to change their lifestyle before plaque formation starts. In the beginning of fat deposition, pharmaceutical treatment is prescribed to the patient. After a period of drug treatment, the patient's quality of life is expected to be improved, and the artery gradually recovers (Figure 10) (3). However, in some cases artery is not cured with drugs, and the plaque formation causes narrowing or completely obstructing the lumen which are the critical stages of arteriosclerosis (17). Three different treatment approaches are used in the critical level obstruction as angioplasty, stent and surgery (Figure 11).

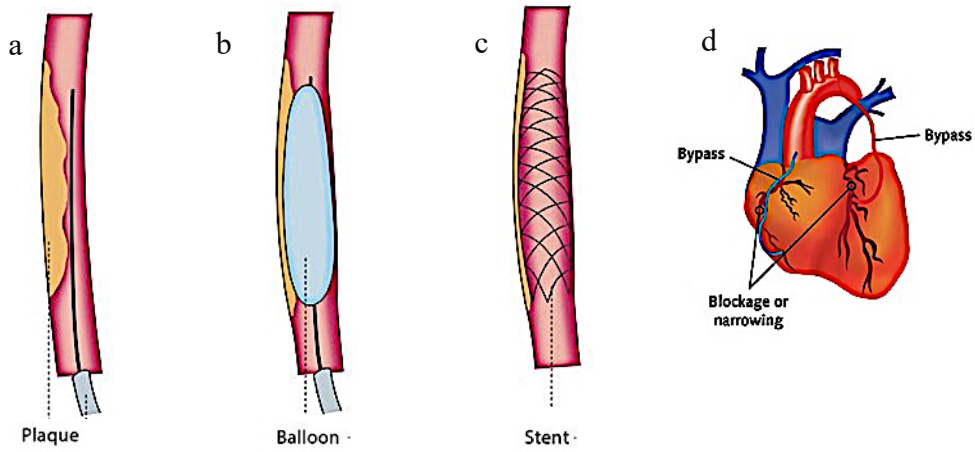

Figure 11. (a) Advanced plaque formation, and treatment strategies: (b) angioplasty, (c) stent and (d) bypass surgery.

Reference: https://www.cirse.org/patients/ir-procedures/angioplasty-and-stenting/ Accessed date 30.05.2020.

Angioplasty is carried out in the early stages of plaque formation to restore blood circulation in clogged arteries (Figure 10 and 11b) (3). In coronary angioplasty, a long catheter is implanted via the femoral artery, moves up the aorta and reaches the coronary arteries. By using radioactive dye, stenosis location is determined, and the balloon on the catheter is inflated to provide mechanical expansion. These mechanical forces help increasing in lumen size and blood flow via compression, and lead to redistribution of the plaque in lumen of the vessel wall. However, restenosis which means the re-narrowing the lumen of arteries is seen in 30-50% of the patients after 4-6 months (17). Restenosis is mostly associated with the high proliferation rate of SMCs causing the hyperplasia in the lumen, and elastic recoil of the arterial wall (3, 17). If the side effects occur during angioplasty, permanent stents are usually included in the procedure (3).

Stents may help to reduce the negative effect of angioplasty (Figure10 and 11c). Stents are expandable tubes which are made up of wire mesh which is placed to angioplasty site. Stents help to protect the circular shape of the lumen by acting as

scaffold. Thus, it may prevent the restenosis (17). However, stents also may have complications in long term or short term. In the short term, thrombosis may occur within 7 days in 1-3% of the patients. When the stent is placed into the vessel, it damages the endothelium. Since the disruption of the endothelial lining leads to accumulation of platelet and fibrous tissue, the stent is embedded in an endothelium-lined layer of intimal fibrosis, and scar formation occurs. In the long term, 50% of the patients face with restenosis within 6 months. The immune response can also be a possible side effect of the stents as related to the tissue-stent interface (17).

When blood flow is completely prevented due to arterial occlusion, the obstructed site is needed to be bypassed by the help of surgery (Figure 10 and 11d). Both autologous grafts or synthetic grafts can be used for bypass operations in the clinic (16). In fact, it was awarded to Nobel Prize in 1912 who invented the arteriovenous anastomoses (19). Saphenous vein is the most widely used autograft in small-diameter arterial bypass surgery since it is easy to access and harvest (20). But due to their mechanical properties do not match with the artery, it leads to intimal hyperplasia, arteriosclerosis, and aneurysm (3). Although the limited number of saphenous veins are available in the body, numerous surgeries can be needed within years to provide revascularization (21). Therefore, there is a necessity for alternative grafts and these requirements have been overcome by the development of biomaterials (22).

Vascular grafts are fabricated from synthetic materials such as polyethylene terephthalate (Dacron®) and polytetrafluoroethylene (Teflon®) (23). Dacron and Teflon meet expectations in large diameter arteries (>8 mm) and in medium arteries (6-8 mm) due to their high blood flow velocity. As the blood vessel diameter decreases like in small diameter arteries (<6 mm), blood flow velocity decreases, and commercial synthetic grafts do not perform well in that situation (24, 25). In the case of Dacron and Teflon application to the small arteries, they cause the intimal hyperplasia and thrombosis. Hyperplasia may lead to immune reaction in the patients. In addition, the patients must use anticoagulant for a long time to prevent side effects.

Despite the low clinical performance of synthetic grafts, the market value is expected to exceed $ 3.6 billion by 2024 (26).

Due to limited availability of autologous grafts and poor mechanical properties of the synthetic grafts, conventional treatment approaches cannot meet the expectation in the clinic especially in the small-diameter vascular problems (3). Therefore, alternative treatment strategies are needed in the clinic. Tissue engineering and regenerative medicine can be promising advancements to develop ideal tissue substitutes and to enhance healing process.

2.4 Principles of Tissue Engineering

Tissue or organ failure, resulting from injuries or accidents, is the most frequently occurred and most expensive health care problem. It costs over $ 400 billion in USA (4). Millions of people suffer from tissue loss or end-stage organ failure, in fact every 9 minutes new patients are added to the organ waiting list in the USA, and only a limited number of transplantation is performed due to donor shortage (4, 27). In surgical treatments of vascular disease, autograft applications are commonly used but there are some limitations such as donor site morbidity, insufficient structural and mechanical properties, unavailability of tissue (3). In addition, many types of biomaterials are widely used in the clinic such as vascular grafts. These cell-free biomaterials have also some limitations such as insufficient structural and mechanical properties, the risk of thrombosis and intimal hyperplasia in small diameter arterial grafts (3). In the past, biological units such as cells were not often combined with biomaterials (28). However, with the advancement in the biomaterials field, incorporation of cells into the biomaterials emerges as a new approach called tissue engineering. Vacanti J.P. and Langer R. described the tissue engineering as “an interdisciplinary field that applies the principle of engineering and life sciences toward to the development of biological substitutes that maintain, restore and improve tissue function”(4).

Main purpose of the tissue engineering is to fabricate biological equivalent to overcome organ or tissue failure. Another outcomes of the tissue engineering are to 1) investigate correlation between the organization and function of cells; 2) build *in vitro* tissue models to be used in high throughput drug screening, 3) establish *in vitro* disease models to understand mechanism of that disease, and thus reduces the animal experiments (29, 30). The ideal tissue-engineered medical devices should contain: 1) a scaffold, or a cell carrier, to provide supportive niche for cells, 2) appropriate cells depend on target tissue, 3) bioactive molecules to guide cells for proliferation, migration and/or differentiation on the scaffold (31, 32) (Figure 12). In the concept of tissue engineering, the importance of ECM needs to be understood and studied to develop tissue-specific scaffold and to mimic the tissue under *in vitro* conditions. The main components of ECM are collagen, proteoglycans, and adhesive glycoproteins which provide not only physical support to cells and also provide a matrix where cells can adhere and communicate with each other. Some ECMs are specialized according to the property of tissue (33).

In tissue engineering, the scaffolds are intended to mimic the distinct architecture and functions of ECM in orchestrating cell migration, proliferation, differentiation, and angiogenesis because an ideal tissue repair environment can be provided by replicating the specific properties of the natural tissue (34). The scaffolds are the 3D structures and they have to be highly porous to allow cell penetration, culture medium exchange and moving out the metabolic waste from the environment. The scaffolds are fabricated with various biodegradable synthetic or natural polymers, and their degradation rate should match the tissue growth *in vivo*. It is crucial for scaffolds to takes over the roles such as mechanical, chemical, and biological until the damaged tissue is fully healed (28, 32). Consequently, the cell carriers, scaffolds, need to have proper 3D architecture, and also provide mechanical support to new formed tissue, and specific signals for the cells.

Cell source is another important consideration in tissue engineering to enhance healing process and to achieve adequate regeneration in damaged tissue and organ. The cells can be obtained from many sources such as from patients, autogeneic cells, from another human, allogeneic cells, or from another species, xenogeneic cells. But xenogeneic and allogeneic cells have immune rejection risk. Even autogeneic cells seem to be the best cell source, there are some limitations such as questionable health of cells and difficulty of expansion of cells under culture condition. Within tissue engineering, stem cells are promising cells source since they have potential to differentiate into various cell types and have a high proliferation capacity, and besides they can be obtained from various tissues (32, 35).

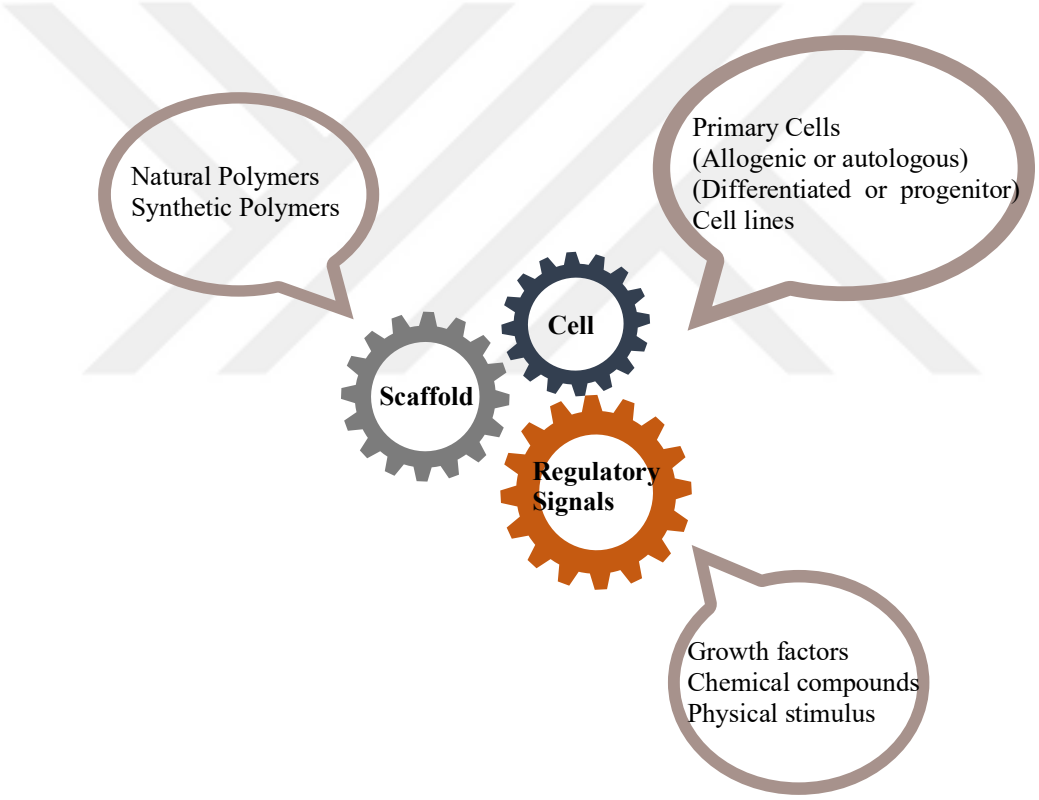

Figure 12. Components of the tissue engineering.

2.5 Blood Vessel Tissue Engineering

The main purpose of the vascular tissue engineering is to design blood vessel equivalents which have similar properties with native blood vessel in terms of architecture and function. Therefore, the ideal blood vessel equivalent should meet numerous criteria (3). The vascular substitute should be biocompatible and not trigger immune response when implanted into body. In addition, vascular equivalent should not lead to thrombosis or blood coagulation, in other words it should be hemocompatible (36). The other important criterion is its mechanical properties. The vascular equivalents should have similar mechanical properties with the native blood vessels or at least the burst pressure should be equal to that of the saphenous vein which is the best option in the surgical treatment to withstand blood pressure without burst (Table 2) (37). Moreover, the ideal blood vessel substitute should be responsive, living conduits with similar functional and mechanical properties to the native blood vessel, easily sutured, grow, and also be available in different sizes in the market (16).

Table 2. Mechanical properties of some blood vessels.

Type of blood vessel		Young`s modulus (MPa)	Ultimate Tensile Strength (MPa)	Elongation at break (%)	Burst Strength (mmHg)
Saphenous vein	Long	23.7	6.3	83	1680-3900
	Circ.	4.2	1.8	241	
Left internal mammary artery	Long	16.8	4.3	59	2000
	Circ.	8	4.1	134	
Femoral artery	Long		1.67	87	
	Circ.	9-12	1-2	63-76	

Reference: Stekelenburg M, Rutten MC, Snoeckx LH, Baaijens FP. Dynamic straining combined with fibrin gel cell seeding improves strength of tissue-engineered small-diameter vascular grafts. Tissue Eng Part A. 2009;15(5):1081-9.

*Long; Longitudinal *Circ ; Circumferential

As with the general tissue engineering principle, tissue-engineered blood vessels are mainly composed of appropriate scaffold and tissue specific cells (Figure 13). The endothelial cells, smooth muscle cells and fibroblasts found in native blood vessel are the main cell sources used in vascular tissue engineering. These cells should be easily obtained, and should retain their characteristic functions in the scaffolds (38). The mature cells can be obtained from patients or donors, but sometimes it is difficult to find viable and available cell sources due to patient's condition or donor age. In addition, due to their low proliferation rate the number of mature cells may be insufficent to be used in tissue engineering. Stem cells like mesenchmal stem cells and induced pluripotent stem cells could be a good alternative to overcome these limitations (39).

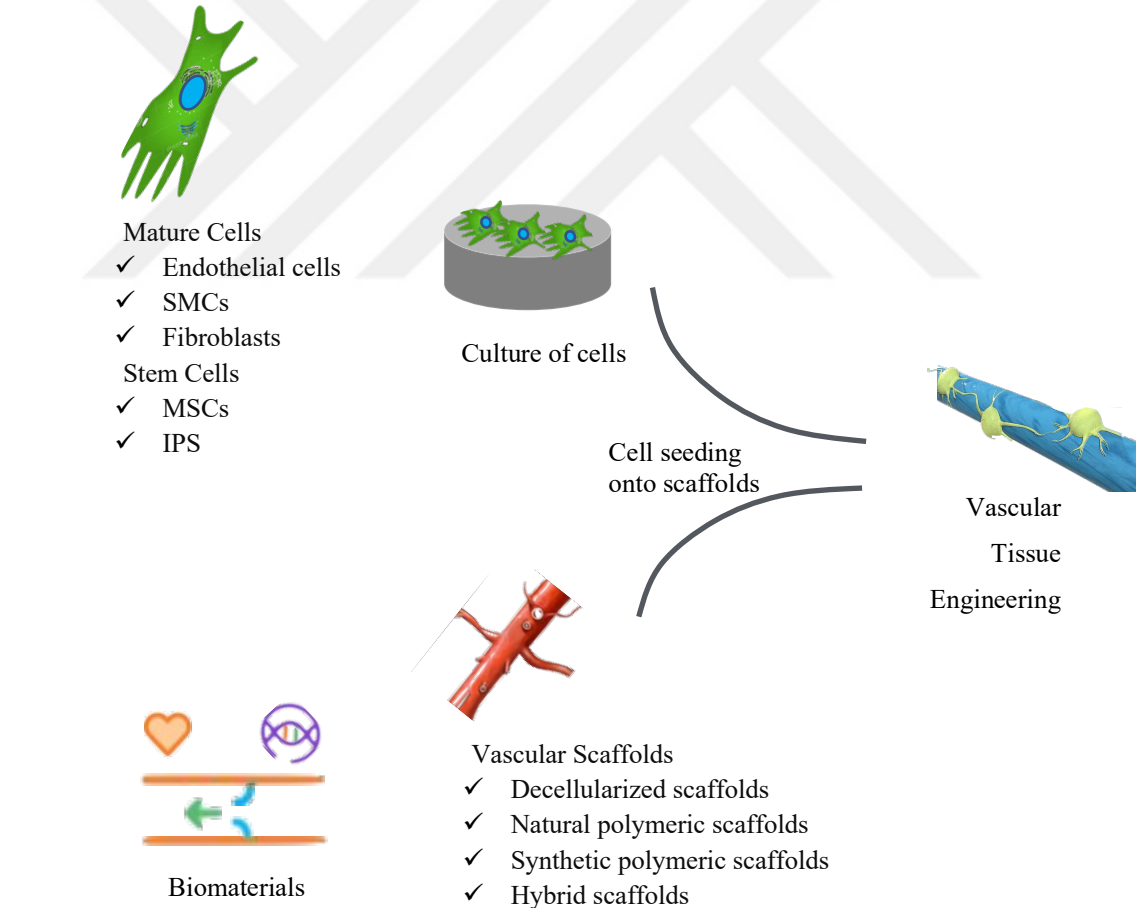

Figure 13. Fundamentals of blood vessel tissue engineering.

2.5.1 Scaffolds for blood vessel tissue engineering

Tissue-engineered vascular equivalents have advantages over cell-free vascular grafts like being responsive in both mechanically and biologically to the hemodynamic microenvironment (40). The success of the particularly small to medium-sized vascular substitute is related to its ability to perform similar structure and function of the native blood vessel (41). The 3D scaffolds serve as ECM, besides ensuring cell adherence, they provide guidance to cells during tissue development by regulating cellular proliferation, organization, migration and even differentiation (16, 42, 43). The scaffold should be tubular form with its smooth and appropriate sized lumen. The ideal vascular scaffold should have a large surface area to increase cell attachment and provide proper environment in which cells maintain their phenotype (44). The porosity of the scaffold is also an important subject because interconnected porosity is required for cell penetration into scaffoldand tissue growth by providing nutrients diffusion through porous network (44, 45). The scaffold should be biodegradable with an appropriate degradation rate to match tissue regeneration rate. The ideal vascular scaffold should resemble the histological properties of blood vessel, as close as possible. The scaffolds can be fabricated from natural or synthetic polymers or decellularized natural vessels can be used as a scaffold (3).

2.5.1.1 Decellularized scaffolds

Decellularized ECM of allogeneic or xenogeneic tissues are used as scaffolds by recellularization in tissue engineering (3)**.** The considerable part of the ECM consists of collagen and elastin, and these proteins usually do not trigger immune response after implantation (46). However, if the cells in the ECM are not removed properly, the remained allogeneic or xenogeneic cells often exhibit immunogenic response (3). Therefore, the aim of decellularization is to remove antigenic cells from the tissue, while preserving the ECM with its structural (47). In decellularization processes, taking care that the intercellular matrix structure is not affected by the process, the cell

components are destroyed in the appropriate solution for required time, then the cell lysates are removed from the tissue (Figure 14) (3). In case the structure and composition of native blood vessel is protected after the decellularization process, decellularized tissue may be used as scaffold for vascular tissue engineering (48). But, decellularized xenogeneic tissues have no clear advantage over alternative grafts and also their cost is higher than the synthetic grafts (16, 49). It was indicated that when the decellularized human blood vessel is used as a scaffold, it could be more responsive to the aneurysm and also there is some ethical consideration to taking account (16, 50). Besides the inefficiently decellularized matrix can trigger the immune response in the patients, the availability of the decellularized matrix with different sizes and shapes is limited (16).

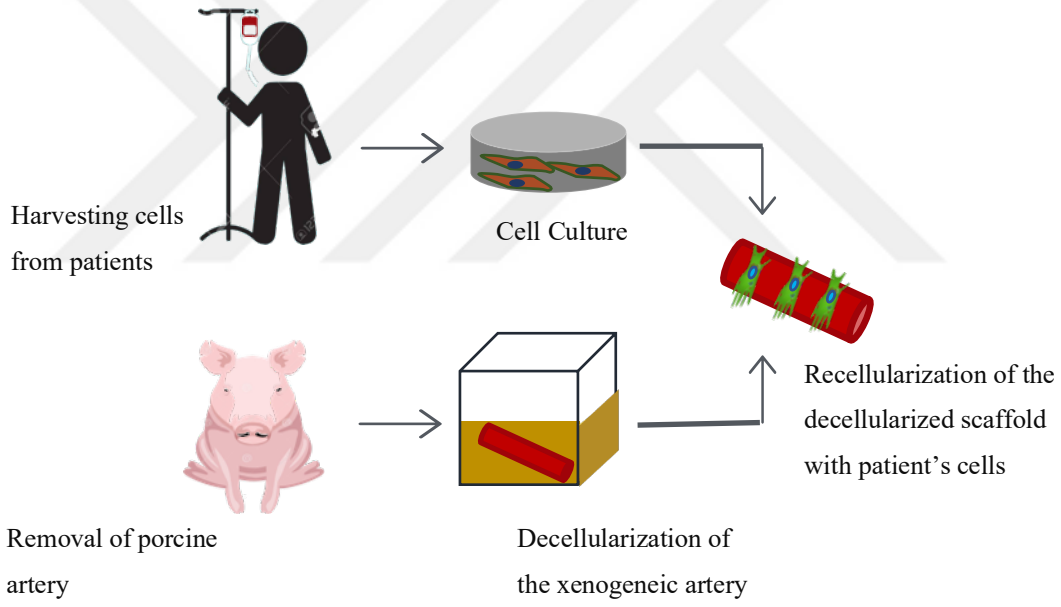

Figure 14. Schematic illustration of decellularized scaffold use in vascular tissue engineering.

2.5.1.2 Natural polymer-based scaffolds

Natural polymers like proteins and polysaccharides are preferred in tissue engineering application since they are readily accepted by the body. The difference between decellularized scaffolds and natural polymer-based scaffolds is that the decellularized scaffold has a conserved architecture, while natural polymers are isolated from tissues as a mixture or pure polymers and then be processed in scaffold fabrication. Different types of natural polymers can be obtained from various sources (Table 3).

The natural polymers exhibit desirable properties such as high biocompatibility, cell-induced proteolysis and ligand-receptor interaction that provide biological recognition (32). Despite of their advantages, natural polymers have considerable limitations such as difficulties in their purification and possible immune response due to inadequate purification. Their mechanical properties are also very poor since enzymes found in the biological system can easily degrade them. Winnberg and Bell fabricated the first living natural polymer-based vascular graft in 1986. They fabricated collagen-based cell-seeded construct; however, the mechanical properties of the substitute were very poor. Therefore, they had to support collagen-based construct with a synthetic mesh to increase its mechanical properties, and then the construct become usable in the clinic (51). This may be springboard in blood vessel tissue engineering. Combining synthetic polymers with natural ones is a good solution to overcome all the disadvantages of natural polymers (32).

Table 3. Types of natural polymers used in tissue engineering and their sources.

Source	Polymer Type
Plant	Cellulose
Animal	Collagen Chondroitin sulfate Hyaluronic acid
Microorganism	Polyesters
Insects	Silk
Crustacean	Chitosan Chitin
Algae	Alginate

Reference: Hasirci V., and Nesrin H. Introduction. Fundamentals of Biomaterials. New York, NY: Springer 2018. p. 1-36.

2.5.1.3 Synthetic polymer-based scaffolds

Different types of synthetic polymers, especially biodegradable ones, are commonly used in tissue engineering (Table 4). The biodegradable synthetic polymers have numerous advantages over natural polymers such as controllable mechanical properties, adjustable degradation profile, relatively low cost, processability into desired shape and structure, and allowing to custom design (32). The lack of bioactivity and harmful effect of degradation product could be the limitations of synthetic polymers (52). However, synthetic polymer-based scaffolds can be bioactive by coating the scaffold with bioactive agents like proteins (53). Moreover, the end product of some synthetic polymers after degradation could lead to some problems. For example, polyglycolic acid one of the most commonly used synthetic polymers in vascular tissue engineering degrades into lactic acid, and it changes the pH of the microenvironment (54). The negative effect of degradation products of synthetic polymers can be eliminated by controlling the degradation rate, for example by blending these polymers with other synthetic polymers or natural polymers. Since

these obstacles related to synthetic polymers could be addressed, they are widely used in tissue engineering studies.

Table 4. Synthetic polymers commonly used in vascular tissue engineering.

Name	Formula
Polycaprolactone (PCL)	$(C_6H_{10}O_2)_n$
Polyglycolide (PGA)	$(C_2H_2O_2)_n$
Polylactides (PLA)	$(C_3H_4O_2)_n$
Poly (lactide-co-glycolide) (PLGA)	$[(C_6H_8O_4)_x(C_4H_4O_4)_y]_n$
Polyurethanes (PU)	$C_{27}H_{36}N_2O_{10}$

Reference: Nair LS., Laurencin C.T. Biodegradable Polymers as Biomaterials. Progress in Polymer Science. 2007;32, :762- 98

2.5.1.3.1 Polycaprolactone (PCL)

Polycaprolactone is a homopolymer made up of ε -caprolactone monomer. This semi-crystalline polyester is synthesized by ring-opening polymerization which results in chain growth polymerization of ε -caprolactone (Figure 15) (55). PCL is widely used in vascular tissue engineering studies due to its biocompatibility, biodegradability and elastomeric properties (56, 57). The melting point of PCL is between 55-60^{o}C and the glass transition temperature is around -60^{o}C. The PCL is soluble in a large scale of organic solvent, which makes it highly processible. PCL can be blended with different types of polymers in an appropriate solvent (Table 5). Due to its hydrolytically labile aliphatic ester bond, it undergoes hydrolytic degradation. Its degradation rate ranges between 2-3 years. Although PCL has a relatively low tensile strength, it displays high elongation at break which can be higher than 700%. The mechanical properties of PCL

can be altered by blending with other polymers or by synthesizing the co-polymer of PCL with PLA or PGA (55, 58).

Table 5. Thermal and mechanical properties of PCL.

Polymer	T_g (ºC)	T_m (ºC)	Tensile Strength (MPa)	Elongation at Break (%)	Degradation Time (Years)
Polycaprolactone	- 60	55-60	≈ 23	>700	2-3

Reference: Nair LS., Laurencin C.T. Biodegradable Polymers as Biomaterials. Progress in Polymer Science. 2007;32, :762- 98.

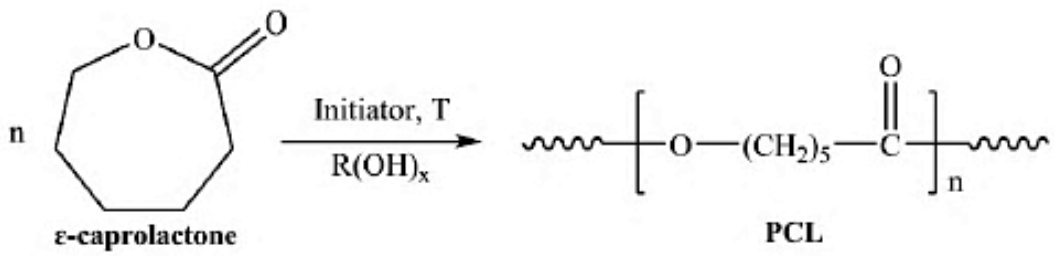

Figure 15. Synthesis of PCL by ring opening polymerization.

Reference: Karaseva S, Botvin V, Filimoshkin A. Synthesis of poly-ε-caprolactone/hydroxyapatite composite materials by in situ and mechanical mixing methods and investigation of their physico-chemical properties. IOP Conference Series: Materials Science and Engineering. 2019;597:012007.

2.5.1.3.2 Poly(lactide-co-glycolide) (PLGA)

Poly(lactide-co-glycolide) is the copolymer of the lactic acid and glycolic acid (Figure 16) (59). Poly(glycolic acid) (PGA) and poly(lactic acid) (PLA) are commercially available, USA Food and Drug Administration (FDA) approved synthetic polymers. The PGA and PLA undergo hydrolytic degradation and their end products can be removed from the body. PLA and PGA have different chemical, mechanical and physical properties (Table 6). PLA has a lower degradation rate

compared to PGA. PLGA, a linear copolymer, can be obtained with different ratios of its monomers, PLA and PGA (Table 6) (59). By altering the LA/GA ratio and molecular weight, the degradation rate can be adjusted depend on the application. For example, PLGA with a ratio of 50/50 (LA/GA) is degraded in 1-2 months, while PLGA (75/25; LA/GA) degrades in 4 to 5 months and PLGA (85/15; LA/GA) degrade in 5-6 months (55). Its good biocompatibility, being approved by FDA and having adjustable degradation rate had made PLGA a favorable polymer to be used in scaffolds for vascular tissue engineering applications (60).

Table 6. Thermal and mechanical properties of PGA, PLA, and PLGA (85/15; 75/25; 50/50).

Polymer	T_g (°C)	T_m (°C)	Tensile Strength (GPa)	Elongation at Break (%)	Degradation Time
Poly(glycolic acid) (PGA)	35-40	>200	12,5	15-20	6-12 months
Poly(lactic acid) (PLA)	60-65	175	4,8		6 months
Poly(lactide-co-glycolide) (85/15)	>37		2	3-10	5-6 months
Poly(lactide-co-glycolide) (75/25)	>37		2	3-10	4-5 months
Poly(lactide-co-glycolide) (50/50)	>37		2	3-10	1-2 months

Reference: Nair LS., Laurencin C.T. Biodegradable Polymers as Biomaterials. Progress in Polymer Science. 2007;32, :762- 98.
Gentile P, Chiono V, Carmagnola I, Hatton PV. An overview of poly(lactic-co-glycolic) acid (PLGA)-based biomaterials for bone tissue engineering. Int J Mol Sci. 2014;15(3):3640-59.

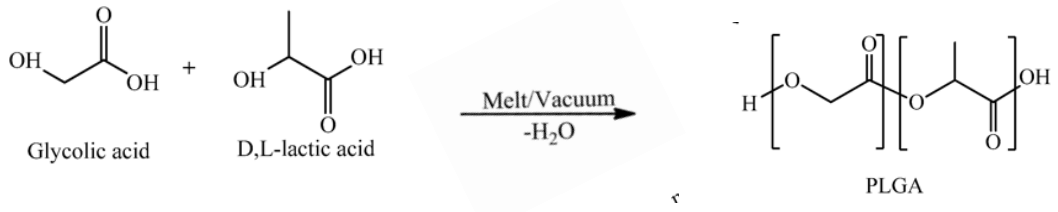

Figure 16. Synthesis of PLGA by ring opening polymerization.

Reference: Ayyob M. And Kim Y.J Effect of Chemical Composition Variant and Oxygen Plasma Treatments on the Wettability of PLGA Thin Films, Synthesized by Direct Copolycondensation. Polymers 2018, 10(10), 1132

2.5.1.3.3 Poly(L-lactide-co-D,L-lactide) (P(L-D,L)LA)

PLA can be two homopolymer forms which are poly(L-lactic acid) (PLLA) or poly(D,L-lactic acid) (P(D,L)LA). PLLA shows high crystallinity, while P(D,L)LA has a semi-crystalline, amorphous structure. PLLA is resistant to hydrolysis due to its high crystallinity. On the contrary, its amorphous structure makes P(D,L)LA more sensitive to hydrolysis (61). PLLA degrades slower than P(D,L)LA (Table 7) (62). A copolymer of racemic P(D,L)LA and stereoregular PLLA is called poly(L-lactide-co-D,L-lactide) (P(L-D,L)LA) (Figure 17) (63). The chemical and physical properties of P(L-D,L)LA are changed depend on the ratio of P(D,L)LA and PLLA. As a combination of PLLA and P(D,L)LA, the needed degradation profile can be achieved by the use of P(L-D,L)LA. Although P(L-D,L)LA is a convenient polymer with its controllable degradation, some features like having rigid structure, high elastic modulus, and low elongation may limit the use of the polymer (62). Therefore, blending of P(L-D,L)LA with another polymer can improve mechanical properties and enhance tissue interaction (64). P(L-D,L)LA, which is generally used in bone and drug delivery studies, is also used in vascular tissue engineering applications to increase mechanical strength (65-67).

Table 7. Thermal and mechanical properties of PLLA, PDLLA, and P(L-D,L)LA

Polymer	T_g (ºC)	T_m (ºC)	Tensile Strength	Elongation at Break (%)	Degradation Time
Poly-L-Lactic Acid (PLLA)	60-65	175	~ 4.8 GPa		2-5 years
Poly-DL-Lactic Acid (P(D,L)LA)	55-60		~ 1.9 GPa		12-16 months
Poly-L-DL-Lactic Acid P(L-D,L)LA	54		26 MPa	8.70	

Reference: Nair LS., Laurencin C.T. Biodegradable Polymers as Biomaterials. Progress in Polymer Science. 2007;32, :762- 98.
Ciambelli GS, Perez MO, Siqueira GV, Candella MA, Motta AC, Duarte MAT, et al. Characterization of poly (L-co-D,L Lactic Acid) and a study of polymer-tissue interaction in subcutaneous implants in wistar rats. Materials Research. 2013;16:28-37

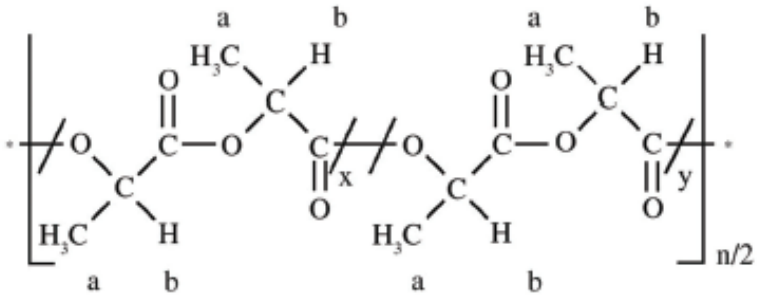

Figure 17. Molecular structure of P(L-D,L)LA

Reference: Martins K.F., Messias A.D., Leite F.L., and Duek E.A.R. Preparation and Characterization of Paclitaxel-loaded PLDLA Microspheres. Materials Research. 2014; 17(3): 650-656.

2.5.1.4 Hybrid polymeric scaffolds

The blends of polymers can be used in the scaffolds to obtain desired properties that cannot have in their individual form (67, 68). Application-specific polymers can be blended in an appropriate solvent which is suitable for each polymer type (68). The scaffold can be fabricated from natural polymer blend, synthetic polymer blend or

from the combination of synthetic and natural polymers which called hybrid scaffold (Figure 18) (16, 69). Hybrid polymers, combination of natural and synthetic polymers, are commonly used to improve chemical and physical properties of the polymer, like bioactivity, mechanical properties, degradation profile, etc. By the use of hybrid polymers the desired mechanical properties of the synthetic polymer can be combined with the biological cues of the natural polymer (16). The hybrid scaffold can be obtained both by coating the surface of the synthetic scaffold with natural proteins such as gelatin, fibronectin, or by combining natural and synthetic polymers during the manufacturing of the scaffold (65, 70). If the important points are considered, such as temperature, which disrupts the natural structure of proteins or polymer, hybrid polymeric scaffolds could offer a potential vascular scaffold by exploiting the best features of synthetic and natural polymers (16, 71).

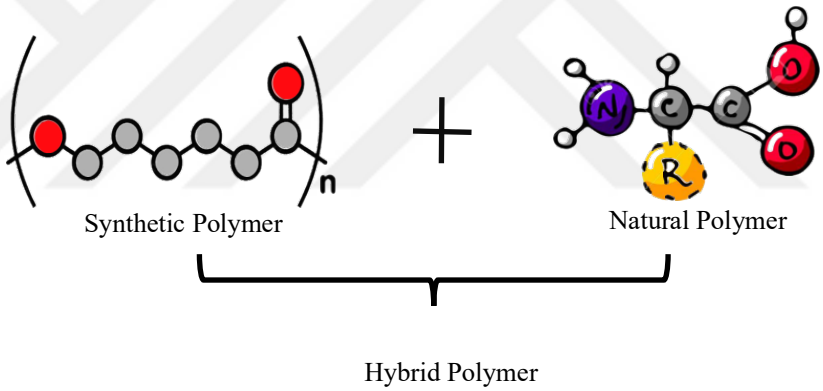

Figure 18. Hybrid polymer component.

2.5.1.5 Fabrication methods of scaffolds

The scaffold serves as an ECM and regulates cell behavior like adherence, proliferation, apoptosis, migration and differentiation. The scaffold should have the following features: 1) highly porous three-dimensional structure with interconnected porosity to supply nutrients and to allow gas exchange; 2) biodegradability of which rate should match with the rate of tissue regeneration *in vivo*; 3) proper surface

chemistry to support cell attachment and growth; 4) appropriate mechanical and topographical properties to meet the properties of the target tissue (32). Scaffolds can be fabricated by various techniques to obtain different scaffold forms such as foam, mesh or film with different textures like porous, random or oriented. The most common techniques used in scaffold fabrication are lyophilization, particle leaching, solvent casting, dip-coating, and electrospinning (Table 8) (28).

Table 8. List of some scaffold fabrication methods and the resultant scaffold morphology

Methods	**Texture and form of scaffolds**
Lyophilization	Porous foams
Particulate leaching	Porous foams
Solvent Casting	Patterned or smooth films
Dip coating and solvent casting	Porous or non-porous, tubular or flat films
Wet Spinning	Micro-fibrous meshes
Electrospinning	Align or random micro or nano-fibrous mats

Reference: Hasirci V. and Nesrin H. Tissue Engineering and Regenerative Medicine. Fundamentals of Biomaterials. New York, NY: Springer 2018. p. 281-302.

2.5.1.5.1 Dip coating

One of the methods of obtaining thin films of the polymer solution on substrate is dip coating (72). Dip coating is the process of immersing the substrate into the coating solution for a time and removing from the solution at a constant speed then dried. The dip-coating process consists of 3 stages; the first is to immerse the substrate into the coating solution at a constant rate, the second step is the dwell time of the substrate in the coating solution, and the last step is withdrawn the substrate from the coating solution at a constant speed. The liquid film is formed on the substrate surface, and then the thin film is obtained on the substrate by evaporating the solvent of the solution (Figure 19). Dip-coating is a consistent, low-cost and reliable technique. By changing the parameters such as dipping number, coating solution concentration or dwell time,

the thickness of the film can be adjustable. By adding porogen into the coating solution, porosity of the scaffold can be achieved with the removal of the porogen after solvent evaporation (73). The tubular or flat scaffold, which may have different morphology depending on whether it contains porogen or not, can be fabricated with dipping-coating by altering the substrate shape (74, 75).

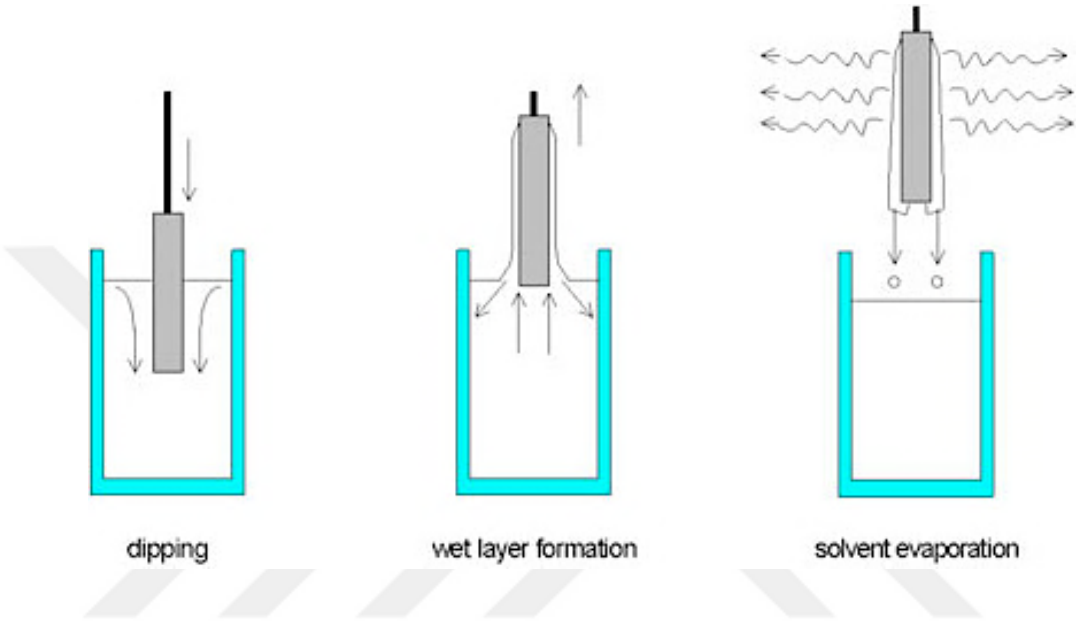

Figure 19. Stages of dip-coating.

Reference: http://www.apexicindia.com/technologies/dip-coating-technology/ Access date 30/05/2020

2.5.1.5.2 Electrospinning

The natural ECM has a fibrillar structure to support the cell physically and biologically. It is important to fabricate scaffold similar to native ECM to mimic the natural tissue in a structural and functional manner (76). Electrospinning is one of the efficient method to fabricate fibrous scaffolds which offer desired properties in tissue engineering field (32). Electrospinning is the technique of producing fibers from polymer solutions with electric force. The electrospinning set-up is composed of power supply to apply potential, a syringe containing polymer solution, syringe pump to feed polymer solution at a constant flow rate, and a grounded metallic collector. The electrospinning system has numbers of parameters which can be controllable and

affect fiber diameter, shape and orientation (Figure 20). These parameters can be listed as the concentration and viscosity of polymer solution, the flow rate of the polymer solution, the distance between collector and syringe needle, the applied potential, solvent conductivity, the rotation speed for mandrel system, temperture, and so on. Fine, continuous, micro or nano-scale fibers can be obtained with the electrospinning after optimizing parameters (77). Fibrous mats obtained with electrospinning provides a large surface area to volume ratio which supports cell attachment, proliferation, and growth. In addition, by using different collector types, random or aligned fibrous structures can be fabricated to obtain structurally similar scaffolds with natural ECM of target tissue (78). By changing the polymer type, parameters or collector type, the target tissue-specific fibrous scaffolds can be obtained via electrospinning. For instance, mandrel systems with rotating drum collectors are commonly used in vascular tissue engineering studies to obtain tubular fibrous scaffolds (77).

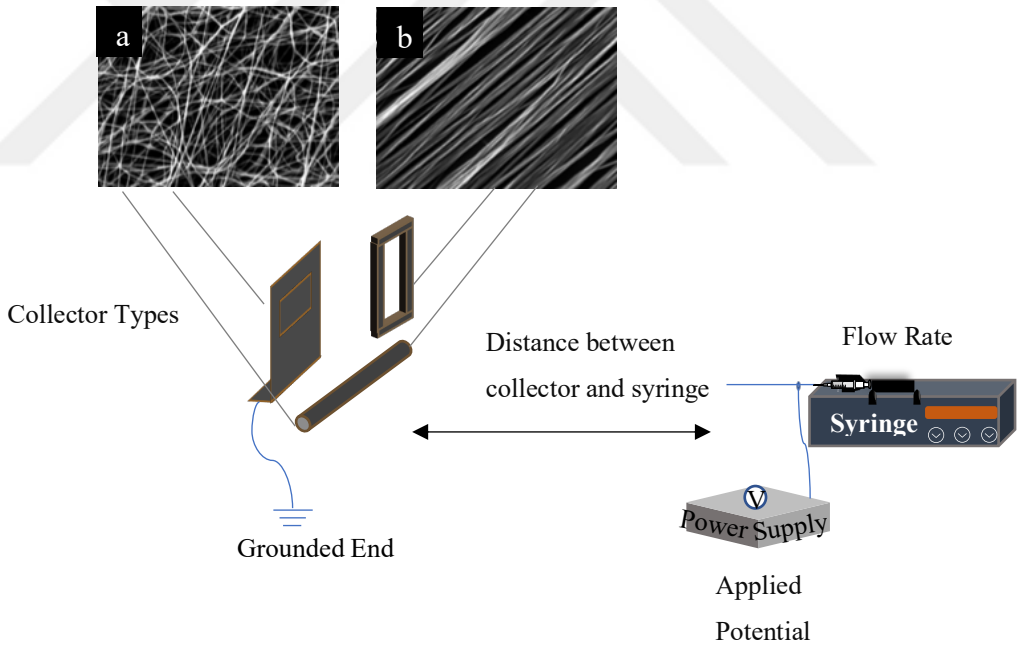

Figure 20. Illustration of electrospinning set-up with its controllable parameters and different collector types that allow to obtain (a) random of (b) aligned fibrous mats.

2.5.2 Cell sources used in blood vessel tissue engineering

Cells are the living part of the tissues and play an important role in healing and regeneration of tissues. In tissue engineering, cells from different sources can be used, such as autogeneic cells of patients, allogeneic cells of another person, or xenogeneic cells of another species. Autogeneic cells are preferable in most of clinical studies since allogeneic and xenogeneic cells have a risk of immune rejection. Cell types commonly used in tissue engineering are mature somatic cells, embryonic stem cells, induced pluripotent stem cells, tissue specific stem cells, and mesenchymal stem cells (32). In terms of vascular tissue engineering, vascular tissue mature cells such as endothelial cells, smooth muscle cells (SMCs), fibroblasts, and also stem cells such as mesenchymal stem cells, are used in blood vessel tissue engineering (Table 9) (16).

Table 9. Cell types used in vascular tissue engineering

Cell Types	
Mature Cells	Stem Cells
Endothelial Cells (ECs)	Induced Pluripotent Stem Cells (iPSCs)
Smooth Muscle Cells (SMCs)	Mesenchymal Stem Cells (MSCs)
Fibroblasts	Embryonic Stem Cells (ESCs)

Reference: Pashneh-Tala S, MacNeil S, Claeyssens F. The Tissue-Engineered Vascular Graft-Past, Present, and Future. Tissue Eng Part B Rev. 2016;22(1):68-100.

2.5.2.1 Mature cells

ECs, SMCs, and fibroblasts are the main cell types of the blood vessel wall. ECs line the lumen of the blood vessel and regulate the contraction of SMCs by secreting biochemical molecules, as well as they are responsible for the regulation of blood vessel metabolism and remodeling. SMCs are responsible for the contraction of the blood vessel which is important for maintaining the mechanical properties of the blood

vessels and for the secretion of the extracellular matrix components (79). The ideal tissue-engineered graft should be supported with ECs and SMCs to mimic native vascular tissue (80). Autogeneic ECs, SMCs, and even fibroblasts are utilized in many vascular tissue engineering studies (65, 81). However, the use of autogeneic mature cells brings some drawbacks, such as another surgery requirement for the isolation of that cell, donor site morbidity and low proliferation capacity of the cell under culture condition. The stem cells are good alternatives to overcome these limitations of mature cells (16, 79).

2.5.2.2 Stem cells

Stem cells are unspecialized cells which have self-renewal and differentiation capability. Self-renewal is the process that cells produce their copies by cell division to increase in number, and stem cells protect their undifferentiated state and differentiation capability when they undergo self-renewal. On the other hand, the differentiation is the process that the cells become specialized cells having specific functions under certain conditions (28, 35). Stem cells are classified according to their tissue origin or stage of development (Figure 21). In addition, stem cells are categorized depending on the breadth of differentiation capacity which also called their potency. Four main types of stem cells according to their potency are: 1) totipotent stem cells; 2) pluripotent stem cells; 3) multipotent stem cells; and 4) unipotent stem cells (35).

Totipotent stem cells, for example zygote and blastomeres before blastocyst stage, have capability to differentiate into three embryonic germ layers and extraembryonic tissues. Pluripotent stem cells have a potential to differentiate into all cell types in the body except extraembryonic tissues (82). The best-known pluripotent stem cells are embryonic stem cells (ESCs) which are originated from the inner cell mass of blastocytes. Multipotent stem cells have an ability to differentiate into multiple specialised cell types found in a specific tissue. Adult stem cells like hematopoietic

stem cells, skin stem cells, neural stem cells, etc. are multipotent stem cell that can differentiate into tissu-specific, limited number of cells. They divide more slowly than the pluripotent stem cells and expansion capacity lower than the pluripotent stem cells (35). However, working with multipotential stem cells does not cause specific ethical problems, unlike pluripotent stem cells (83). It was believed that mesenchymal stem cells were multipotent and have a limited differentiation capacity, they can differentiate only into cells derived from mesoderm. However, this notion has been changed when the researchers revealed that MSCs were able to differentiate into various cell types, also derived from endoderm and ectoderm, under certain induction conditions. Unipotent stem cells or progenitor cells are tissue-specific cells that can differentiate into single cell lines (35)

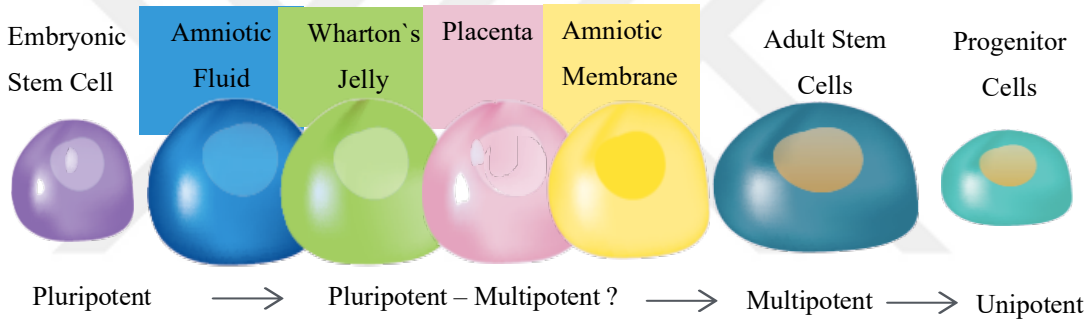

Figure 21. Stem cell classification based on both potency and ontogenesis.

Reference: Pappa KI, Anagnou NP. Novel sources of fetal stem cells: where do they fit on the developmental continuum? Regen Med. 2009;4(3):423-33.

2.5.2.1.1 Mesenchymal stem cells

Friendenstein and colleagues published a protocol regarding isolated bone marrow mesenchymal stem cells using the adhesion profile of cells on a culture plate (35, 84). Afterward, MSCs have been obtained from various different tissues that have mesenchymal origin such as fat, umbilical cord, dental pulp, etc. The Mesenchymal and Tissue Stem Cell Committee of the International Society for Cellular Therapy was

established three criteria to define a cell as MSC (Table 10). MSCs should have adherence plasticity on the culture plate and express certain MSCs markers while exhibiting negative expression of some markers like hematopoietic stem cell markers. The last criteria is that MSCs should differentiate into osteoblast, chondroblasts, and adipocytes under *in vitro* conditions (85). Besides their differentiation capabilities, MSCs have preferred functional properties such as secretion of trophic factors that have an influence on the other cells as paracrine effect, enhancing regeneration and remodeling of tissues (35). Even if not fully understood, these cells have immune modulation role via cell-to-cell contact or secretion of soluble factors, and thus they are able to enhance tissue regeneration (86). MSCs are utilized in tissue engineering to be integrated into scaffold, and are differentiated into target tissue-specific cell with physical or chemical cues, such as topography of scaffolds or growth factors (87).

Table 10. Minimal criteria to identify MSC

1) Adherency to plastic in standart culture condition		
2) Phenotype	Positive ≥ 95	Negative ≤ 2
	CD105	CD45
	CD73	CD34
	CD90	CD14 or CD11b
		CD79 or CD19
		HLA-DR
3) *In vitro* differentation: osteoblasts; adipocytes and chondroblasts (demonstrated by staining of *in vitro* cell culture)		

Reference: Dominici M, Le Blanc K, Mueller I, Slaper-Cortenbach I, Marini F, Krause D, et al. Minimal criteria for defining multipotent mesenchymal stromal cells. The International Society for Cellular Therapy position statement. Cytotherapy. 2006;8(4):315-7.

MSCs can be obtain from both extraembryonic tissues or adult tissues. MSCs can be isolate from different types of extraembryonic tissues such as placenta, amniotic fluid, amniotic membrane, umbilical cord blood and umbilicol cord matrix (Figure 21) (88). Stem cells obtained from the matrix part of umbilical cord are referred to as Wharton`s Jelly mesenchymal stem cells (WJ MSCs). WJ MSCs exhibit intermediate stem cell characteristics between properties of pluripotent ESCs and multipotent adult MSCs. Unlike adult MSCs, WJ MSCs consistently express some ESC markers such

as Sox-2, Nanog, Oct-4, and Rex-1 (89). Since WJ MSCs isolated from normally discarded tissues and so not have ethical concerns, it is an ideal source for stem cell utilized studies compared to the ECS (88). In terms of differentation ability, WJ MSCs differentation potential is higher than the adult MSCs (89). In addition, the immunomodulation capability of WJ MSCs is broader than the adult MSCs, and these cells have low level express of HLA-ABC, almost no expression of HLA-DR (90). These cells also display all distinctive properties of MSCs (Table 10). Isolation of the cells without ethical concern from discarded tissue, expandability in the long term culture, differentiation capacity and possess immune-privileged properties make WJ MSCs promising cell source for tissue engineering and regenerative medicine studies (89).

2.5.3 Growth factors used in blood vessel tissue engineering

Growth factors are one of the biological agents used in tissue engineering (32). They are in the protein structure and play important role in many cellular processes such as migration, differentiation, and survival. Growth factors are also important for tissue regeneration and healing (28, 32). Depending on the purpose, different types of growth factors can be incorporated into the scaffolds or added into the growth medium of cells.

Considering blood vessel tissue, the function of endothelial cells are modulated by various trophic factors that can be found in circulation or secreted by SMC or fibroblast. Function and dysfunction of the endothelial cells cause inflammation and cardiovascular disease (91). Therefore endothelial cell culture is an important matter to mimic the vascular structure and requires various types of growth factors to culture cells under *in vitro* conditions (Table 11). Another important growth factor for vascular tissue engineering is transforming growth factor-beta (TGFβ) which acts as a regulator in vascular development (92). TGFβ1 which belongs to the TGFβ superfamily stimulates the phenotypic differentiation of MSC into smooth muscle cells by

regulating the expression of contractile proteins such as a-SMA, Calponin which are the specific smooth muscle markers (92, 93).

Table 11. Biological molecules used in endothelial cell growth and their functions.

Biological molecules in Endothelial Cell Medium	Role of biological molecules
basic Fibroblast like Growth Factor (bFGF)	Vascular development and maintaining vascular integrity (94)
Epidermal Growth Factor (EGF)	Serve as a mitogen and induce cell differentiation and proliferation (95)
Vascular Endothelial Growth Factor (VEGF)	Inhibition of the expand of endothelial cells and increase the survival of endothelial cell (95)
Insulin Like Growth Factor (IGF)	Modulation of cell growth and apoptosis (95)
Heparin	Inhibition of blood coagulation and improvement in cell stability by binding to growth factors (95)
Hydrocortizole	Reduce cell toxicity and inhibition of disease related vasodilation by decreasing the NO release(95)
Ascorbic Acid	Crucial for cell growth and maintaning specific cobblestone morphology of endothelial cells (95)

2.6 Promising Substitues for Blood Vessel Tissue Engineering

There are numerous tissue engineering approaches aimed to treat vascular disorders. The scaffolds made of various natural or synthetic polymers or hybrid polymers are used in vascular tissue engineering studies. Natural polymers particularly collagen, fibrin and elastin are widely used in vascular tissue engineering applications since they support cell adhesion and tissue regeneration (96, 97). However, natural polymers show fast biodegradation and poor mechanical properties. Synthetic polymers such as polyglycolic acid (PGA), polylactic acid (PLA), poly L-lactide acid (PLLA), polycaprolactone (PCL), polyglycerol sebacate (PGS), etc. are employed in

blood vessel tissue engineering (81, 98). The poor cell adherence or even lack of cell attachment is the main problem with synthetic polymer-based scaffolds. The limitations of synthetic and natural polymers mentioned above can be solved by the use of hybrid polymeric scaffolds such as collagen-PLA, collagen-PCL, elastin-PCL, etc (99). Cell carries used in vascular tissue engineering can be obtained in different forms such as film, porous membrane, fibrous mesh or hydrogel (56, 100, 101). It is important to design cell carriers that provide cell orientation to mimic natural tissue-like organization in blood vessel tissue engineering studies (102). Advances in the production methods of scaffolds have allowed integrating topographic and chemical cues to scaffold design. Topographic cues such as patterned surfaces or aligned fibrous structure can guide cell organization and their behavior (103, 104). In vascular tissue engineering, scaffolds are genereally supported with mature endothelial, smooth muscle or fibroblast cells (81, 99-101). By the advancement in stem cell field, these potential cell sources have been widely used in tissue engineering studies. The use of stem cells, which are capable of self-renewal and differentiate into many different types of cells, in tissue engineering promises to produce patient-specific tissue product, reduce the risk of immune response, and design complex tissues such as vessels, nerves and bones (35).

In the literature, a large number of single, bilayered (51, 60, 65, 81, 99, 102, 105-107) and multilayered vascular substitutes (56, 100, 101, 108) have been developed in the form of tube. Niklason and Langer with their colleagues were the first that produced a single-layer synthetic PGA based small-caliber artificial artery *in vitro*. The outer side of the vascular scaffold was supported with bovine SMC and endothelial cells were integrated to the inner side. Cells were grown on the scaffold with the bioreactor system. They revealed that the patency of the tissue engineered construct was 100% after 4 weeks of implantation in pigs and the burst strength was higher than 2000 mmHg (81).Wise and his colleagues designed bilayered hybrid small-diameter vascular constructs to mimic the internal mammary artery (IMA). They fabricated the vascular scaffold with electrospinning. The inner side of the scaffold was obtained from human synthetic elastin (SE) to increase the endothelization and

the outside of the scaffold was obtained from PCL. The lumen side of the scaffold was seeded with HUVEC. It was revealed that SE supported HUVEC attachment and proliferation. They concluded that mechanical properties of the scaffold were insufficient when fabricated from synthetic elastin, therefore PCL was incorporated intoto scaffold to provide mechanical support. Although the elastic modulus of the scaffold was close to the IMA, tensile strength was higher than IMA depending on PCL concentration (99).

In recent years, fabrication of multilayered vascular substitutes has been a challenge in vascular tissue engineering. Khademhossini and his colleagues developed a perfusable tri-layered vascular construct within the microfluidic system by using layer by layer organization of mature blood vessel cells, fibroblast, SMC and endothelial cells. Fibroblasts and rat aortic SMCs were laden in crosslinkable GelMA, and firstly GelMA laden fibroblasts were formed over the outer side of the small-diameter needle, then GelMA laden SMC was injected to the inner side of the needle. HUVECs were seeded into the lumen side of the construct. It was observed that HUVEC formed as a monolayer on 2D GelMA and the viability of the fibroblast was related to GelMA concentration. It was also revealed that the mechanical properties of tri-layered construct were lower than the native blood vessel due to being made up of hydrogel (100). In 2020, Chen at al. was obtain the tri-layered vascular scaffold from biodegradable polymers to mimic the native structure of the blood vessel. The innermost layer of the scaffold was PCL based electrospun mesh. The middle porous structure was obtained from PLGA by using freeze-drying and is wrapped over the inner layer. The outermost layer of the scaffold was fabricated by polyurethane (PU) over the bilayered scaffold. Layers were attached to each other via thermal linking. The scaffold was supported with either EC or SMC but not co-cultured on the construct. It was observed that the mechanical properties of the graft were not sufficient compared to the native artery (101).

The scope of this study was to develop a multilayered, tubular vascular substitute and to investigate its performance with *in vitro* studies. For this purpose, the multilayered scaffold was prepared by the following processes: 1) formation of porous tubular film by dip coating as the inner layer of the construct, 2) deposition of circumferentially aligned electrospun fibers over porous film as the intermediate layer of the construct, and 3) wrapping random electrospun fibrous around aligned fibrous layer as the outer layer of the construct. Human WJ MSCs and HUVEC were used as cell sources to be seeded on the intermediate and the inner layers, respectively. The vascular substitute was designed taking into account the histological properties of native muscular artery tissue by imitating intima, media and adventitia layers of blood vessel.

3. MATERIALS AND METHODS

3.1 Materials

Polycaprolactone (PCL) (Mw 124000 g/mol), poly(lactic-co-glycolic acid) (PLGA) (Mw 153000 g/mol) and poly(L-lactide-co-D ,L-lactide) (P(L-D,L)LA) (Mw 1500000 g/mol) were obtained from Purac, Corbion Company. Dexamethasone, ascorbat-2-phosphate, chloroform, DAPI, trypsin-EDTA, silver nitrate, sodium thiosulfate, collagenase, FITC-Phalloidin, fibronectin, WST-1, proline, sodium pyruvate and insulin-transferrin-selenite were obtained from Sigma-Aldrich (St. Louis, Missouri, USA), and DMF was purchased from Merck Company (NJ, USA). PEG (Mw 1000) was obtained from Fluka, BioChemika. Hank`s Balanced Salt Solution (HBSS) (HBSS1-A) was purchased from Capricorn Scientific. DMEM-F12, penicillin-streptomycin and FBS were obtained from Gibco. The antibodies, CD105, CD73, CD90, CD44, CD34, CD45, HLA-DR, HLA-ABC, Isotype IgG1, Isotype FITC IgG1, Isotype PerCP IgG1, Isotype PE IgG1 and Isotype PerCP IgG2 were purchased from BD Biosciences. In addition, CD31 is obtained from Dako. ß-glycerophosphate was obtained from AppliChem. ALP was purchased from Randox. Antibody against VE-Cad was obtained from Thermo Scientific. Antibody against α-SMA was obtained from Syc-Tek, while anti-smooth muscle heavy chain (SMC HC) was purchased from Abcam.

3.2 Methods

3.2.1 Construction of the multilayered polymeric scaffolds

Polymer based multilayered tubular scaffolds were prepared as three layers composed of porous film as the inner layer, circumferentially aligned fibers as the intermediate layer and random fibrous mat as the outer layer. The inner layer, porous tubular film was fabricated by dip coating using a polymer blend of PCL and PLGA. The intermediate and the outer layers were fabricated by electrospinning technique using a polymer blend of PCL, PLGA and P(L-D,)LLA. The solvent type, composition and concentration of polymer blends were optimized considering the required properties and the fabrication methods of layers. Firstly, polymers were dissolved in different solvents at different concentration and composition to determine the optimum conditions for the polymer blends (Table 12). Polymer solutions prepared in different solvents with different ratios were poured into glass petri dish, and air dired under hood overnight to evaporate solvent of polymer solutions. The thin polymeric films obtained by solvent casting were peeled off from the surface, and then examined under light microscope.

Table 12. List of used polymers with their concentration and composition and the solvent types used to determine the optimum polymer blend conditions.

Polymers, Concentrations and Compositions	Solvent
10% PCL-PLGA (w/v, 8:2; w:w)	Chloroform
10% PCL (w/v)	Chloroform
10% PCL-PLGA (w/v, 8:2; w:w)	Dichloromethane
10% PCL (w/v)	Dichloromethane

3.2.1.1 Preparation of the porous tubular film

The porous tubular film as to be the inner layer of the multilayered scaffold was fabricated by dip coating method. A polymer blend solution of PCL-PLGA (5-10%, w/v, 8:2, w:w) was prepared. Stainless steel metal rods (316LVM Medical Grade, 3 mm in diameter, 13 cm in length) were dipped into PCL-PLGA solution containing PEG (Mwt 1000 Da) (5-15%) as a porogen (Figure 22). Dip coating process was repeated 4-15 times to obtain proper film structure. Following each dip coating cycle, it was waited for the evaporation of solvent. At the end, polymeric film coated rods were placed in dH_2O to obtain porous tubular film by removal of PEG. Samples were frozen and freeze-dried (Labconco, 7934031) to preserve porous structure. Different concentrations of PEG (5-15%) were tested to optimize porosity, and the thickness of polymeric films was optimized by changing the number of dip coating cycle (Table 13).

According to the results given in section 4.1.2, the porous tubular films were prepared using polymer blend solution of 5% PCL-PLGA (8:2, w:w, dissolved in DCM) containing 10% PEG and applying 4 times dip coating in the further studies.

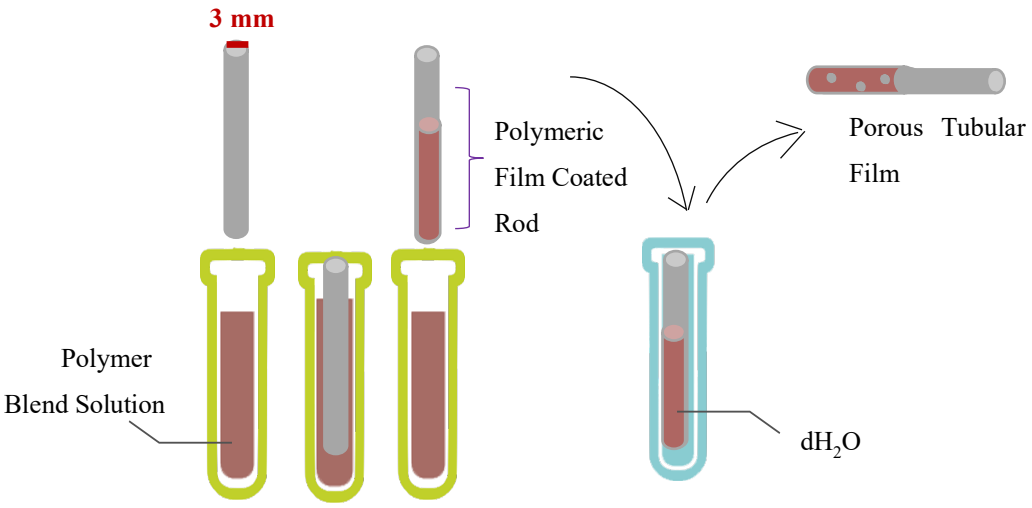

Figure 22. Schematic presentation of porous tubular films by dip coating and solvent casting.

Table 13. The polymer concentrations and number of dip coating cycles used to optimize porosity and thickness of tubular film

Polymer Blend Concentration	PEG Concentration	Number of dip coating cycles
10 % PCL-PLGA	5, 10 and 15 %	15
5% PCL-PLGA	10 %	4, 6, 8 and 10

3.2.1.2 Fabrication of the electrospun fibrous mats

The aligned and random fibers for the intermediate and outer layers were obtained by electrospinning (Innovenso, NE100), respectively. The different fiber topography was achieved by changing the collector diameter and drum rotation speed. Electrospinning set up is composed of power supply, syringe pump and grounded collector. A polymer solution was placed into syringe and pushed through the syringe needle with a constant flow rate by syringe pump. A high voltage was applied between the needle and the collector to create an electric field. Positive electrode was linked to the nozzle of the syringe, then high voltage introduced to system to make polymer droplet charged. When voltage was high enough to overcome surface tension of the polymer, polymer droplets was stretched and took the shape of cone known as taylor cone. To keep polymer droplet jet constantly, critical voltage value adjusted and applied to the system. As the polymer solution was ejected from nozzle of the syringe to the grounded collector, solvent was evaporated, and the stretched polymer was collected on grounded-collector as fibrous mat. Depending on the collector type, fibers with different topograpghy could be achieved. In order to obtain fine, bead-free fibers on the collector, electrospinning parameters such as the applied potential, flow rate, distance between collector and nozzle, rotation speed of drum collector, concentration of polymer and solvent ratios were optimized (Table 14).

Table 14. Optimization of electrospinning parameters.

Polymer Concentrations and Compositions	Solvent Type	Applied Potential (kV)	Distance (cm)	Flow Rate (µL/min)
8.5 % PCL-PLGA (8:2; w:w)	CHL-Methanol (5:1)	8,10,15,18, 20, 25	10, 12, 15, 17, 20	4, 8, 14, 20, 33, 40
5%, 8% and 10% PCL-PLGA (8:2; w:w)	CHL-DMF (5:1, 8:2, 9:1, 19:1)	8, 10, 15, 16, 20, 25	10, 12 15, 18, 20, 25	4, 8, 30, 33
10%, 15% PCL-PLGA (8:2,w:w	DCM-DMF (8:2, 9:1, 19:1)	8, 9, 10, 11,12, 13, 14, 15	18, 19, 20, 21, 22, 25	5, 8, 10, 11, 12, 13, 14, 15, 20
5%, 15% PCL-PLGA-PLDLLA (6:2:2, w:w:w) (5:2:3, w:w:w) (4:2:4 w:w:w)	DCM-DMF (19:1)	10, 11, 12, 13, 15	20, 25	5, 6, 8, 12, 15, 20

CHL: Chloroform, DCM: Dichloromethane; DMF: Dimethylformamide

According to the optimization results given in the section 4.1.3.1, PCL-P(L-D,L)LA-PLGA (5%, 4:4:2, w:w:w) prepared in DCM:DMF (19:1) was used for fabrication of the intermediate and the outer part of multilayered scaffold in the further studies. The optimized elecrospinning parameters were determined as; applied potential of 15 kV, with flow rate of 15 µL/min, distance of 25 cm. The thin porous film coated metal rods (3 mm in diameter) were used as a collector in madrel system to deposit circumferentially aligned fibers, as the intermediate layer of the scaffolds over porous tubular film. The circumferential alignment was obtained when the drum was rotated at the 3000 rpm (Section 4.1.3.1). Thus, the bilayered scaffold was obtained as circumferentallly aligned fibers over porous tubular film (Figure 23). On the other hand, the outer random fibrous mat was collected on a drum of 4 mm diameter metallic rods. Random topography of the fibers was achieved by decreasing the rotation speed of drum collector to 500 rpm. Then, the obtained random fibrous mat was wrapped over circumferentially aligned fibrous mat as the outer layer of the scaffold (Figure 23). Eventually multilayered scaffolds composed of porous tubular

film, circumferentially aligned fibers, and random fibers were obtained and characterized.

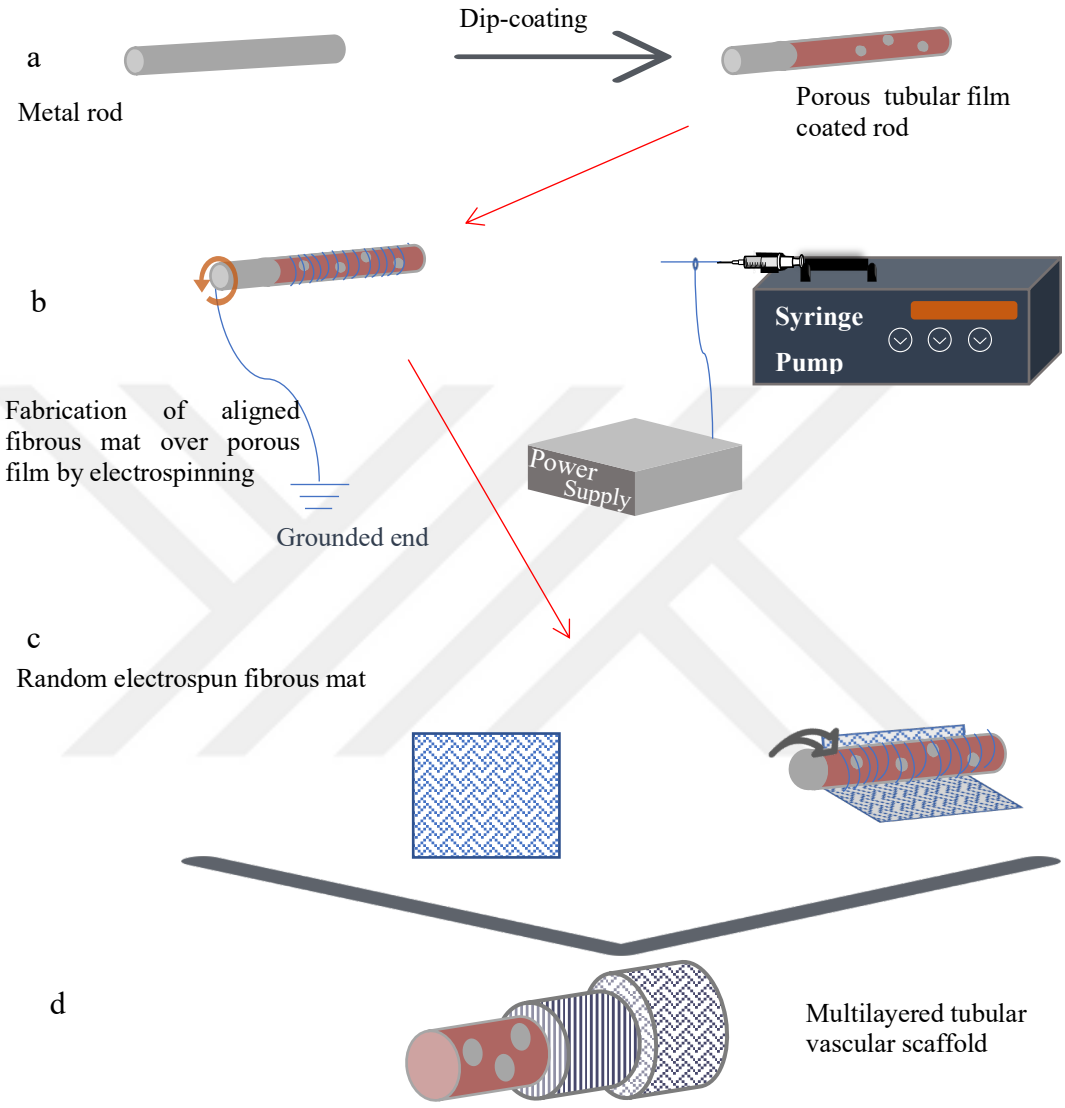

Figure 23 Illustration of multi-layered scaffold preparation. (a) Porous tubular film fabrication on metal rod by dip coating, (b) production of intermediate layer of the scaffold by depositing the circumferentially aligned fibrous mat over porous film, (c) Random fibrous mat wrapping over aligned fibers as the outer layer and (d) the obtained multilayered vascular scaffold.

3.2.1.3 Characterization of scaffolds

3.2.1.3.1 Scanning electron microscopy

Surface morphology of multilayered scaffold parts including the porous tubular film, circumferentially aligned fibrous mat, random fibrous mat were investigated with Scanning Electron Microscopy (SEM). Samples were coated with gold in 55 nm thickness with vacuum sputter coater (Leica EM ACE600), and the images were taken by scanning electron microscope (Thermo Quatrro ESEM at Acıbadem Mehmet Ali Aydınlar University), at 5 kV-10 kV.

3.2.1.3.2 Analysis of fiber diameter and orientation

The distribution of fiber diameter and orientation was analyzed with Fibro Quant 1.3 software using SEM images (three images from different areas) of electrospun fibrous mats obtained under optimum electrospinning process conditions. The fiber diameters and the deviation angles of fibers, indicating fiber orientation, were calculated according to reference fiber given to the software

3.2.1.3.3 Mechanical analysis

The mechanical properties of the polymeric films were determined with mechanical tester (CellScale – Univert, Canada). Polymeric films (1cm in width, 4 cm in length), 5% PCL-PLGA (8:2, w:w, in DCM), 5% PCL-PLGA (8:2, w:w, in DCM) prepared using 10% PEG were attached to the holders of the instrument. The samples were tested under 1 mm/min test speed. The stress-strain curve was obtained for each sample. The young`s modulus of the sample was calculated from the slope of the stress-strain curve (straight line-elastic region of the stress-strain curve). Mechanical

test of the polymeric films was analyzed at Center of Excellence in Biomaterials and Tissue Engineering, Middle East Technical University (METU, BIOMATEN).

3.2.1.3.4 Permeability test

The inner porous tubular film was designed to allow fluid flow but not permit cell penetration. Therefore, the porous film was tested in terms of colored medium passage through the tubular film wall. The porous tubular film was fabricated as explained in Section 3.2.1.1. The non-porous tubular film was obtained from 5% PCL-PLGA polymer solution without PEG and used as a control. The tubular films were placed into petri dish and 200 µL colored medium was placed into the lumen of the tube. The passage of colored medium through the film was followed and photographs of the films were taken to compare the liquid leakage between the porous film and the non-porous film.

3.2.2 *In vitro* studies

In this study, human Wharton's Jelly mesenchymal stem cells (WJ MSCs)-derived smooth muscle cells (SMCs) and endothelial cells were used as cell sources. Human WJ MSCs were obtained from the umbilical cord matrix, while the human umbilical vein endothelial cells (HUVEC) were isolated from the vein tissue. The human derived cells were used with the approval of ethical committee (Acibadem Mehmet Ali Aydınlar University, İstanbul, ATADEK 2018/2 given in Appendix D). Cellular experiments were conducted in accordance with the principles of the Helsinki Declaration and local ethical regulations

3.2.2.1 Isolation, culture and characterization of human umbilical vein endothelial cells (HUVEC)

HUVECs were isolated from umbilical cord vein by enzymatic culture method. Umbilical cords were obtained from three different donors (n=3) after birth. Tissue was transferred from hospital to laboratory in HBSS solution. The cell isolation procedure was carried out within 24 hours of the delivery of baby. Two arteries and a vein were identified, and PBS solution was passed through the vein of the tissue to remove excess blood. The vein was filled with 0.1 % collagenase solution (w/v, in PBS) by clamping the ends. Then, the tissue was transferred into 50 mL falcon tube containing PBS, and placed in water bath at 37 ^{o}C for 25-30 min. After incubation, the clamp was loosened, and the cell suspension was poured into the falcon tube. The vein was rinsed with PBS to obtain the remained cells. The cell suspension was centrifuged at 1500 rpm for 5 min and the pellet was resuspended in endothelial cell specific growth medium, EGM-2 containing EGF (5 ng/mL), bFGF (10 ng/mL), R3-IGF (20 ng/mL), VEGF (0.5 ng/mL) ascorbic acid (1µg/mL), heparin (22.5 µg/mL), hydrocortizone (0.2 µg/mL) and FCS (2%), then the cells were seeded into gelatin (1%) coated T25 flasks for 30 min at 37^{o}C. Cells were examined under light microscope every 2 days to follow their growth. When the cells reached 80-90% confluency (around day 5), cells were subcultured via trypsinization. Cells were detached from the surface with 0.05% Try-EDTA and centrifuged at 1500 rpm for 5 min. Pellet was resuspended in EGM-2 growth medium, and passaged. Cells were frozen in 10% DMSO and stored at liquid nitrogen vapor.

Identification of isolated HUVECs was conducted by determination of expression of endothelial-specific markers, CD31 and Vascular Endothelial Cadherin (VE-Cad) via immunostaining. HUVECs (P3) were seeded on gelatin coated 24 well plate as 5× 10^3 cells/well. After 3 days of culture, cells were fixed with 4% PFA for 30 min at room temperature. The fixed cells were incubated in 100 mM glycine solution (in PBS) for 15 min at room temperature to saturate PFA groups, and then washed with PBS for

3 times by 5 min intervals. Cells were permeabilized with 0.1%Triton X-100 (in PBS) (PBST) for 10 min at room temperature and washed with PBS for 3 times by 5 min intervals. Samples were incubated in 1% BSA (in PBST) for 30 min at 37 ^{o}C, and cells were incubated with primary antibodies as VE-Cad (1:100, in 0.1% BSA) and CD 31 (1:40, in 0.1% BSA) overnight at +4^{o}C. After washing with PBS, cells were incubated with secondary antibodies, Alexa Fluor 488 (1: 100) against VE-Cad and Alexa Fluor 555 (1: 200) against CD-31, at 37 ^{o}C for 1 hour. Samples were washed with PBS, and counterstained with DAPI (1:5000, in PBS) for 10 min at room temperature. Samples were rinsed with PBS and were examined with fluorescence microscope (Zeiss, Axiovert A1).

3.2.2.2 Isolation and culture of Wharton's Jelly mesenchymal stem cells (WJ MSCs)

WJ MSCs were isolated from umbilical cord matrix with explant culture. Umbilical cords were obtained from three different donors (n=3) after birth. Tissue were transferred from hospital to laboratory in HBSS solution. The cell isolation procedure was carried out within 24 hours of the delivery of baby. Tissues were washed with PBS for once to remove excess blood and to identify arteries and vein (Figure 24 a and b). Two arteries and a vein were removed from the tissue (Figure 24 b). The matrix part of tissue was sliced into small pieces which were transferred into 6 well plates. Tissues were cultured in a growth medium composed of DMEM: F12 (1:1) supplemented with 10% FBS, 100 U/mL penicilline /100 µg/mL streptomycin and 1ng/mL bFGF at 37^{o}C in a humidified CO_2 incubator. The tissues were examined under light microscope to follow cell growth on culture plate. Then tissue sections were removed, and cells were subcultured. Cells were detached with 0.05% Try-EDTA after 5 min incubation at 37^{o}C, centrifuged for 5 min at 1500 rpm, and pellet was resuspended in the growth medium. Cells were frozen in 10% DMSO, and stored in liquid nitrogen vapor.

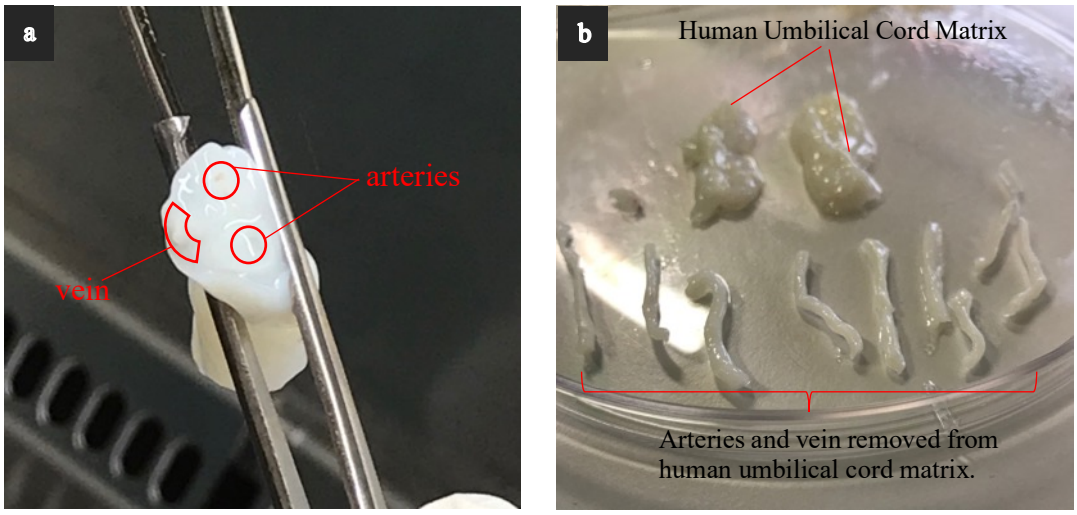

Figure 24. Isolation of WJ MSCs from human umbilical cord matrix. (a) Human umbilical cord tissue and (b) removal of the arteries and vein from the tissue matrix.

3.2.2.3 Characterization of WJ MSCs

WJ MSCs were characterized according to the standards of the Mesenchymal and Tissue Stem Cell Committee of the the International Society for cellular therapy (ISCT) by flow cytometry, determination of osteogenic differentiation capability (85). Moreover, growth kinetics of isolated WJ MSCs was determined. All experiments carried out with cells at P3 unless otherwise specified.

3.2.2.3.1 Evaluation of cell morphology

Morphology of WJ MSCs was examined under light microscope. Moreover, WJ MSCs were stained with FITC conjugated phalloidin and 4', 6-diamidino-2-phenylindole (DAPI) for cytoskeletal actin organization and nucleus, respectively. For that purpose, cells were seeded on 24 well plates and cultured in the growth medium. They were fixed with 4% PFA for 30 min at room temperature. Cells were permeabilized with 0.1% Triton X-100 for 5 min and rinsed with PBS. Samples were incubated in 1% BSA solution for 30 min at 37°C. The cells were stained with FITC-

Phalloidin (1:100, in 0.1% BSA) for 1 hour at 37°C. Then, the cells were counterstained with DAPI (1:5000, in PBS) for 10 min at room temperature. Cells were examined under fluorescence microscope (Zeiss, Axiovert A1).

3.2.2.3.2 Growth kinetics of the isolated WJ MSCs

Growth behavior and doubling time of cells were determined with cell proliferation assay, WST-1. WST-1 is a colorimetric assay based on the cleavage of tetrozolium salt WST-1 into formazan by cellular mitochondrial dehydrogenases. This bioreduction reaction occurs in viable cells. Therefore, amount of formazan production is proportional to the metabolic activity of cells. Formazan dye can be quantified by reading the absorbance at 440 nm.

WJ MSCs (P3) were trypsinized as explained in section 3.2.2.1, and then seeded on 24 well plate with a density of 5×10^3. WST-1 working solution was prepared in the growth medium of cell (20:1, medium: WST1), and 500 µL of this solution was added onto the cells. After incubation for 2 hours at 37°C in CO_2 incubator, the color product was transferred into 96 well plate as duplicate, and the absorbance was measured at 440 nm. The obtained OD value was converted into cell number using the calibration curve (Appendix A.2). Cell numbers were determined at the end of 24, 48, 72, 96, 144, 192 and 240th hours, and logarithmic cell number vs time graph was plotted. Each time point was worked as triplicate. Logarithmic cell number against time graph was used to calculate doubling time of the cells.

The doubling time of the cells was calculated by using following equation:

$$G = \frac{t}{3.3 \times \log b/B}$$

G: Generation time (doubling time)

t: time interval between beginning of the exponential phase and end of the exponential phase

log b: logarithmic cell number at the end of the beginning cell number

log B: logarithmic cell number at the beginning of the beginning cell number

3.2.2.3.3 Immunophenotype determination with flow cytometry

The expressions of cell surface antigens of isolated cells were analyzed with flow cytometry. The isolated WJ MSCs (P3) were trypsinized, and collected into 15 mL falcon tubes, and then centrifuged at 1500 rpm for 5 min. Cell pellet was resuspended in the growth medium, and the cells were transferred into tubes as 5×10^5 cells/tube in 1% BSA (in PBS). Samples were centrifuged at 1500 rpm for 5 min at 4°C, then the cells were incubated with antibodies (FITC-CD105, PerCP-CD73, PerCp-CD90, PE-CD44, FITC-CD45, PE-CD34, PerCp-HLA-DR, PE-HLA-ABC, PerCp-IgG2α, FITC-IgG1, PerCp- IgG1 and PE- IgG1) for 1 hour at +4°C. After incubation, the cells were washed with PBS twice, and fixed with 1%PFA for 10 min at room temperature. Cells were centrifuged at 1500 rpm for 5 min at +4°C, and resuspend in PBS. The cell suspension was transferred into flow tubes and analyzed with flow cytometer (BD FACS Verse).

3.2.2.3.4 Osteogenic differentiation of the isolated WJ MSCs

WJ MSCs (P3) were trypsinized and seeded into 24 well plates as 5×10^3 cells/well. Cells were incubated in the growth medium for 24 hours, and then the growth medium was replaced with osteogenic induction medium (Table 15). Cells were incubated in osteogenic induction medium for 14 or 21 days. Undifferentiated WJ MSCs cultured in the growth medium were used as control. Osteogenic differentiation was evaluated by determining specific alkaline phosphatase activity (ALP), which is characteristic for osteoblasts. In addition, von Kossa staining was done for calcium phosphate deposition which is seen in bone tissue.

Table 15. Osteogenic induction medium

Growth Medium	Osteogenic Induction Medium
DMEM: F12	DMEM Low Glucose
10% FBS	10% FBS
100 U/mL penicillin /100 µg/mL streptomycin	100 U/mL penicillin /100 µg/mL streptomycin
1ng/mL bFGF	100 nM Dexamethasone
	50 µg/mL Ascorbat 2- Phosphate
	10 mM ß-Glycerophosphate

For specific ALP activity, cells were lysed with 0.1% Triton X-100 (in 0.1 M Tris buffer, pH 9.0), and then cell lysates were transferred into eppendorf tubes. To freeze and thaw cells, the lysates were kept at -80 ^{o}C for 10 min, and then kept at 37^{o}C for 10 min. This process was repeated three times, and lysates were sonicated (Omni Ruptor 4000 sonicator) for 10 min with 30 second break intervals. The lysates were centrifuged at 5000 rpm for 10 min at +4^{o}C. Then, 50 µL of 0.1% Triton X-100 and 50 µL of supernatant were placed in 96 well plates, and 20 µL of ALP substrate was added onto it. Absorbance was determined at 405 nm for 16 min in every 2 min. Specific ALP activity was expressed as nmol of substrate converted to product/min.total protein concentration of the cell lysate. considering the calibration curve of the enzymatic product (Appendix A.5). The working solution in the absence

of cell lysate was used as a blank. Total protein concentration was determined by BCA assay (Appedix A.6).

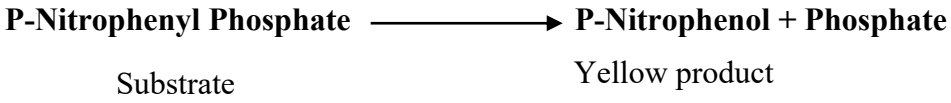

For von Kossa staining, cells were fixed with 4% PFA for 30 min at room temperature on day 14 and 21. Cells were incubated with 1% silver nitrate solution for 1 h under UV light. Unreacted silver was removed with 5% sodium thiosulfate treatment for 5 min. Cells were washed with PBS for 3 times and were examined under light microscope.

3.2.2.4 Differentiation of WJ MSCs into smooth muscle cells (SMCs)

3.2.2.4.1 Induction of WJ MSCs to differentiate into SMCs

WJ MSCs (P3) were trypsinized and seeded at density of 1×10^3 on fibronectin (50 µg/mL) coated slides. WJ MSCs were cultured in their growth medium until they reached 60-70% confluency, then the medium was replaced with induction medium (Table 17). Cells were cultured in three different induction media for 12 and 24 days. Differentiation of WJ MSCs into SMCs was evaluated with immunocytochemistry.

Table 16. Differentiation mediums for WJ MSC

Growth Medium	SMC Induction Medium 1
DMEM: F12	DMEM Low Glucose
10% FBS	2 % FBS
100 U/mL penicillin /100 µg/mL streptomycin	100 U/mL penicillin /100 µg/mL streptomycin
1 ng/mL bFGF	5 ng/mL TGF β1

SMC Induction Medium 2	SMC Induction Medium 3
DMEM Low Glucose	DMEM Low Glucose
2 % FBS	2 % FBS
100 U/mL penicillin /100 µg/mL streptomycin	100 U/mL penicillin /100 µg/mL streptomycin
300 μM Ascorbic Acid	5 ng/mL TGF β1
	300 µM Ascorbic Acid

3.2.2.4.2 Investigation of SMCs markers expression by immunocytochemistry

After 12 and 24 days of induction in different induction media, cells were fixed with 4% PFA for 30 min at room temperature. The fixed cells were incubated in 100 mM glycine (in PBS) for 15 min at room temperature to saturate PFA groups, and then washed with PBS for 3 times by 5 min intervals. Cells were permeabilized with 0.1%Triton X-100 (in PBS) (PBST) for 10 min at room temperature and washed with PBS for 3 times by 5 min intervals. Samples were incubated in 1% BSA (in PBST) for 30 min at 37 ºC, and incubated with primary antibodies, anti-human α-SMA, anti-human SMC-HC (1:50, in 0.1% BSA) overnight at +4ºC. Samples were washed with PBS, and incubated with secondary antibodies, Alexa Fluor 488 (1:100) for SMC-HC and Alexa Fluor 555 for α-SMA (1:200) at 37 ºC for 1 h. Cells were washed with the PBS, and counterstained with DAPI (1:5000, in PBS) for 10 min at room temperature. Cells were rinsed with PBS, and examined with laser scanning confocal microscope (Zeiss, LSM 700).

3.2.2.5 Evaluation of cellular behavior on the scaffolds

3.2.2.5.1 Cell seeding onto the scaffolds

To investigate the behavior of WJ MSCs and HUVEC on the scaffolds in terms of adherence, cell morphology and growth, cells were mono-cultured and co-cultured on the bilayered tubular scaffolds, composed of inner porous tubular film and circumferentially aligned fibrous mat.

The scaffolds were sterilized with 70% EtOH for 2 hours, and air dried overnight. Firstly, the outer side of the scaffold was coated with 50 µg/mL of fibronectin solution (in PBS) by incubating at 37 ºC for 2 hours, while the inner side of the tubes was coated with 1% gelatin (in PBS) by incubating at 37 ºC for 2 hours. After protein coating, scaffolds were transferred into the 24 well plates and kept at 37 ºC overnight to dry.

WJ MSCs and HUVECs were cultured in their growth media on tissue culture flasks at 37ºC in CO_2 incubator (indicated in section 3.2.2.1 and 3.2.2.2) to obtain enough cell number for seeding on scaffolds. WJ MSCs (P3) and HUVECs were trypsinized and counted. WJ MSCs were seeded onto the outer side of bilayered tubular scaffold with a density 5×10^4cells/tube. HUVECs were seeded onto the inner side of bilayered tubular scaffold with a density of 2×10^4cells/tube. Three groups of samples were prepared as bilayered scaffolds which were seeded with only WJ MSCs, only HUVECs and both WJ MSCs and HUVECs. Only HUVEC and only WJ MSC seeded groups were culture as monoculture in their own growth media. However, in co-culture group for both WJ MSCs and HUVEC the mixture of cell specific growth medium (1:1, EGM-2 containing growth factors (3.2.2.1): DMEM- F12 (1:1) supplemented with 10% FBS, 100 U/mL penicillin /100 µg/mL streptomycin and

1ng/mL bFGF) was used. In the first group, WJ MSC was mono cultured on the outer side of the scaffold (Figure 25a). The second group was the HUVEC which was monocultured in the inner side of the scaffold (Figure 25b). In the last group, WJ MSC and HUVEC were seeded together on the outer side and the inner side of the scaffold, respectively, and cells were co-cultured on the scaffolds (Figure 25c).

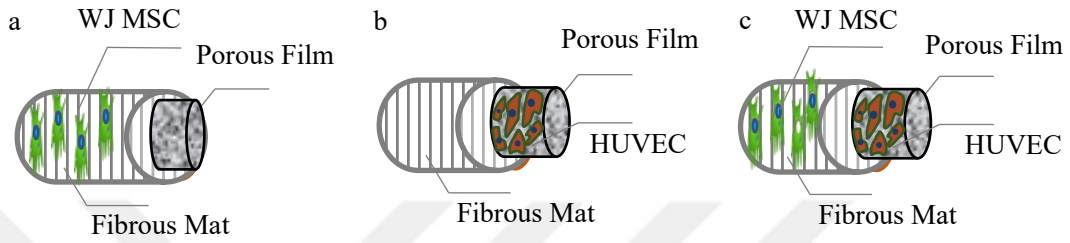

Figure 25. Illustration of experimental groups for the analysis of cell behavior on scaffolds. (a) WJ MSC mono-cultured on the outer side of the tube, (b) HUVEC mono-cultured in the inner side of the tube and (c) WJ MSC and HUVEC co-cultured on the tube.

3.2.2.5.2 Proliferation and morphology analysis of cells on the scaffold

To evaluate cell attachment and proliferation on the scaffolds, WJ MSC and HUVEC cell numbers were quantified with MTS assay at day 7, 14 and 21 after the cell seeding. The samples were studied as triplicate for each time point and for each experimental group. Moreover, cells on the scaffolds were stained with FITC-Phalloidin-DAPI and examined with laser scanning confocal microscope to investigate the distribution and organization of cells on scaffolds.

For MTS assay, 10% MTS solution was prepared in DMEM Low Glucose containing 10% FBS, 100 U/mL penicillin /100 µg/mL streptomycin and 1ng/mL bFGF for WJ MSC (WJ MSC-MTS solution), and in EGM-2 growth medium for HUVEC (HUVEC-MTS solution). For monoculture groups, 500 µL appropriate MTS solution was added onto the scaffolds depend on the cell type which was seeded on it.

For the co-culture group, WJ MSCs were incubated in 10% WJ MSC- MTS solution, while HUVECs were incubated in 10% HUVEC- MTS solution. Cells were incubated in these MTS solutions for 2 h at 37 ^{o}C. The color product (200 µL) was transferred into 96 well plates as duplicate, and the absorbance was measured at 490 nm with plate reader. Absorbance values were converted to the cell number via calibration curves (Appendix A.1, A.3 and A.4).

On 7, 14 and 21 days of culture, cells on the tubular scaffolds were fixed with 4% PFA solution and stained with FITC-Phalloidin and DAPI according to the procedure given in section 3.2.2.3.1. The distribution and organization of WJ MSCs and HUVEC on the scaffolds were examined with laser scanning confocal microscope.

3.2.2.6 Construction of the multilayered vascular substitute

WJ MSCs with a density of 7.5 $\times 10^4$ cells / tube were seeded onto the intermediate layer of the scaffold as given in detail in Section (Figure 28). WJ MSCs were cultured in their growth medium for 3 days, and then the medium was replaced with the SMC induction medium 1 which was composed of DMEM Low Glucose, 2% FBS, 100 U/mL penicillin /100 µg/mL streptomycin and 5 ng/mL TGF β1. WJ MSCs were differentiated into SMC in induction medium for 24 days. The induction medium was refreshed every 3 days. Before starting co-culture, the bilayered scaffold was wrapped with random fiber mats as the third layer. HUVECs were seeded onto the inner side of tube with a cell density of 5 $\times 10^4$ cells / tube. After 3 h of cell attachment, multilayered scaffolds were transferred into 24 well plates. HUVECs on the inner side and SMC on the intermediate layer of the multilayered tubular scaffold were co-cultured in co-culture medium (1:1, SMC Induction Medium1: EGM-2) for 4 days.

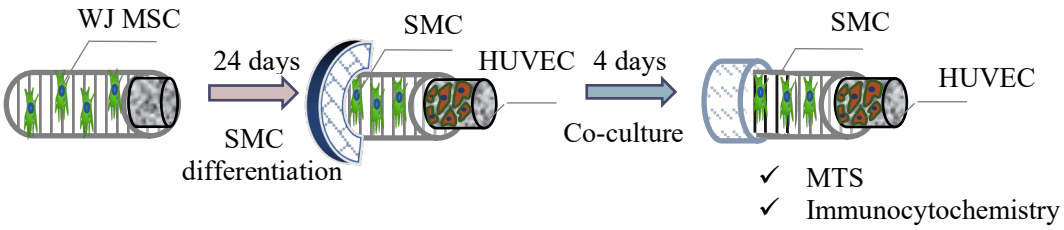

Figure 26. Illustration of experimental design to investigate behavior of WJ MSC-derived SMCs and HUVEC on the multilayered scaffold.

3.2.2.6.1 Proliferation of HUVEC and WJ MSC-derived SMCs on multilayered scaffolds

At the end of culture, cell number of co-cultured HUVEC and WJ MSC-derived SMCs on the multilayered scaffolds, WJ MSC-derived SMCs on multilayer scaffolds, and WJ MSC-derived SMCs on the bilayered scaffolds was quantified with MTS assay according to the protocol given in section 3.2.2.5.2 to evaluate the effects of steps followed during construction of multilayered blood vessel substitute under *in vitro* conditions.

3.2.2.6.2 Protein expression analysis of HUVEC and SMCs on polymeric scaffolds with immunocytochemistry

At the end of culture, cells were fixed with 4% PFA for 2 hours at room temperature. The fixed cells were incubated in 100 mM glycine (in PBS) for 15 min at room temperature to saturate PFA groups, and then washed with PBS for 3 times by 5 min intervals. Cells were permeabilized with 0.1%Triton X-100 (in PBS) (PBST) for 10 min at room temperature and washed with PBS for 3 times by 5 min intervals. Samples were incubated in 1% BSA (in PBST) for 30 min at 37 ºC. WJ MSC derived SMC incubated with primary antibodies, anti-human α-SMA, anti-human SMC-HC (1:50, in 0.1% BSA) and HUVECs were incubated with primary antibody, anti-human

CD31 (1:40, in 0.1% BSA) overnight at +4°C. Samples were washed with PBS, and incubated with secondary antibodies, Alexa Fluor 488 (1:100) for SMC-HC and Alexa Fluor 555 for α-SMC and CD31 (1:200) at 37 °C for 1 h. Cells were washed with the PBS, and counterstained with DAPI (1:5000, in PBS) for 10 min at room temperature. Cells were rinsed with PBS, and examined with laser scanning confocal microscope (Zeiss, LSM700).

3.3.3 Statistical Analysis

Statistical analysis was performed using GraphPad Prism 5.0 (GraphPad Software, San Diego, CA, USA). All experiments were carried out as triplicate unless otherwise specified. All values were averaged and expressed as means ± standard deviation (SD). Statistical differences were determined with the single-tailed or two-tailed student's t-test. $p<0.05$ were considered as statistically significant.

4. RESULTS

4.1. Characterization of the Multilayered Polymeric Scaffolds

4.1.1 Determination of appropriate solvent for the polymer blend solutions

In order to obtain suitable scaffolds in terms of biodegradation and mechanical properties according to target tissue, the polymers can be used as alone or in combination (109). The solubility of polymers can vary in different solvents, therefore an appropriate solvent in which all components are miscible should be chosen for blends. In this study, the multilayered tubular scaffold was prepared by using blends of PCL, PLGA and P(L-D,L)LA considering their degradation and mechanical properties. The blend of PCL and PLGA was used to produce the inner porous film layer, while the blend of PCL, PLGA and P(L-D,L)LA was used to fabricate the middle and outer fibrous layers. For the inner layer of the scaffold, the solution of PCL-PLGA (10%, w/v; 8:2, w:w) was prepared in chloroform (CHL) (110, 111). Both polymers were dissolved separately, and then mixed. However, when the polymers were mixed, it was observed that some polymer particles were not completely dissolved and remained on the wall of the glass bottle. In addition, the viscosity of PCL-PLGA (10%, w/v; 8:2, w:w) solution was very low for the electrospinning process, and the middle and the outer fibrous mesh layers could not be obtained. Then, it was revealed that both PCL and PLGA have high solubility in dichloromethane (DCM), and also the spinnability of PCL and PLGA in DCM is better than in CHL due to its higher evaporation time and higher conductivity (112, 113). To compare chloroform and dichloromethane in terms of solubility of polymer blends and the solution viscosity, PCL-PLGA (10%, w/v; 8:2, w:w) were prepared in both CHL and DCM, and thin films were obtained (Figure 27). Light microscopy images and macroscopic observations indicated that polymer blends were dissolved better in DCM compared to in CHL. It was observed that PCL films displayed homogenous, granular

morphology, and this granular appearance was prominent especially in the ones dissolved in CHL (Figure 27a and b). The homogeneous, granular morphology was also slightly seen in the polymer blend solution dissolved in both DCM and CHL (Figure 27c and d). The results showed that the granular morphology was due to chemical structure of PCL not due to blending of polymers. It was concluded that DCM would be used as a solvent for polymer blends in the further studies.

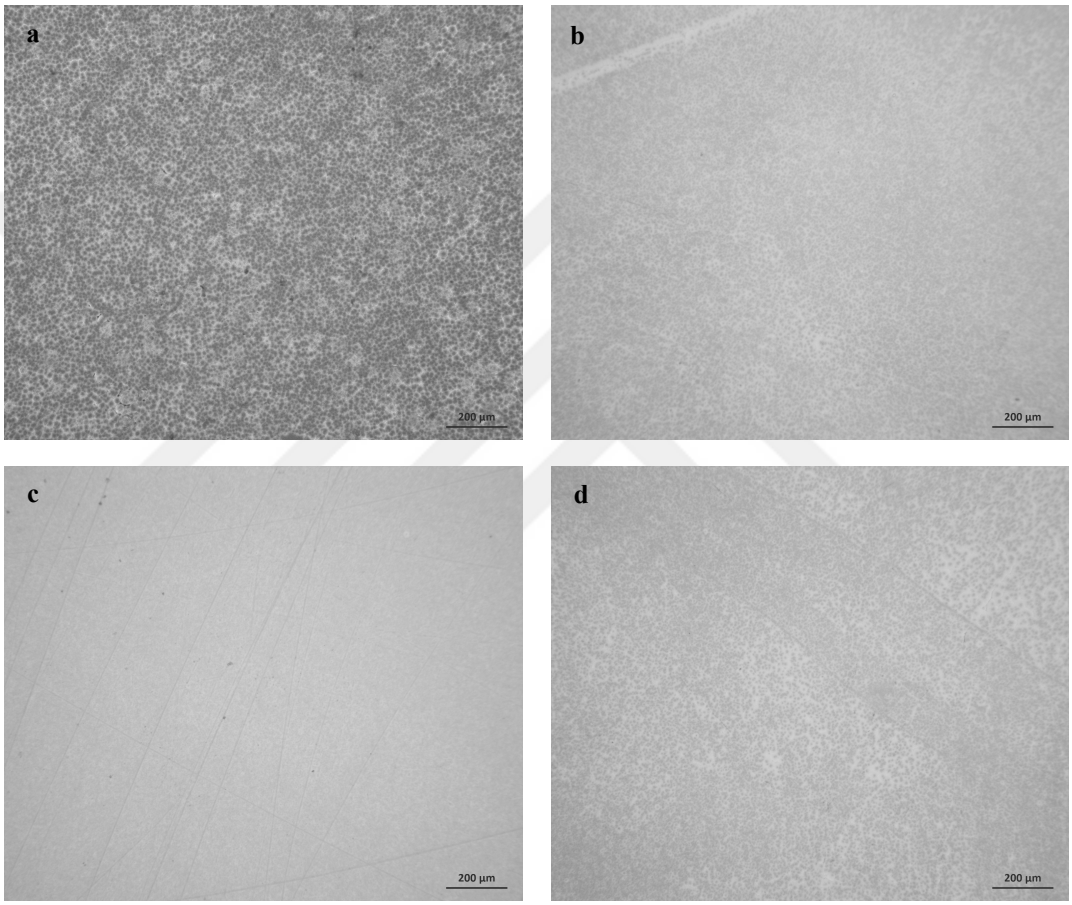

Figure 27. Light microscopy images of thin films of polymer solutions prepared in different solvents. PCL (10%, w/v) prepared in (a) CHL and in (b) DCM. PCL-PLGA (10%, w/v; 8:2, w:w) in (c) CHL and (d) DCM. Magnification: X5, scale bar: 200 µm.

4.1.2 Morphology analysis of the porous tubular films

The inner layer was planned to be porous tubular film to mimic tunica intima of the native blood vessel and obtained by dip coating and solvent casting. Tunica intima is composed of endothelium, basal lamina and subendothelial connective tissue in native muscular artery (10). Endothelial cells attach to the basal lamina via adhesion molecules (12). The porous film was designed to serve as a basal lamina for the attachment of endothelial cells like in native tissue. The porosity of the film would be optimized in a manner that to allow medium exchange while acting as barrier for cell penetration. For that purpose, in order to provide porosity polyethylene glycol (PEG) was added to PCL-PLGA polymer solution (10%, w/v; 8:2, w:w) as a porogen, and then was leached out with distilled water after solvent casting. Different concentrations of PEG as 10% and 15% were tested in terms of porosity (Figure 22). A sample prepared without PEG was used as a control to investigate the effect of PEG on porosity. It was observed that there was almost no pore structures on the tubular film prepared in the absence of PEG (Figure 28a, b). SEM results showed that the porosity was increased by increasing the concentration of PEG as expected (Figure 28). The tube prepared with 10% PEG solution displayed less than 10 μm pore size (Figure 28c, d). The pore size and interconnectivity of pores in that group could provide sufficient medium exchange through the wall of the tube. The tube obtained using 15% PEG was also exhibiting interconnectivity of pores along the tube wall, while the pore size of the tube increased to 20 μm, which was larger than the cell size (Figure 28e, f). These large pores may result in undesired cell penetration from lumen side to the intermediate layer. Therefore, the porous tubular films obtained with the use of polymer solution PCL-PLGA (8:2; w:w) containing 10% PEG (w/v) were used in the further studies. After porosity optimization, the thickness of the film was optimized by altering polymer concentration and number of dip coating cycle to provide the sufficient fluid diffusion throughout the tube wall.

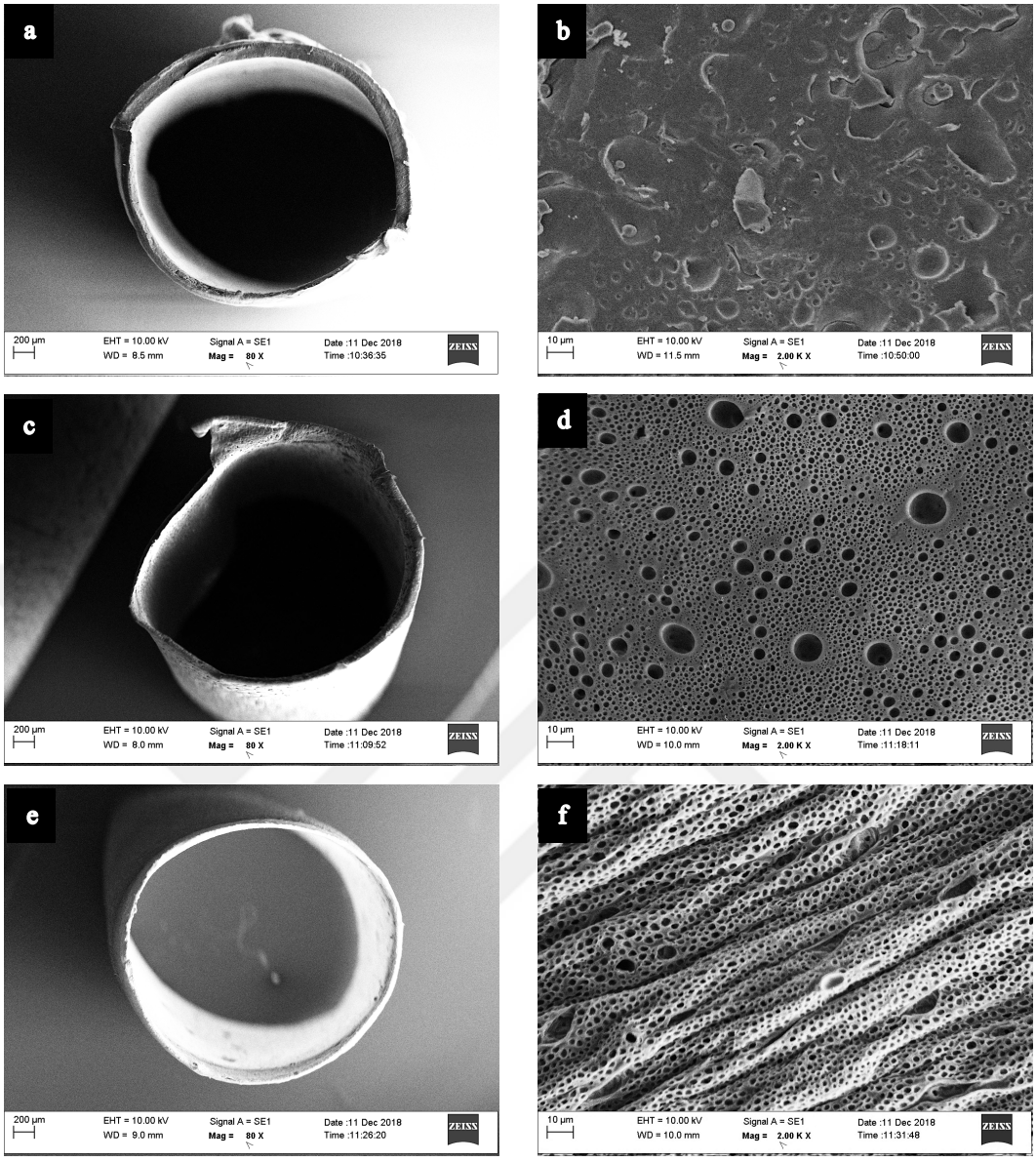

Figure 28. SEM images of cross-section and exterior surface of the porous tubular films obtained with 10% PCL-PLGA (8:2; w:w). Tubular films prepared (a, b) without PEG, (c, d) with 10% PEG, and (e, f) with 15% PEG. Magnifications: (a,c,e) X80, scale bar: 200 µm, (b,d,f) X2000; scale bar: 10 µm.

The thickness of the tube wall obtained with the solution of 10% PCL-PLGA (8:2; w:w) containing 10% PEG (w/v) by 15 times dip coating was 70 µm (Figure 28c), which would be very thick to provide sufficient fluid diffusion along the tube wall. Therefore, the thickness of the film was changed by reducing the polymer concentration from 10% PCL-PLGA (8:2; w:w) to 5% PCL-PLGA (8:2; w:w), while keeping the PEG concentration (10%, w/v) constant. In addition, the effect of the

number of dip coating cycles (10-4 times) on the film thickness was investigated (Figure 29). It was observed that the thinner films were obtained when the number of dip coating cycles was decreased. The thickness of the tube wall was determined as 46.06 ± 2.16 µm, 31.75 ± 1.29 µm, 21.61 ± 1.04 µm, when the tubes were prepared by dip coating 10, 8, 6 times, respectively (Figure 29 a,b,c). The optimum tube wall thickness was obtained by 4 times dip coating, and determined as 21.45 ± 1.07 µm to allow sufficient fluid diffusion along the tube wall.

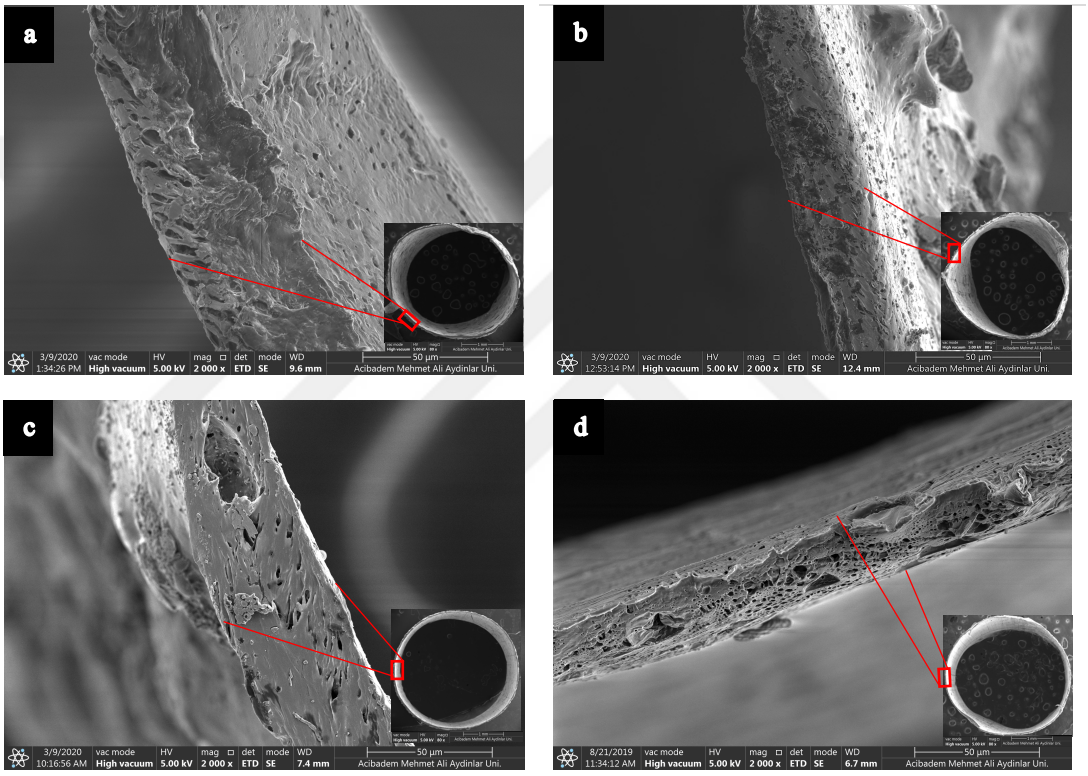

Figure 29. SEM images of wall of the porous tubular films obtained with 5% PCL-PLGA (8:2; w:w) containing 10% PEG by dip coating (a) 10 times, (b) 8 times, (c) 6 times and (d) 4 times. Inserts: cross-section views of tubular films. Magnifications: (a, b, c, d) X2000, scale bar: 50 µm, (inserts) X80, scale bar: 1 mm.

The detailed examination results of the porous tubular film fabricated by 4 times dip coating in the solution of 5% PCL-PLGA (8:2; w:w) containing 10% PEG were given in Figure 30. The lumen diameter of the tubular construct was measured as 3 mm from SEM image (Figure 30a). The wall thickness of the film was determined as 21.45 ± 1.07 µm, and the interconnectivity of the pores was seen along to tube wall

(Figure 30b). The pore size on the inner side was in the range of 1 µm to 5 µm, while it ranged from 4 to 8 µm on the outer side (Figure 30c, d).

.

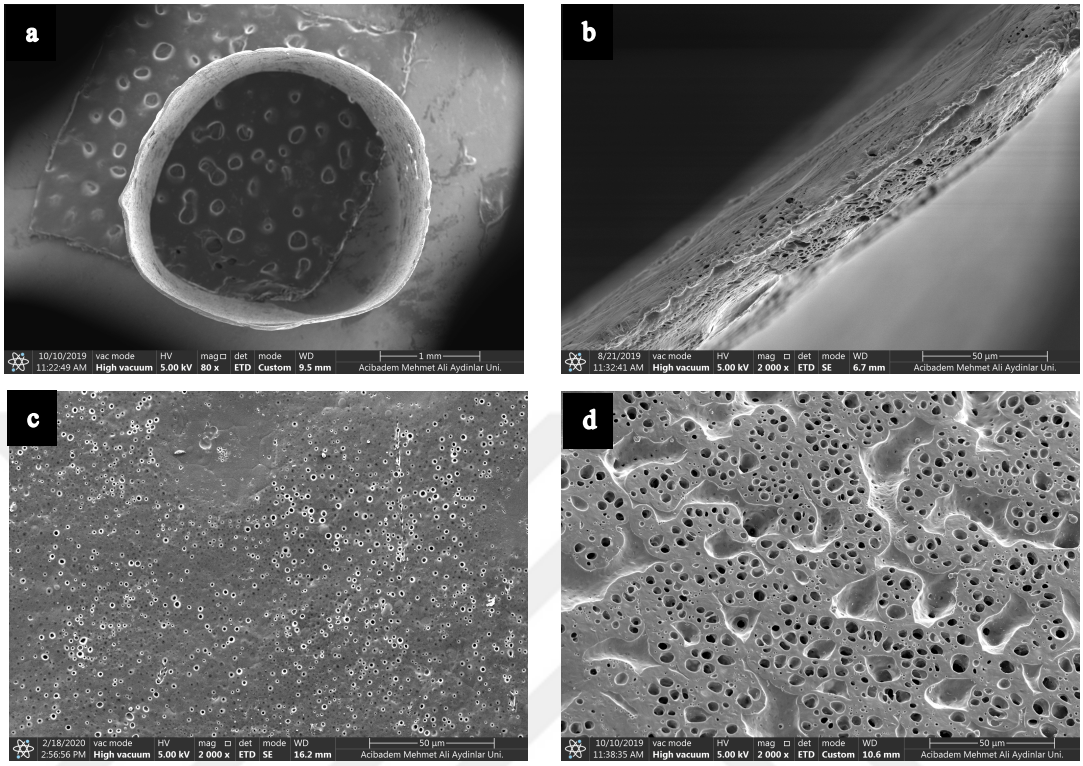

Figure 30. SEM images of the porous tubular film obtained by 4 times dip coating in the solution of 5% PCL-PLGA (8: 2; w: w) containing 10% PEG. (a) Cross-section view of the film, (b) the wall of the film, (c) the inner side and (d) the outer side of the film. Magnifications: (a) X80, scale bar: 1 mm, (b, c, d) X2000, scale bar: 50 µm.

4.1.3 Construction of the multilayered scaffolds via deposition of the electrospun fibrous mats over the porous tubular films

4.1.3.1 Morphology and topography analysis of the electrospun fibers

Tunica media of the native muscular arteries is composed of circumferentially arranged smooth muscle cells (SMCs) and connective tissue containing collagen fibers and a few elastic materials. The collagen fibers are arranged in lamellae, and the

thickness of the tunica media can be differ due to number of lamellae ranges from 25 to 35 (10, 114). It was aimed to mimic organization of tunica media by deposition of circumferentially oriented fibers over porous tubular film via electrospinning. The parameters of electrospinning such as polymer concentration, applied potential, flow rate, distance between the needle and drum collector, rotation speed of drum was optimized to obtain uniform, bead-free, aligned fibers. Firstly, the polymer blend solution 8.5% PCL-PLGA (8:2, w:w, chloroform: methanol, 5:2, v:v) was electrospun under a constant voltage 25 kV, with flow rate 40 µL/min, distance 15 cm, speed 3000 rpm, and it was observed that numerous beads were formed and the fibers were fused as a bundle (Figure 31a). Then, using the same polymer concentration and keeping the rotation speed constant, the applied potential and flow rate was reduced to 20 kV and 33 µL/min, respectively, and the distance between collector and syringe was increased to 20 cm (Figure 31b). However, the beads were still observed on the fibers. Then, DMF was added to the polymer blend solution of 8% PCL-PLGA (8:2, w:v; chloroform:DMF, 8:2, v:v) to increase conductivity, and thus to reduce the bead formation (115). In addition, the applied potential and flow rate were substantially decreased to 10 kV and 4 µL/min, respectively. In that case, very delicate, tiny fibers with numerous beads were formed (Figure 31c). The polymer concentration was increase to 10% PCL-PLGA (8:2, w:w; chloroform:DMF, 8:2, v:v) to obtain more viscous polymer solution, but it lead to larger beads and increased the fusion of fibers (Figure 31d). Various processing conditions were tested with different polymer solutions using different solvent ratios as indicated in Table 14; however, uniform, bead-free electrospun fibers could not be obtained when the polymers dissolved in chloroform (data were not given).

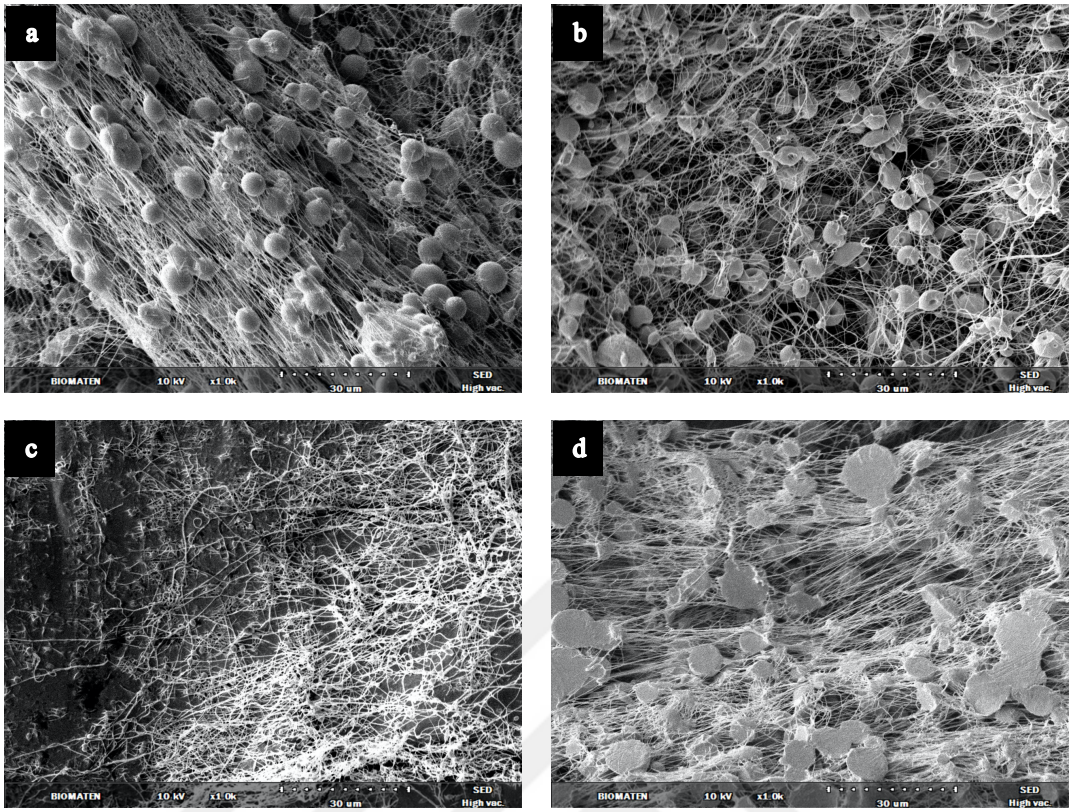

Figure 31. SEM images of electrospun fibrous mat obtained during electrospinning optimization. The polymer blend solution of 8.5% PCL-PLGA (8:2, w:w; CHL: methanol, 5:2, v:v) was electrospun with (a) 25 kV, 40 µL/min, 15 cm, 3000 rpm, (b) 20 kV, 33 µL/min, 20 cm, 3000 rpm, (c) 8% PCL-PLGA (8:2, w:w; CHL: DMF, 8:2, v:v) with 10 kV, 4 µL/min, 20 cm, 3000 rpm, (d) 10% PCL-PLGA (8:2, w:w; CHL: DMF, 8:2, v:v) with 25 kV, 40 µL/min, 12 cm, 3000 rpm. Magnifications: X1000; scale bar: 30 µm. (applied potential, kV; flow rate, µL/min; distance between needle and collector, cm; rotation speed of drum, rpm).

The main solvent of the polymer blend was replaced as dichloromethane, after showing that both PCL and PLGA were soluble in DCM in section 4.1.1, and also DCM was preferred especially because of its spinnability since it has higher conductivity than CHL (115, 116). When the electrospinning was carried out using 10% PCL-PLGA solution dissolved in DCM (8:2, w:w; DCM:DMF, 8:2, v:v) by applying 10 kV voltage, with distance 20 cm, flow rate 5 µL/min, rotation speed 2000 rpm, more uniform fibers were obtained compared to the fibers obtained with the same polymer blend solution dissolved in chloroform (Figure 32). Even though the morphology of fibers gets better, beads were still observed on the fibers.

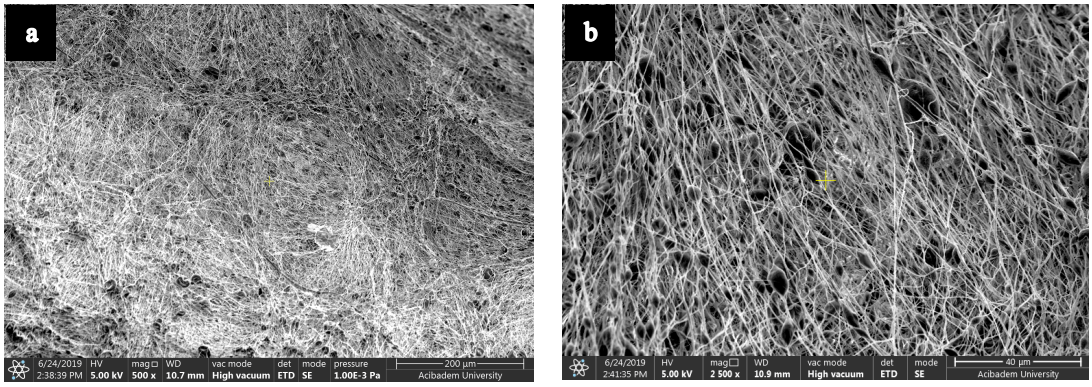

Figure 32. SEM image of electrospun fibrous mat of 10% PCL-PLGA (8:2, w:w; DCM:DMF, 8:2, v:v) under voltage 10 kV, flow rate 5 µL/min, distance 20 cm, speed 2000 rpm. Magnification (a) X500, scale bar: 200 µm, (b) X2500, scale bar: 40 µm.

Solution viscosity is one of the main factor that affects the electrospinning process and bead formation. The higher viscosity may help to produce bead-free fibers. In addition, as the viscosity of the polymer solution is increased, the shape of the beads changes from spherical to spindle-like form (117). Therefore, P(L-D, L)LA was added to the polymer blend solution to increase the viscosity of the spinning solution in order to obtain uniform, bead-free fibers. A solution of 15% PCL-P(L-D,L)LA-PLGA (6:2:2, w:w:w; DCM:DMF, 19:1, v:v) was electrospun under processing conditions; applied voltage 15 kV, flow rate 20 µL/min, distance 25 cm (Figure 33). The alignment of fibers tried to be improved by altering the rotating speed of drum from 500 rpm to 3000 rpm. It was observed that the addition of P(L-D,L)LA enhanced the formation of more uniform fibers but the fibers still had beads (Figure 33 a-d). However, it was revealed that by increasing the rotation speed of drum the shape of the beads was changed from spherical to spindle-like form, and the average distance between beads was increased which was a good sign for the full fiber formation. On the other hand, the alteration of rotation speed did not enhance the alignment of fibers.

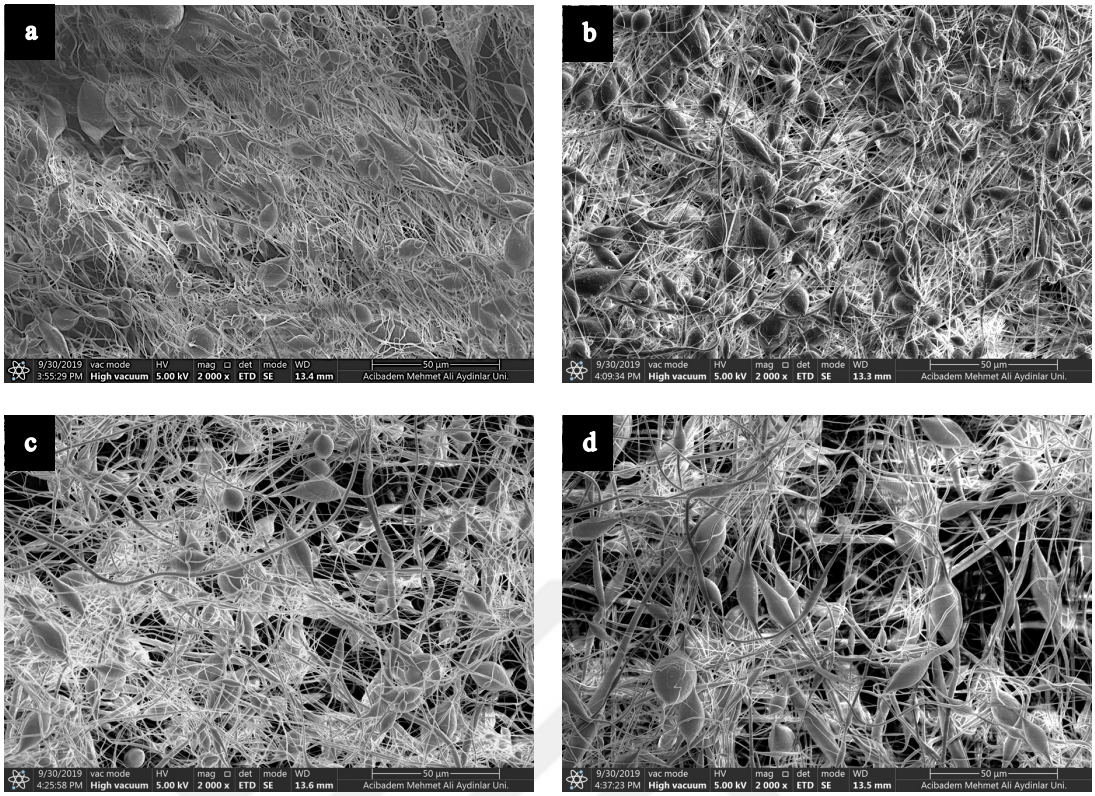

Figure 33. SEM images of an electrospun fibrous mat obtained during electrospinning optimization. The polymer blend solution of 15% PCL- P(L-D,L)LA -PLGA (6:2:2, w:w:w; DCM: DMF, 19:1, v:v) was electrospun under voltage 15 kV, with flow rate 20 µL/min, distance 25 cm and rotation speed of drum (a) 500 rpm, (b) 1500 rpm, (c) 2000 rpm and (d) 3000 rpm. Magnifications: X2000; 50 µm.

In order to obtain appropriate viscosity to prevent bead formation, the polymer blend solution of 5% PCL-P(L-D,L)LA-PLGA (4:4:2, w:w:w, DCM:DMF, 19:1, v:v) was electrospun by applying 15 kV voltage, with 20 µL/min flow rate, 25 cm distance and 3000 rpm drum rotation speed. A tubular electrospun fibrous mat was obtained with 3 mm lumen diameter and 120 µm wall thickness (Figure 34a and b). The obtained fibrous mat had no beads both on the inner and the outer surfaces. It was determined that the fiber diameter ranged from 1 µm to 1.5 µm (Figure 34c and d). The uniform, bead-free fibers were obtained successfully using this polymer blend composition and concentration. However, since the fibers did not exhibit alignment, processing parameters would be adjusted to improve fiber alignment. The speed of the drum collector has to be high enough to stretch polymer before being deposited on the collector so that aligned fiber can be formed on the mandrel (115). However, in our spinning set up, even if the drum was rotated at the maximum speed as 3000 rpm,

fibers were slightly aligned (Figure 35 a and b). In order to enhance the fiber alignment, the flow rate was reduced, considering that more time was given to polymer for stretching before deposited on the collector. It was observed that the fiber alignment was significantly improved when the flow rate of polymer solution was reduced from 20 µL/min to 15 µL/min (Figure 35 b and d). However, this improvement in fiber alignment was not observed when the flow rate was reduced to 10 µL/min or 5 µL/min (Figure 35f and h). In fact, the fiber alignment was worsened compared to 15 µL/min (Figure 35 d,f,h).

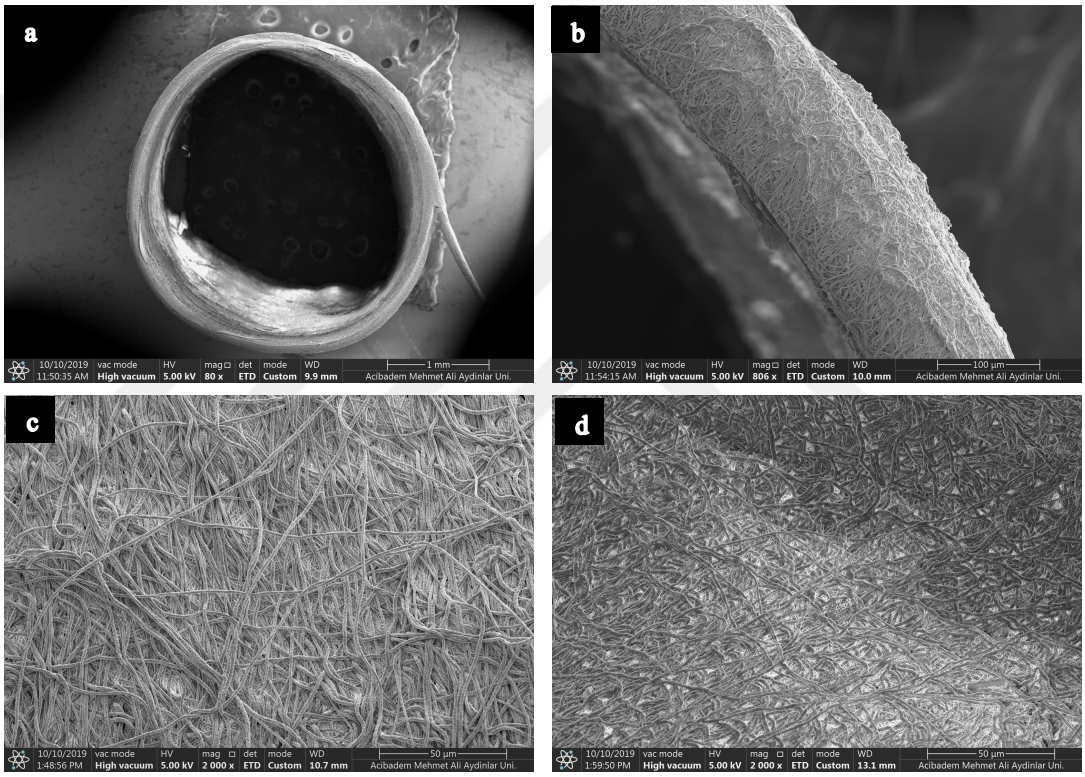

Figure 34. SEM images of electrospun mat prepared with 5% PCL-P(L-D,L)LA-PLGA (4:4:2, w:w:w; DCM:DMF, 19:1, v:v) under processing conditions: voltage 15 kV, flow rate 20 µL/min, distance 25 cm, rotation speed of drum 3000 rpm parameters. (a) Cross-section view, (b) tube wall, (c) the outer side of the tube and (d) the inner side of the tube. Magnifications: (a) X80, scale bar: 1 mm, (b) X800, scale bar: 100 µm, (c, d) X2000; scale bar: 50 µm.

.

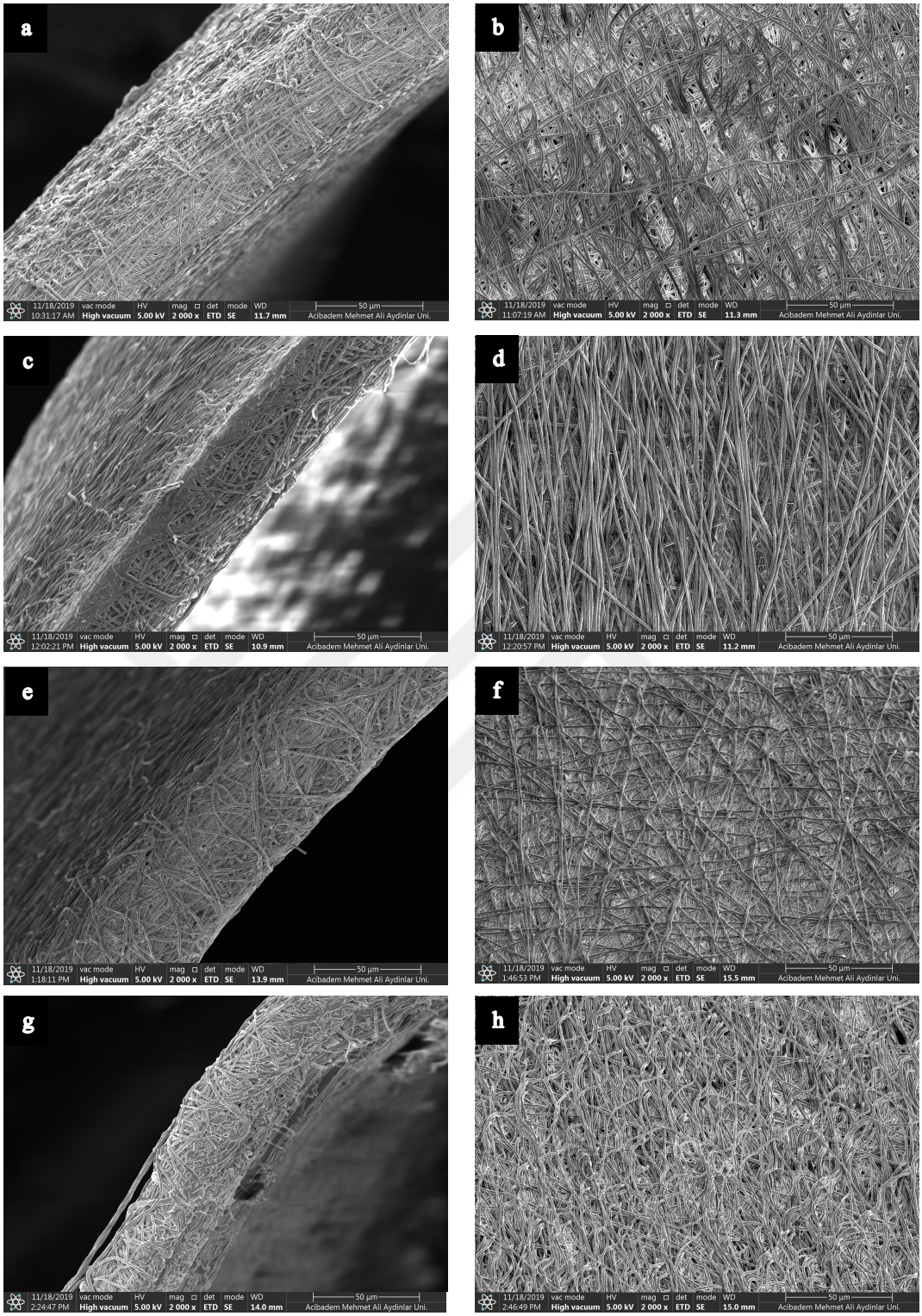

Figure 35. SEM images of an electrospun mat prepared with 5% PCL-P(L-D,L)LA-PLGA (4:4:2, w:w:w; DCM:DMF, 19:1, v:v) under processing conditions: voltage: 15 kV, distance 25 cm, rotation speed of drum 3000 rpm and flow rate (a, b) 20µL/min, (c, d) 15 µL/min, (e, f) 10 µL/min and (g, h) 5 µL/min. Magnifications: (a, c, e, g) images from wall of the tube, X2000; scale bar: 50 µm and (b, d, f, g, h) images from the outer side of the tubeX5000; scale bar: 50 µm.

The multilayered tubular scaffold was constructed by the following steps in this order: 1) fabrication of porous tubular film as the innermost layer; 2) deposition of circumferentially aligned electrospun fibers over porous film as the intermediate layer; and 3) deposition of random electrospun fibers over aligned fibers as the outermost layer (Figure 36). The porous tubular film was obtained by dip coating 4 times using 5% PCL-PLGA (8:2; w:w) containing 10% PEG solution (Figure 36a, b, c). The circumferentially aligned mat was deposited over the porous tubular film using 5% PCL-P(L-D,L)LA-PLGA (4:4:2, w:w:w, DCM:DMF, 19:1, v:v) under the optimized processing conditions: applied potential 15 kV, flow rate 15 µL/min, distance 25 cm and rotation speed of drum 3000 rpm (Figure 36a, b, e). The lumen diameter of the multilayered scaffold was measured as 3 mm and the thickness of the middle layer was determined as 57.07± 4.39 (Figure 36a and b).

The tunica adventitia, composed of loose connective tissue, is the outermost layer of the native muscular artery (10). The extracellular matrix of the tunica adventitia mainly composed of collagen fibers. The collagen fibers in the adventitia layer not only give stability to the blood vessel but also provide nourishment and oxygen to the smooth muscle cells. The thickness of the tunica adventitia can be varied depending on the type and location of the artery (2, 10). The external layer of the scaffold was fabricated as random fibrous mat to give support to the scaffold (Figure 36a, b, d). The same polymer blend solution 5% PCL-P(L-D,L)LA-PLGA (4:4:2, w:w:w, DCM:DMF, 19:1, v:v) was used to obtain random fibrous mat by electrospinning under the same processing conditions as the ones used in fabrication of middle layer of the scaffold except the rotation speed of drum. In order to obtain random fibers, the rotation speed of drum was reduced to 500 rpm, and thus the random electrospun mat was successfully deposited over aligned electrospun mat (Figure 36a, b, d). The thickness of the outermost layer, random fibrous mat was measured as 67.32 ± 0.89 µm (Figure 36b).

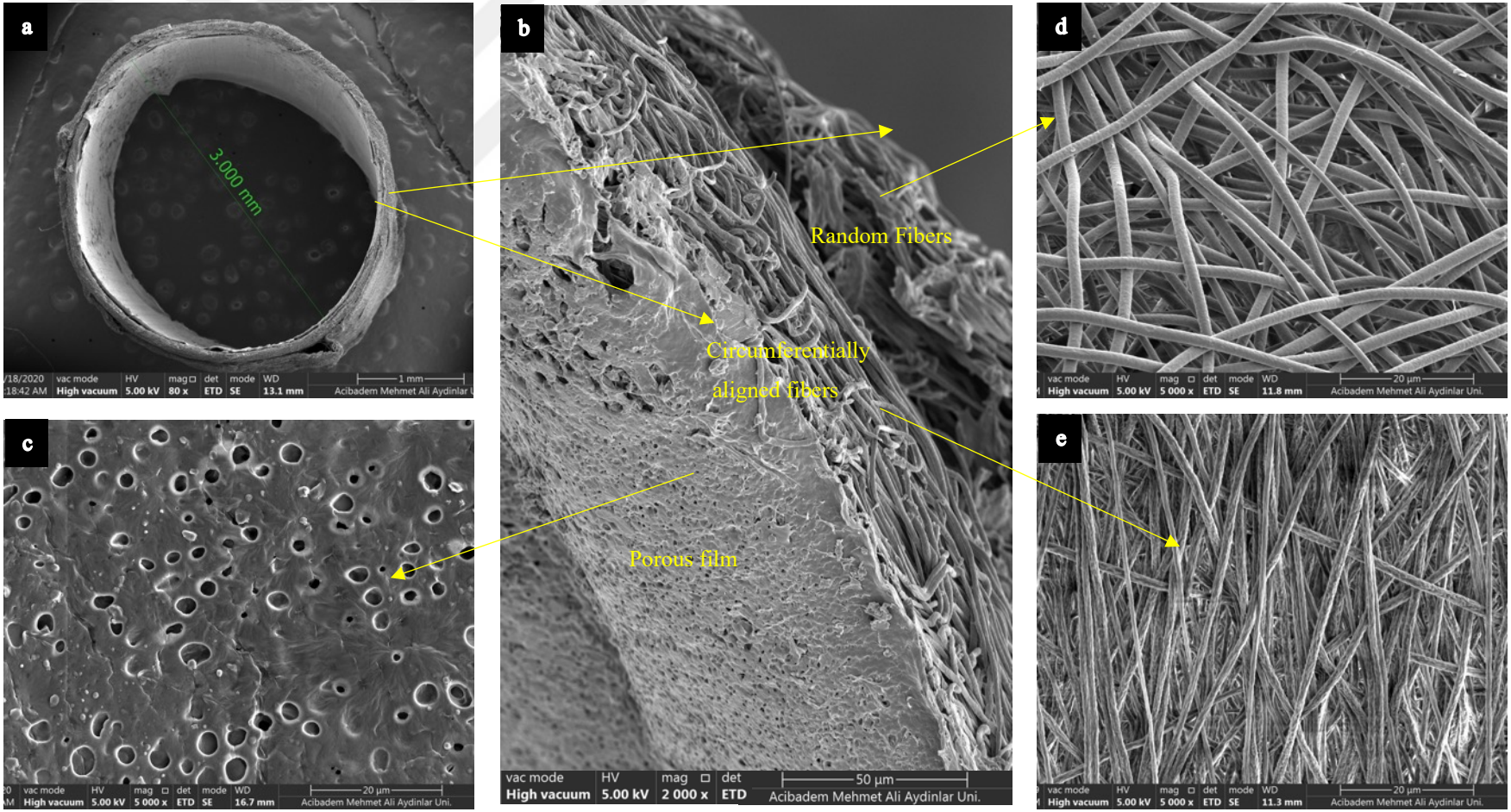

Figure 36. SEM images of the multilayered vascular scaffold. (a) Cross-section view of the tubular scaffold, (b) tube wall, (c) inner porous tubular film side, (d) outer random fibrous mat side, (e) intermediate circumferentially aligned fibrous mat side of the scaffold. Magnifications: (a) X80, (b) X2000 and (c, d, e) X5000.

4.1.3.2 Analysis of fiber diameter and orientation

Extracellular matrix is composed of three-dimensional organization of proteins such as collagen, elastin, laminin which are found mostly in the fibrous form (118). Each tissue has a specific fibrous protein network that gives tissue distinctive shape and this network gets involved in many cellular processes such as cell organization, communication, proliferation and differentiation. In this study, to mimic tunica media and tunica adventitia of native muscular artery, the intermediate and the outer layers of the scaffold were fabricated as circumferentially aligned fibrous mat and random fibrous mat, respectively (Figure 36). The fiber diameter and fiber orientation were quantified with Fibro Quant 1.3 image processing and analysis software (Figure 37 and 38). Although the fiber diameter in the intermediate layer, circumferentially aligned fibrous mat, ranged from 100 nm to 1400 nm, it was observed that 33.4 ± 6.9% of the fibers had a fiber diameter of 200-300 nm (Figure 37a). The fiber angle distribution graph indicated that most of the fibers were aligned in a parallel manner with a 15° angle deviation (Figure 37b). This extent of deviation can be acceptable, to revealed that the obtained electrospun mat displays a good fiber alignment by exhibiting orientation. Fiber diameter in the outermost layer, random fibrous mat, was measured between 100 nm and 1500 nm, and it was determined that 22.06 % of the fibers were found in the 800-900 nm diameter range (Figure 38a). It was observed that in the random fibrous mat, most of the fibers deviated with different angles (Figure 38b). Although the same polymer solution was used in the electrospinning of the intermediate and outer layer, the difference in fiber diameter distribution is due to the fact that the fibers were obtained with different collectors and at different rotation speeds (Figure 37a and 38a). SEM and orientation analysis results indicated that, as planned for the multilayered scaffold, the fibers in the intermediate layer were circumferentially aligned, while the fibers in the outer layer were randomly organized.

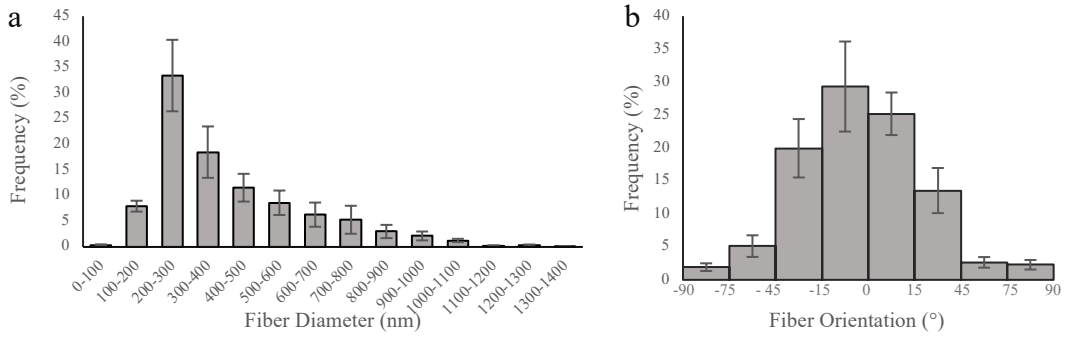

Figure 37. The distribution of (a) fiber diameter and (b) fiber orientation deviation angle of the aligned fibrous mats.

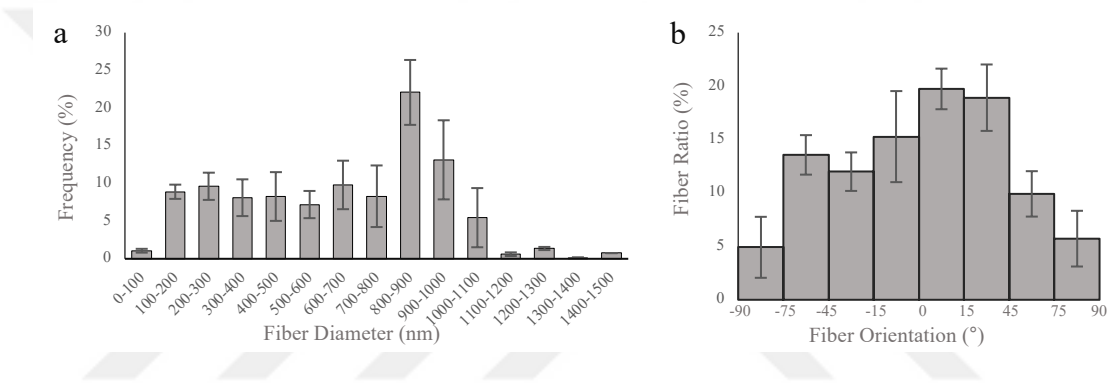

Figure 38. The distribution of (a) fiber diameter and (b) fiber orientation deviation angle of the random fibrous mats.

4.1.4 Mechanical analysis

The blood vessels face with complex mechanical stress environment (Figure 7), therefore the mechanical properties of the vascular substitute should be at least equal to the saphenous vein, which is mostly used autograft in bypass (Table 2).

For tensile testing, a gradually increasing stress condition is applied to the materials until the sample is broken. Strain (ε) is the "length change per unit length" and it is directly proportional to applied stress (σ). The relationship between the stress and the strain is expressed with a stress-strain graph (Figure 39). The initial phase of

plot is the elastic region where the deformation in the material can be reversible. After this region, the applied stress causes permanent deformation in material and this part is called plastic region for viscoelastic materials. The slope of the stress-strain curve in elastic region is called as Young`s modulus (E) and gives information about the stiffness of material. Yield stress is the transition point where the elastic region ends, and plastic region starts. Ultimate tensile strength is the highest stress that a material can withstand. Elongation at break is defined by the ratio between increased length and initial length after breakage of a material.

In this study, two different polymer solution was used to fabricate multilayered vascular scaffold. The inner layer, porous tubular film, was obtained from 5% PCL-PLGA (8:2; w:w) containing 10% PEG solution which was leached out to obtain porosity. The non-porous polymeric film prepared in the absence of PEG was also tested as a control to investigate the effect of porosity on the mechanical properties. The results indicated that the Young's Modulus, stiffness, of non-porous film was 8 fold higher than the saphenous vein, and 12 fold higher than the porous film (Table 17). The Young's Modulus of the porous film was very close to the value of the internal mammary artery and it was slightly lower than the value of the saphenous vein.

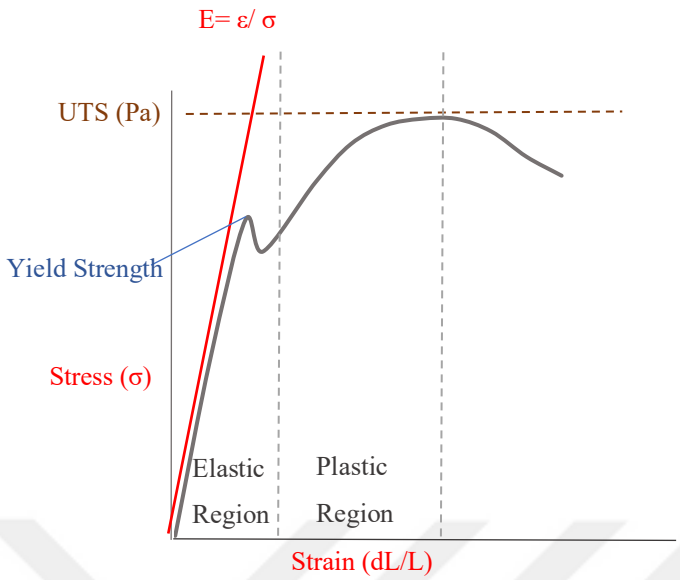

Figure 39. Representative stress-strain curve.

Table 17. Tensile strength of the native blood vessels and the obtained PCL-PLGA films.

Blood Vessels Young`s Modulus (MPa)		Polymeric Films Young`s Modulus (MPa)	
Saphenous Vein	Internal Mammary Artery	Non-porous Film	Porous Film
23.7	16.8	205.3 ± 22.3	16.1 ± 1.1

4.1.5 Permeability test

In order to investigate the diffusion ability of medium, the permeability of the inner layer porous tubular film, the least porous layer, was evaluated (119). It was shown that the non-porous film (prepared in the absence of PEG) could not allow media diffusion along its wall, while the porous film (prepared with 10% PEG) was permeable for media along its wall (Figure 40). The results implied that porous tubular film would provide sufficient diffusion of media to intermediate layer along the tube wall for the cell nourishment and gas exchange.

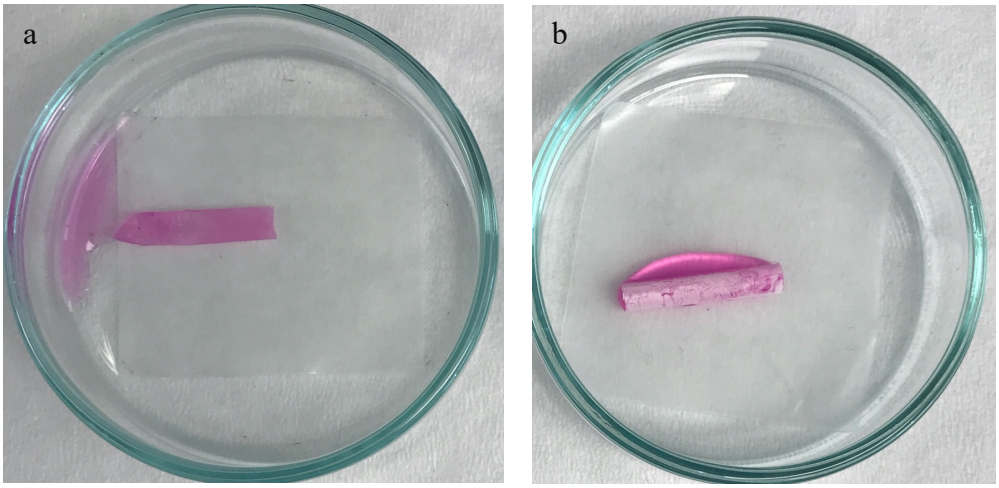

Figure 40. Images of (a) 5% PCL-PLGA (8:2, w:w, without PEG) non-porous tubular film and (b) 5% PCL-PLGA (8:2, w:w, with 10% PEG) porous tubular film.

4.2 *In Vitro* Studies

4.2.1 Isolation, culture and characterization of human umbilical vein endothelial cells (HUVEC)

All type of the blood vessels are lined with epithelium called endothelium. The endothelium exhibits highly characteristic appearance, single layer of continuously elongated, polygonal endothelial cells and it is known as the cobblestone morphology. These cells are arranged in the direction of blood flow. Endothelial cells are very crucial for native tissue since they maintain homeostasis, act as a non-thrombogenic membrane between underlying tissue and blood to prevent thrombus formation, and regulate the immune response (2). Therefore, supporting vascular scaffolds with endothelial cells may help to prevent intimal hyperplasia and thrombosis which are challenges in vascular tissue engineering (3, 120). Endothelial cells can be isolated from different sources such as patients' blood vessels, adult progenitor cells in circulation, and umbilical cord(8, 121). In this study, human endothelial cells were enzymatically isolated from umbilical cord vein. It was observed that the isolated

HUVECs were attached to the culture plate one day after isolation (Figure 41a, b). The cells exhibited clusters-like, cobblestone appearance which is characteristic for endothelial cells. It was observed that the cells proliferated in their growth medium within 3 days, and they reached 70%-80% confluency after 5 days of culture following isolation (Figure 41c-f).

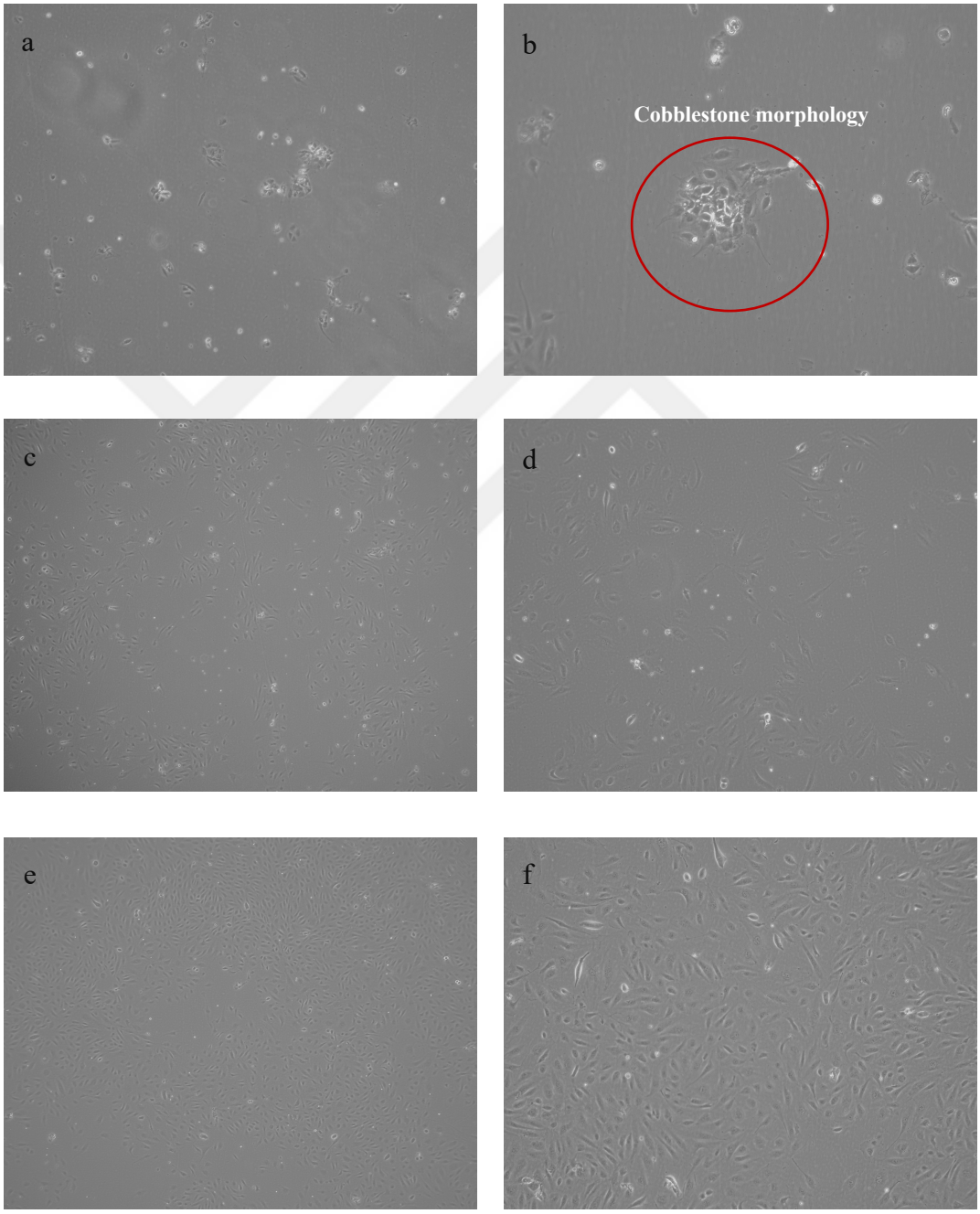

Figure 41. Light microscope images of HUVECs isolated from umbilical cord vein. Cells cultured on gelatin coated TCPS on (a,b) Day 1, (c,d) Day 4, (e,f) Day 5. Magnifications: (a,c,e) X5 and (b,d,e) X10

Since the cells were obtained enzymatically from heterogeneous tissue, the isolated HUVECs were identified by immunocytochemistry staining with endothelial-specific markers such as platelet endothelial cell adhesion molecule (PECAM-1) and vascular endothelial cadherin (VE-Cad). PECAM-1, also known as CD31, is a specialized cell adhesion molecule located in the intercellular contact. VE-Cad is the cell-type-specific adhesion molecule, located on the transmembrane of endothelial cell, helps to maintain cell specific function, and also is required for the cell-to-cell identification (11). Immunocytochemistry results showed that the isolated HUVECs expressed CD31 and VE-Cad on the cell membrane at cell-to-cell contact region along cell borders. All of the cells expressed both CD-31 and VE-Cad (Figure 21a, b) Immunohistochemistry results indicated that HUVECs were successfully isolated and culture in the selective medium.

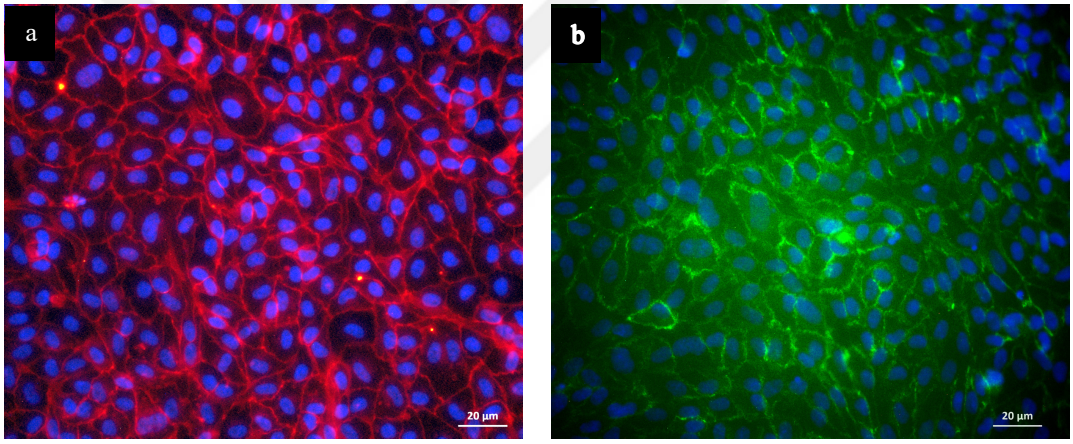

Figure 42. Immunofluorescence analysis for the expression of (a) CD31 and (b) VE-Cad of HUVECs on TCPS. HUVECs were immunostained with antibodies against CD31(red) and VE-Cad (green), and counterstained with DAPI for nucleus (blue). Magnification:X40; scale bar: 20 µm.

4.2.2 Isolation and culture of Wharton's Jelly mesenchymal stem cells (WJ MSCs)

Mesenchymal stem cells (MSCs) are commonly used in tissue engineering due to their self-renewal and differentiation capacity. These cells can be obtained from various sources such as bone marrow, adipose tissue, dental pulp, umbilical cord matrix, etc. (35). They exhibit highly desired properties in the aspect of regenerative medicine and tissue engineering, such as high proliferation rate, differentiation into cell types of target tissues, paracrine effect by secretion of various trophic factors (35). In this vascular tissue engineering study, Wharton's Jelly mesenchymal stem cells (WJ MSCs) were used as a cell source to be differentiated into smooth muscle cells. WJ MSCs were isolated from umbilical cord matrix by an explant culture method as the details given in section 3.2.2.2. Firstly, tissue pieces of umbilical cord matrix were placed into culture plates (Figure 43a, b). It was observed that the cells started to migrate from tissue to culture plate within 7-9 days (Figure 43c, d). After 15 days of culture, WJ MSCs reached confluency on culture plate which showed that the isolated cells were proliferated, and increased in number (Figure 43e, f). It was shown that the isolated cells met one of the required criteria, the adherence to plastic, to be considered a population of MSC. The isolated WJ MSCs exhibited spindle-like shaped fibroblast morphology in the primary culture which is the characteristic feature of the MSCs (Figure 43d) (122). The images of Phalloidin- DAPI staining showed that the isolated WJ MSCs expanded with their organized cytoskeleton (Figure 44a, b).

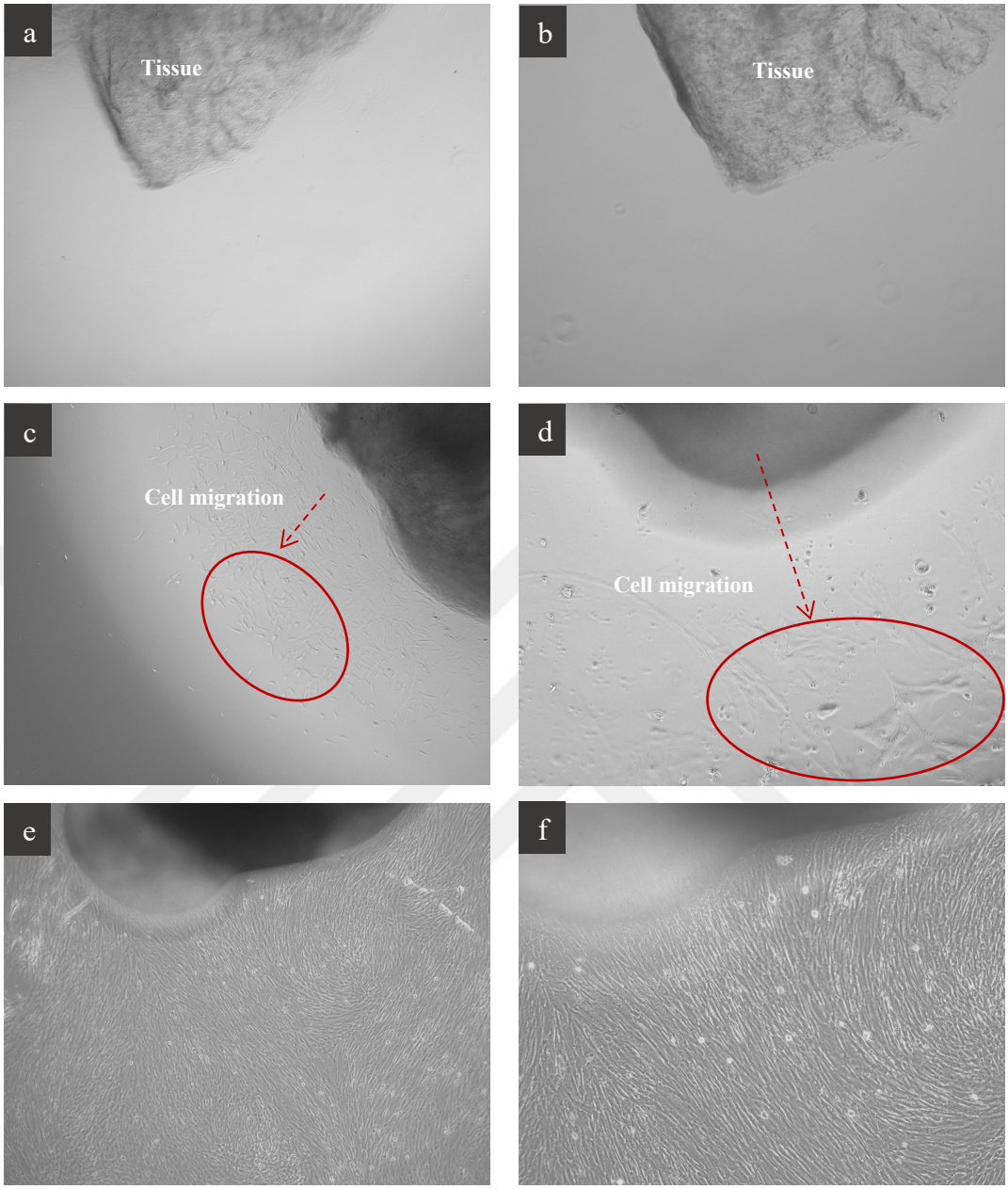

Figure 43. Light microscope images of WJ MSCs isolated from umbilical cord matrix after culture of (a,b) Day 5, (c,d) Day 9, (e,f) Day 15. The dashed arrows show the migration of cells from the tissue to TCPS. Magnifications: (a, c, e) X5 and (b, d, f) X10.

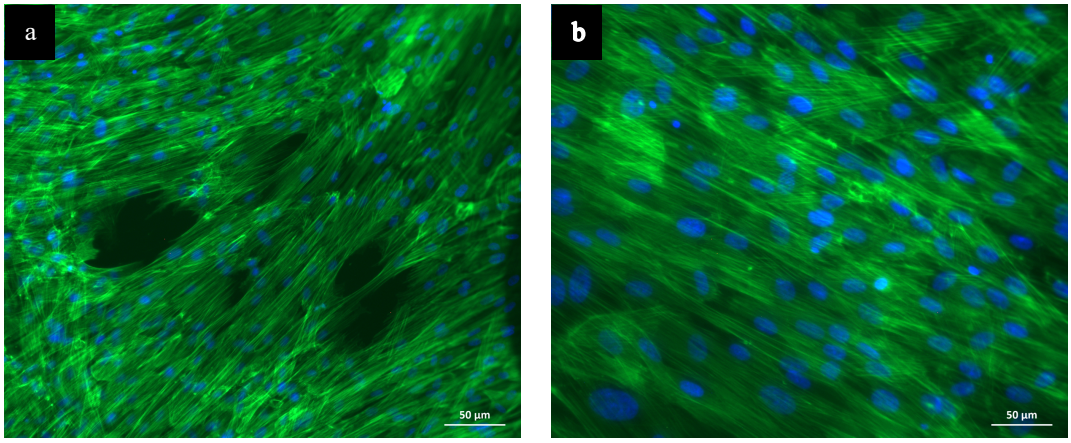

Figure 44. Fluorescence micrographs of Phalloidin-FITC (green) and DAPI (blue) stained WJ MSC on TCPS. Magnification: X20, scale bar: 50 µm.

4.2.3 Characterization of WJ MSCs

4.2.3.1 Growth kinetics of the isolated WJ MSCs

The growth profile of WJ MSCs should be analyzed to determine the doubling time of the isolated cells. The doubling time can be referred as the amount of the time required to double in number of cells. In this study, the growth profile of the isolated WJ MSCs was obtained by plotting the logarithmic number of cells with respect to time (h) (Figure 45). The cell number was determined by WST-1 using calibration curve (Appendix A.1). The doubling time of the cells was calculated from log phase (exponential part) of graph as 22.3 hours.

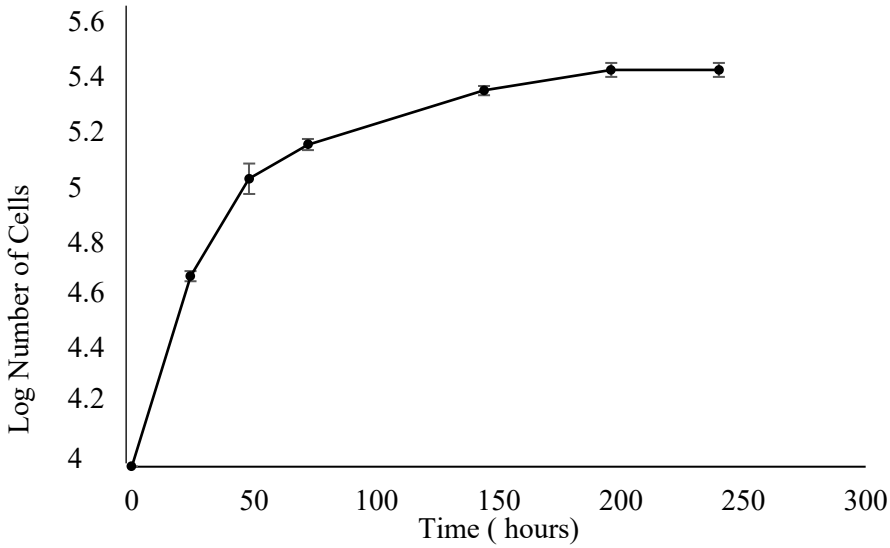

Figure 45. Growth profile of WJ MSCs (doubling time: 22.3 hours).

4.2.3.2 Immunophenotype determination with flow cytometry

WJ MSCs would be characterized to confirm that the isolated cells are mesenchymal stem cells according to the standards of the Mesenchymal and Tissue Stem Cell Committee of the International Society for cellular therapy (ISCT) (85, 123, 124). Besides the cell adherence to plastic, the other criterion to define MSCs is the demonstration of expression of specific surface antigens. For that purpose, the expression of specific surface antigens of isolated WJ MSCs (P3) was analyzed by flow cytometry. Considering the intersection of immunoglobulin isotype control and the sample, the absolute positive cell percentage was calculated (Figure 46). The surface antigen expressions of the isolated WJ MSCs were given in Table 18. MSCs should have positive expression of $CD105^+$, $CD73^+$, $CD44^+$, $CD90^+$ and HLA-ABC^+, and negative expression of $CD34^-$, $CD45^-$ and HLA-DR^- (123). As it is supposed to be, the isolated WJ MSCs were strongly positive for MSC markers $CD105^+$, $CD73^+$, $CD90^+$, $CD44^+$, and also for HLA-ABC, which means that ≥ 95% of the isolated MSCs express these markers (Figure 46 and Table 18). In addition, the isolated MSCs were negative for the expression of hematopoietic markers $CD45^-$, $CD34^-$ and also HLA-

DR^{-} (Figure 46 and Table 18). These results indicated that the isolated WJ MSCs exhibited the characteristic surface antigen expression of MSCs.

.

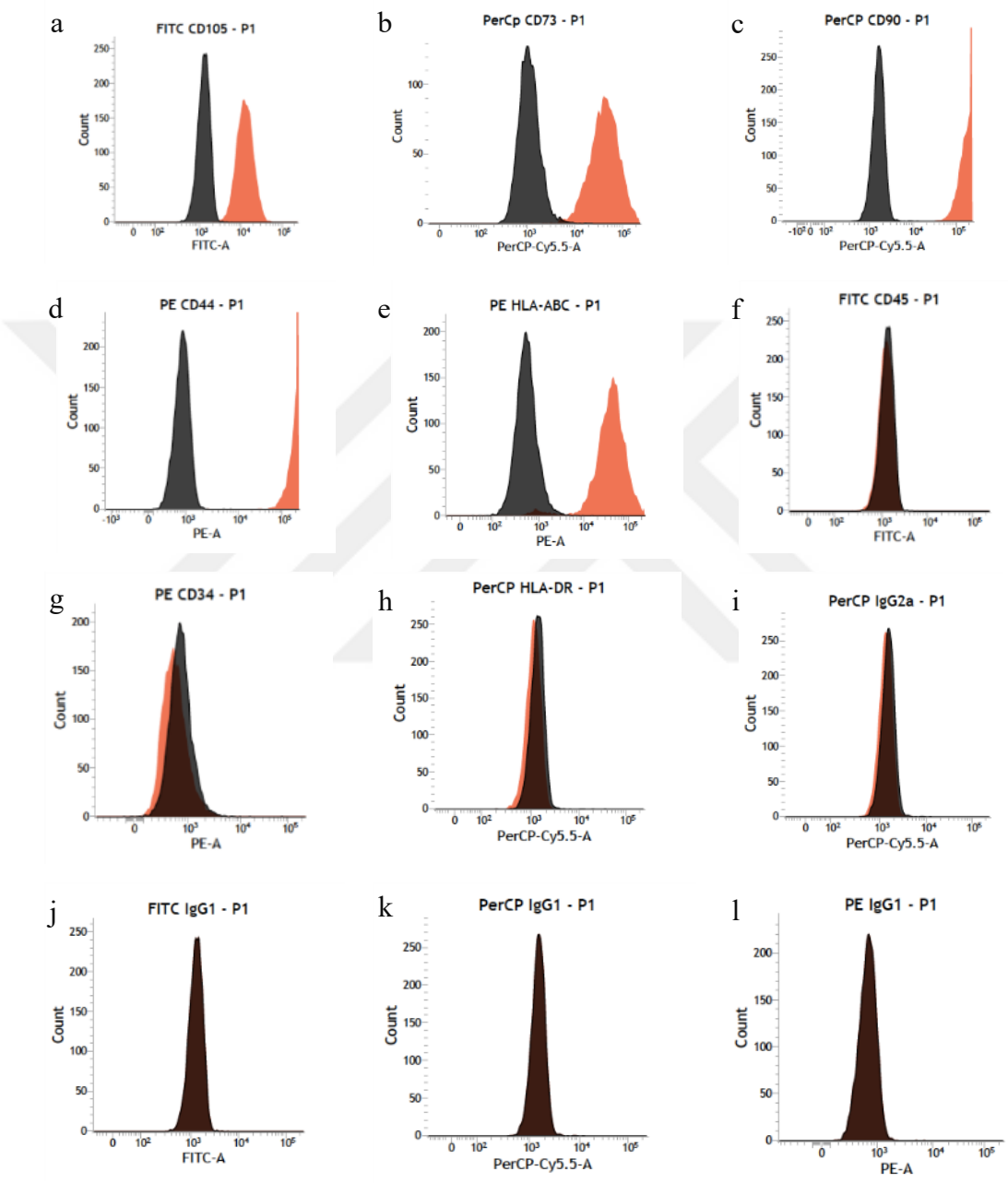

Figure 46. Flow cytometry results of WJ MSCs isolated from human umbilical cord matrix.

Table 18. The expression of surface antigens of WJ MSCs (P3) based on isotypes.

Surface Antigen	WJ MSC%*
CD105	95.25 ±4.01
CD73	99.34 ±0.51
CD90	97.23 ±4.27
CD44	99.53 ±0.65
HLA-ABC	98.76 ±1.80
CD45	2.73 ±3.30
CD34	0.03 ±0.01
HLA-DR	0.52 ± 0.84

*Percentage of the positive cells (Intersection of isotype control and positive sample considered for calculation of absolute positives)

4.2.3.3 Osteogenic differentiation

Another characteristic feature of mesenchymal stem cells is its ability to differentiate into osteogenic, chondrogenic, and adipogenic cells (122). Osteoblasts secrete bone-specific matrix components such as alkaline phosphatase (ALP), calcium-binding proteins, thus they provides calcification and bone formation (125). Osteogenic differentiation of the isolated WJ MSCs was evaluated by determination of ALP activity and CaP deposition with von Kossa staining. WJ MSCs induced to osteogenic differentiation displayed higher specific ALP activity on both day 14 and 21 compared to undifferentiated cells (Figure 47). On the 14th day, the specific ALP activity of induced MSCs was two times higher than the specific ALP activity of control group ($p < 0.05$). In addition, the specific ALP activity of induced WJ MSCs significantly enhanced on day 21 by eight-fold compared to undifferentiated MSCs ($p < 0.0001$). After cells were cultured in osteogenic induction medium for 14 days, it was observed that the shape of the cells changed from spindle-like to cuboidal shape (Figure 48) (126). According to von Kossa staining, there was no calcium-phosphate deposition on 14^{th} day of the induction (Figure 48a, b). However, it was observed that after 21 days of induction calcium-phosphate was slightly accumulated by

differentiated MSCs in comparison to undifferentiated cells (Figure 48c, d). The low calcium-phosphate deposition may implied that since the pluripotency of the WJ MSCs was higher than the other mesenchymal stem cells the time needed for complete osteogenic differentiation of WJ MSCs would be longer than the MSCs derived from other sources (88). In conclusion, the isolated WJ MSCS were able to differentiate into osteogenic cells.

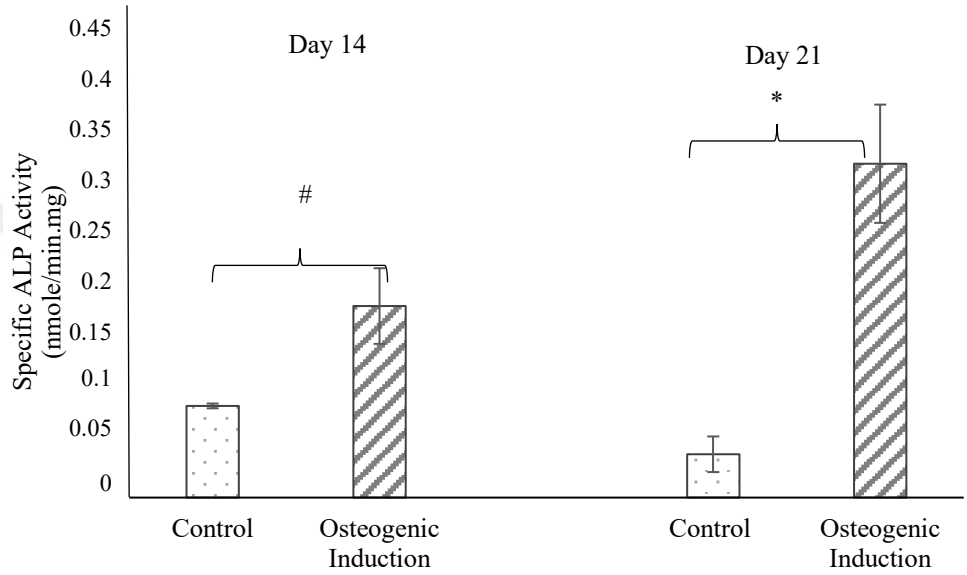

Figure 47. Specific ALP activity of WJ MSCs after 14 and 21 days of osteogenic induction (#: $p < 0.05$, * $p < 0.0001$)

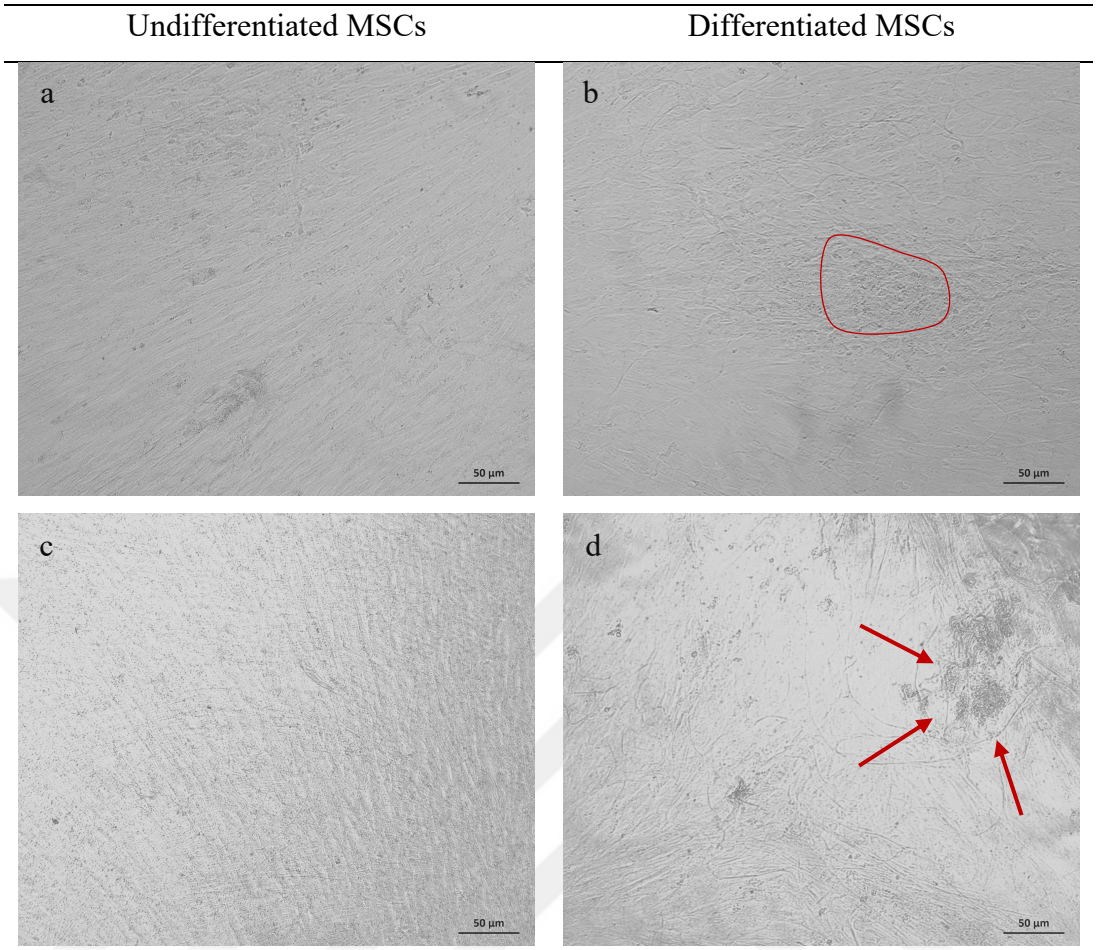

Figure 48. Light microscopy images of von Kossa staining after 14 and 21 days of osteogenic induction. (a, c) Undifferentiated MSCs as control, (b, d) WJ MSCs induced to differentiate into osteogenic cells. Magnification: X20, scale bar: 50µm.

4.2.4 Differentiation of WJ MSCs into smooth muscle cells (SMCs)

Smooth muscle cells (SMCs) found in the tunica media of the native muscular artery, exhibit elongated, fusiform appearance and circumferentially oriented. SMCs aid blood vessels to withstand blood pressure by contraction and relaxation, thus regulate the vasoconstriction and vasodilation (2, 127). Incorporation of SMCs into the vascular scaffold not just mimics the structure of blood vessel tissue but also it may enhance the mechanical features and increase the functionality of artificial blood vessel (128). The mature SMCs are obtained by an extra surgery from healthy blood vessel, and these mature cells may lose their contraction property after isolation, and they may exhibit low proliferation capability depending on donor age. Since a large number of cells needed to seed onto scaffolds, the challenge in tissue engineering is to utilize the cell sources which are obtained non-invasively in high amount and keep their cellular properties (128, 129). Therefore, using MSCs as a cell source and differentiation into cells of the target tissue, for example SMCs like in this study, can solve these issues. Differentiation of stem cells into smooth muscle cells can be carried out in the presence of specific bioactive agents such as TGFβ1 and ascorbic acid. TGFβ1 modulates SMC transition by controlling SMC specific proteins like SMC α-actin and calponin which are responsible for contraction (93). L-ascorbic acid (L-Asc) is known with its antioxidant role, it is important for reducing oxidative stress in smooth muscle cells and for modulation of cholesterol mechanism (130). Arawaka and his colleagues showed that L-Asc stimulates SMC differentiation in pluripotent stem cells (131). Taking consideration these literature knowledge, three different induction media containing 1) only L-Asc, 2) only TGFβ1 and 3) combination of L-Asc and TGFβ1 were investigated for two different time points to determine the induction conditions for differentiation of MSCs to smooth muscle cells. After applying differentiation protocol, the morphology of cells was evaluated by light microscope, and the expression of SMC specific markers at protein level was investigated by immunocytochemistry. On day 12 of induction there was no significant changes in the morphology of the cells in any stimulation groups (Figure 49a, c, e, g). However, it was noticed that undifferentiated cells proliferated more rapidly than the induced

MSCs. It was observed that MSCs induced with 5 ng/mL TGFβ1 exhibited expanded and elongated spindle-shaped SMC like morphology compared to undifferentiated MSCs on day 24 (Figure 49b, d). The typical SMC morphology was not seen when MSCs were induced with only 300 μM L-Asc, even on 24 days of induction (Figure 49e, f). Morphological changes such as increase in cell size and fusiform-like cell shape were observed on day 24 in the induction medium containing both 5 ng/mL TGFβ1 and 300 μM L-Asc (Figure 49h). However, it was thought that this change was due to the effect of TGFβ1, because no prominent change was observed in the cells induced with just L-Asc (Figure 49e, f).

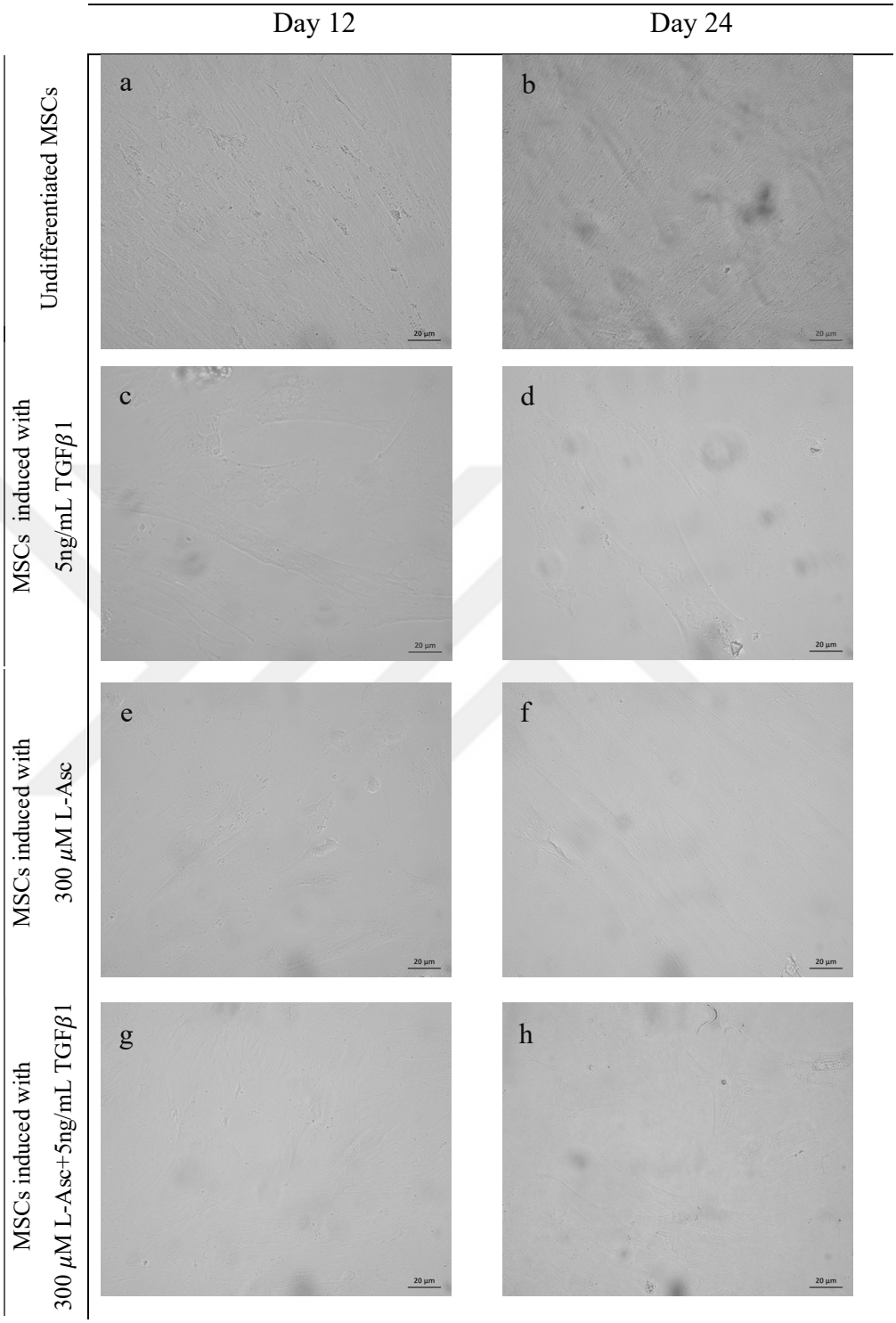

Figure 49. Light microscopy images of WJ MSCs on day 12 and day 24 of SMC induction. (a,b) Undifferentiated WJ MSCs, WJ MSCs induced with (c,d) only 5 ng/mL TGFβ1, (e,f) only 300 μM ascorbic acid and (g,h) combination of 5 ng/mL TGFβ1 and 300 μM ascorbic acid. Magnification: X40, scale bar: 20μm.

After SMC induction to WJ MSCs, the expression of SMC specific markers, α-SMA and SMC-HC, was investigated at protein level by immunocytochemistry. The early marker, α–SMA, is expressed in the beginning of the SMC differentiation and it is related with the contraction of the SMC (93). It was shown that α -SMC is also expressed in MSCs due to being mesodermal origin. The other marker SMC-HC is the late marker expressed in late stage of differentiation (132). According to immunocytochemistry results, there was no detectable expression of α-SMA on 12^{th} day of differentiation within all induction media (Figure 50). It was observed that when the cells were induced with ascorbic acid even for 24 days, there was no significant α-SMA expression like undifferentiated MSCs (Figure 50a, c and Figure 51a, c). However, on 24^{th} day of differentiation the expression of α-SMA was intensely seen in MSCs that were induced with media containing 5 ng/mL TGFβ1 (Figure 51b). Moreover, it was noticed that MSCs induced with TGFβ1 exhibited SMC like expanded and elongated spindle-shape morphology with cell size as 50 μm in diameter and 135 μm in length (Figure 51b) (133).

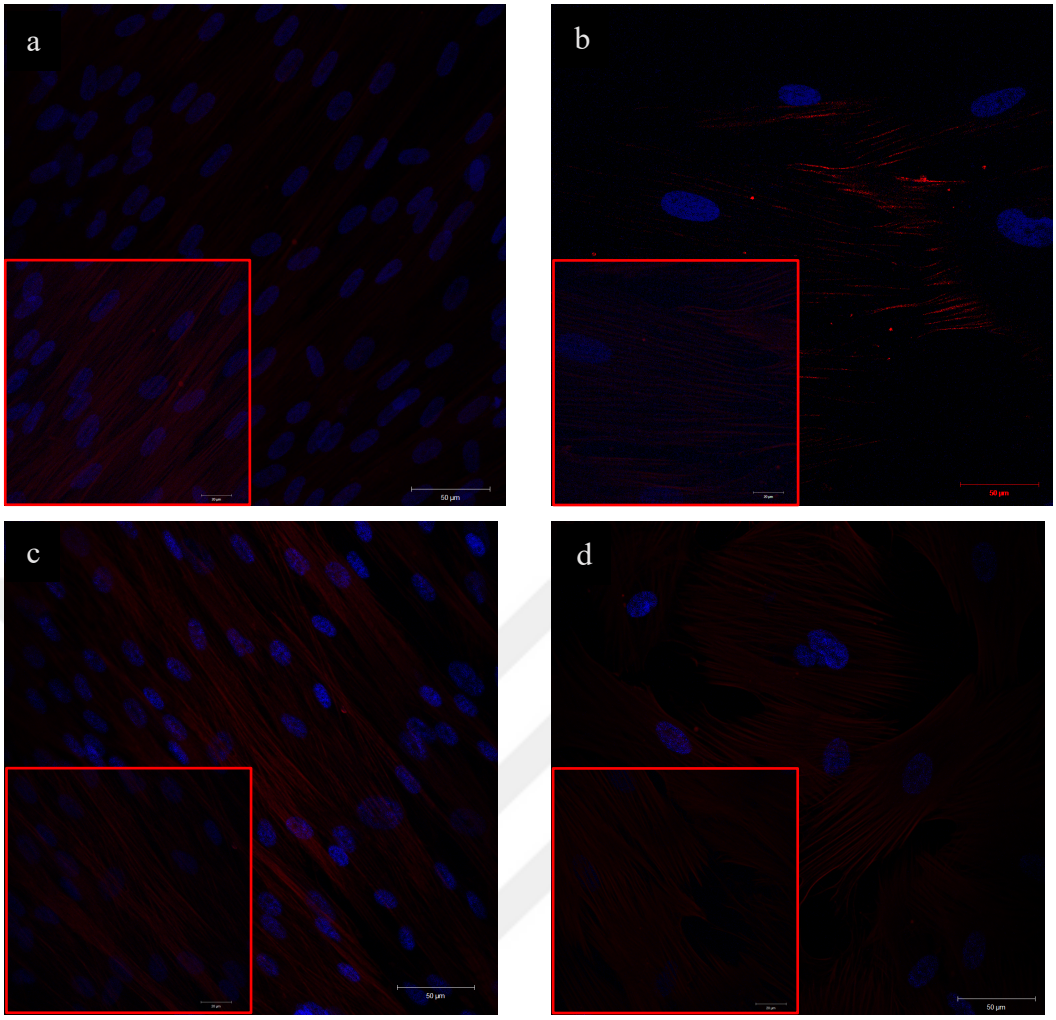

Figure 50. Immunofluorescence analysis of αSMA (red) expression of WJ MSCs at the end of 12 day induction. Confocal micrographs of (a) undifferentiated WJ MSCs, WJ MSCs induced with (b) 5 ng/mL TGFβ1, (c) 300 μM ascorbic acid and (d) combination of 5 ng/mL TGFβ1 and 300 μM ascorbic acid. Inserts: enlarged view of a, b, c, and d. Magnifications: X20, scale bar: 50 µm, inserts X40, scale bar: 20 µm.

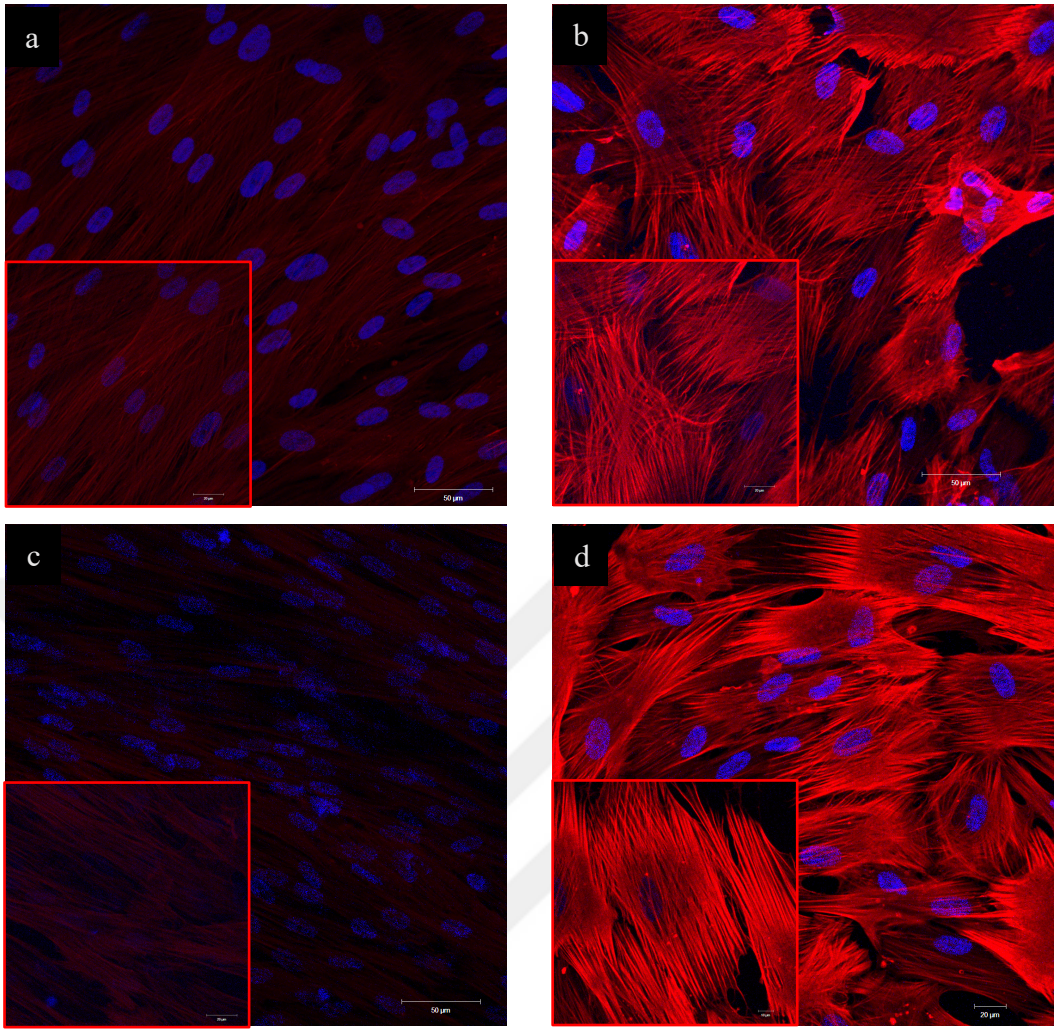

Figure 51. Immunofluorescence analysis of αSMA (red) expression of WJ MSCs at the end of 24 day induction. Confocal micrographs of (a) undifferentiated WJ MSCs, WJ MSCs induced with (b) 5 ng/mL TGFβ1, (c) 300 μM ascorbic acid and (d) combination of 5 ng/mL TGFβ1 and 300 μM ascorbic acid. Inserts: enlarged view of a, b, c, and d. Magnifications: X20, scale bar: 50 µm, inserts X40, scale bar: 20 µm.

The expression of SMC-HC was investigated on 24th day of differentiation since it is the late SMC marker. It was observed that the undifferentiated MSCs were slightly expressed SMC-HC, and there was no difference in expression of SMC-HC of undifferentiated MSCs and MSCs induced with ascorbic acid (Figure 52a, c). However, the expression of SMC-HC was slightly enhanced on day 24, when MSCs cultured in induction media containing only TGFβ1 or combination of TGFβ1 and ascorbic acid (Figure 52b, d). In conclusion, morphology and immunocytochemistry results revealed that the appropriate protocol for differentiation of WJ MSCs into

SMCs was the induction medium containing only TGFβ1 since ascorbic acid showed no significant effect on differentiation. Therefore, this induction medium including TGFβ1 was used in the further differentiation studies.

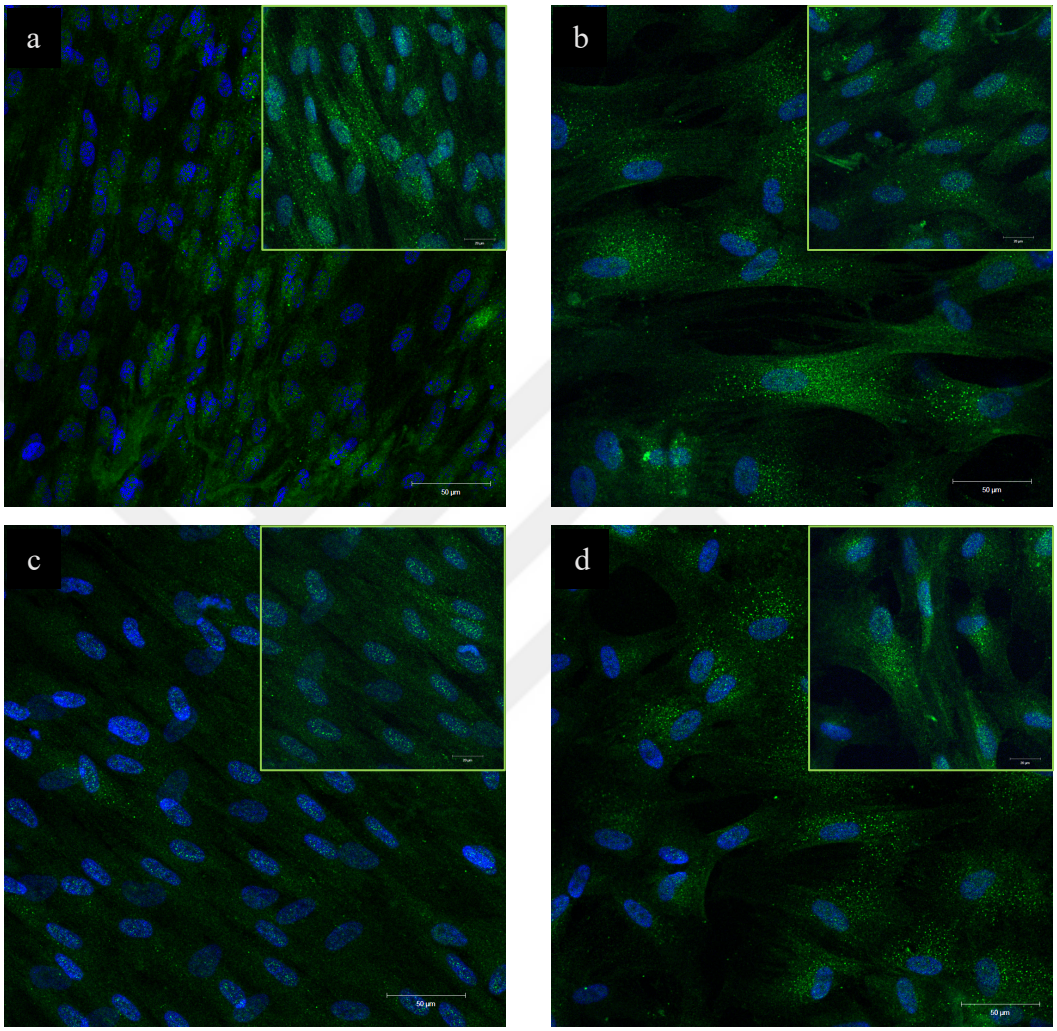

Figure 52. Immunofluorescence analysis of SMC-HC (green) expression of WJ MSCs at the end of 24 day induction. Confocal micrographs of (a) undifferentiated WJ MSCs, WJ MSCs induced with (b) 5 ng/mL TGFβ1, (c) 300 μM ascorbic acid and (d) combination of 5 ng/mL TGFβ1 and 300 μM ascorbic acid. Inserts: enlarged view of a, b, c, and d. Magnifications: X20, scale bar: 50 µm, inserts X40, scale bar: 20 µm.

4.2.5 Evaluation of cell behavior on the polymeric scaffolds

4.2.5.1 Optimization of protein coating for cell adhesion to scaffolds

Scaffolds give three-dimensional milieu for cells to attach, grow, migrate and differentiate like in native tissue. Depend on scaffold chemistry, it may be difficult to attach cells on scaffold due to lack of biomimetic cues provided by ECM. Surface modifications such as coating with protein enhance cell adherence on these scaffolds. Various proteins can be used for that purpose such as collagen, gelatin, laminin and fibronectin (134). In this study, two types of cells, HUVEC and WJ MSCs, were seeded on scaffolds. It was known that HUVEC can attach and grow on gelatin coated surfaces. In order to enhance attachment of WJ MSCs fibronectin and gelatin coating was investigated. Scaffolds were coated with 50 μg/mL fibronectin and 1% gelatin under same conditions, and WJ MSCs were seeded on these protein coated scaffolds. The effect of protein on cell attachment and morphology was evaluated with Phalloidin-DAPI staining for cytoskeleton organization and nuclei, respectively. It was observed that WJ MSCs were attached and spread better on fibronectin coated scaffolds compared to gelatin coated scaffolds (Figure 53). More cells were attached to fibronectin coated scaffolds compared to gelatin coated one (Figure 53 a,b). The spread WJ MSCs seeded on fibronectin coated scaffolds exhibited better actin organization compared to the ones on gelatin coated scaffolds (Figure 53 c,d). It was concluded that fibronectin was more appropriate protein than gelatin for WJ MSCs adhesion. Therefore, further experiments were carried out with 50 μg/mL fibronectin coated scaffolds for WJ MSCs.

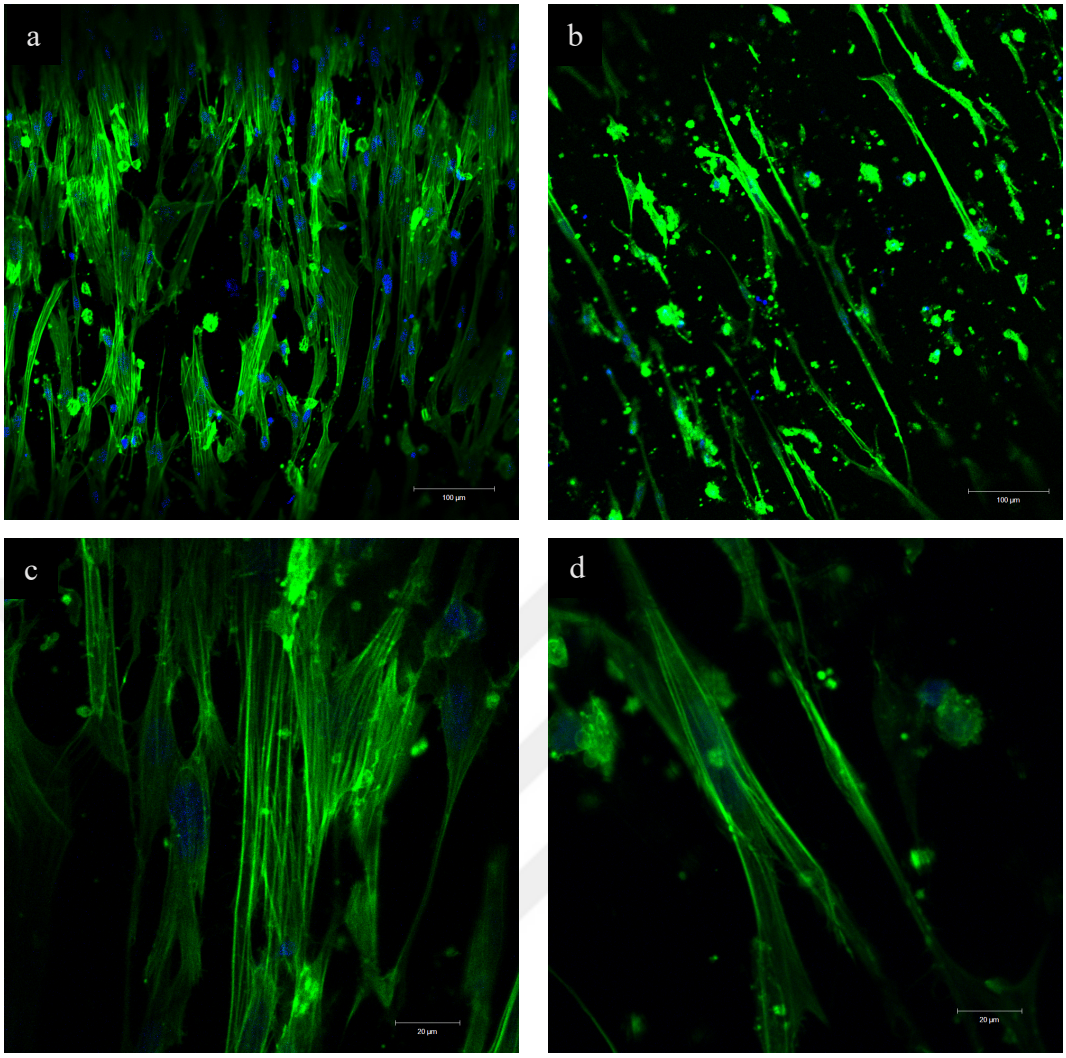

Figure 53. Confocal micrographs of Phalloidin (green)-DAPI(blue) stained WJ MSCs on (a,c) the fibronectin-coated and (b,d) gelatin-coated tubular electrospun mat after 5 days of culture. Magnification: (a,b) X10, scale bar: 100µm, (c,d) X40, scale bar: 20µm.

4.2.5.2 Proliferation and cell activity of cells on bilayered tubular scaffolds

The native tissues usually contain multiple cell types that communicate with each other directly or indirectly. Cell-cell and cell-ECM interactions play important role in cell proliferation, migration, differentiation and secretion of growth factors. Its own ECM and multicellular organization of endothelial cells, smooth muscle cells, and fibroblasts forms the muscular artery tissue. In tissue engineering co-culturing of more than one cell type is required to mimic multicellular target tissues. Co-culture may be

defined as culturing of two or more cells in the same medium. In addition, performing co-culture system within scaffolds provides better understanding of physiology and biology of the native tissue.

The viability and proliferation of WJ MSCs and HUVECs, as mono-culture and co-culture, on bilayered tubular scaffolds were investigated with MTS assay. In addition, the effect of co-culture and scaffold on the cell morphology and organization was studied with Phalloidin-DAPI staining for actin organization and nuclei, respectively. WJ MSCs were seeded onto the outer side of bilayered tubular scaffold at a density of 5×10^4cells/scaffold. On the other hand, HUVECs were seeded onto the inner side of bilayered tubular scaffold at a density of 2×10^4cells/scaffold. A set of samples were carried out as co-culture while the others as mono-culture, and the number of cells were determined with MTS on days 7, 14 and 21 using calibration curve for each cell type (Appendix A.1, A.3). Taking account the seeding density, the number of both cells were slightly low on day 7, in fact, this was expected due to difficulties faced with during cell seeding onto tubular scaffolds (Figure 54 and 55). It was seen that in both cases, in mono-culture and co-culture, the number of WJ MSCs was increased on day 14, this increase was around two fold especially in co-culture condition (Figure 54). The increase in cell number after 14 days was slightly low, and this might be due to cells reaching confluency. It was revealed that the co-culture of WJ MSCs with HUVECs displayed no negative effect on WJ MSCs growth. In fact, it was observed that the proliferation of WJ MSCs was significantly increased with HUVEC co-culture, showing around two fold increase in the number of WJ MSCs (Figure 54) ($p \leq 0.05$). In a similar manner, in both mono-cultured and co-cultured conditions HUVECs proliferated and increased in number within tubular scaffolds by time, especially on day 14 (Figure 55). As in WJ MSCs, co-culturing did not affect HUVEC proliferation negatively. It was observed that HUVECs were grown and increased in number on scaffolds on day 14, even in the presence of WJ MSCs (Figure 55b) ($p< 0.05$). The cell numbers of both WJ MSCs and HUVEC were increased in co-culture condition compared to their cell number in mono-culture (Figure 54 and 55) ($p\leq0.05$ for WJ MSC, $p <0.05$ for HUVEC).

The morphology analysis of mono-cultured and co-cultured, WJ MSCs and HUVEC on the scaffolds confirmed MTS results (Figure 56 and 57). It was observed that in mono- and co-culture conditions both cells attached and spread on the scaffolds on day 7 (Figure 56 and 57 a, d). As the cells increased in number by time, they were spread all over the scaffold and covered the surface (Figure 56 and 57 b, c). In addition, it was observed that WJ MSCs sensed the topography of circumferentially aligned fibers, and orientated parallel to each other in the direction of fiber axis.

Both MTS and Phalloidin-DAPI results revealed that the attached cells were proliferated and spread all over the scaffold by time, regardless of in co-culture or mono-culture. These results imply that cells were not inhibiting each other's growth in co-culture. Williams and colleagues also revealed that SMCs and endothelial cells strongly interact with each other in the co-culture system and upregulate the cell proliferation. In conclusion, the significant increase in cell number with co-culture can be explained by the fact that the molecules secreted from both cells affect each other positively by time, and thus there might be a mutual benefit between two cells.

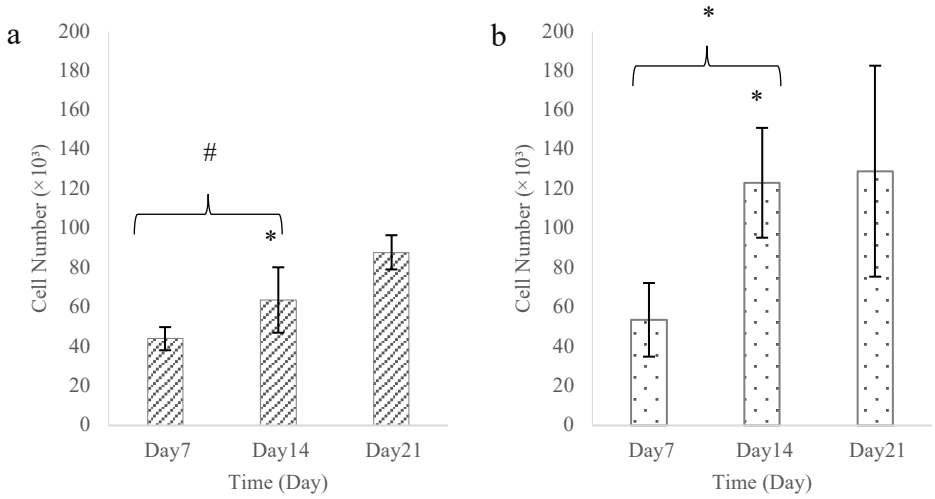

Figure 54. Proliferation of WJ MSCs cultured on bilayered scaffolds as (a) mono-culture and (b) co-culture with HUVECs (# $p > 0.05$, * $p \leq 0.05$).

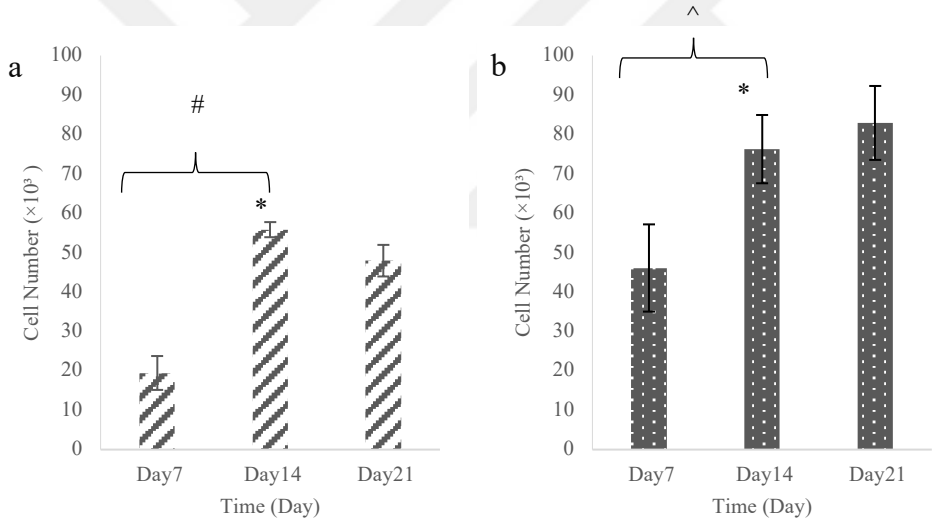

Figure 55. Proliferation of HUVEC cultured on bilayered scaffolds as (a) mono-culture and (b) co-culture with WJ MSCs (# $p > 0.05$, * $p < 0.05$, ^$p < 0.0001$)

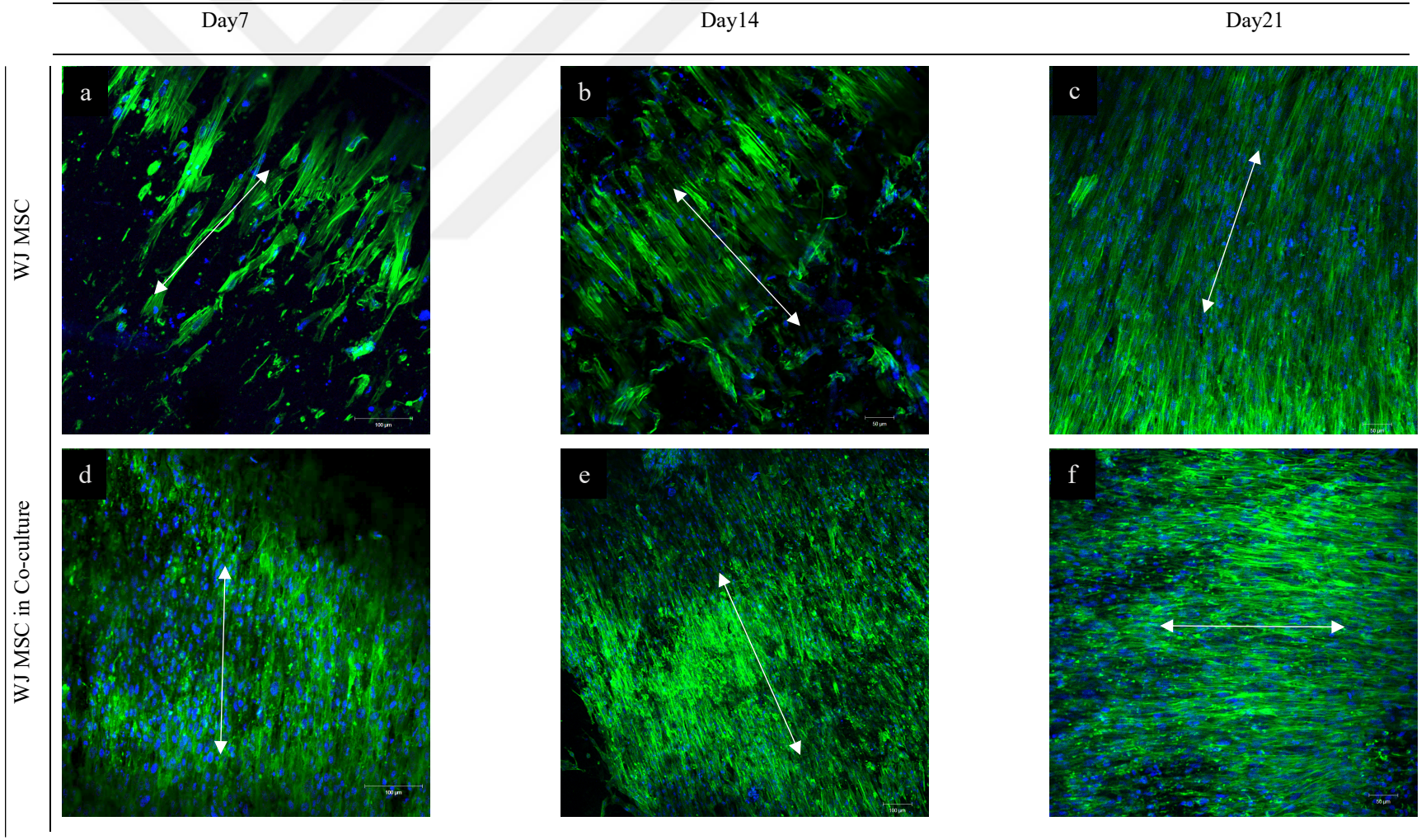

Figure 56 Confocal micrograph of Phalloidin (green)-DAPI(blue) stained WJ MSCs on the outer side of bilayered tubular scaffolds under (a,b,c) mono-cultured and (d,e,f) co-cultured conditions on day 7, 14 and 21. Magnifications: X10, scale bar: 100 µm (two sided arrows indicate the aligned fiber axis)

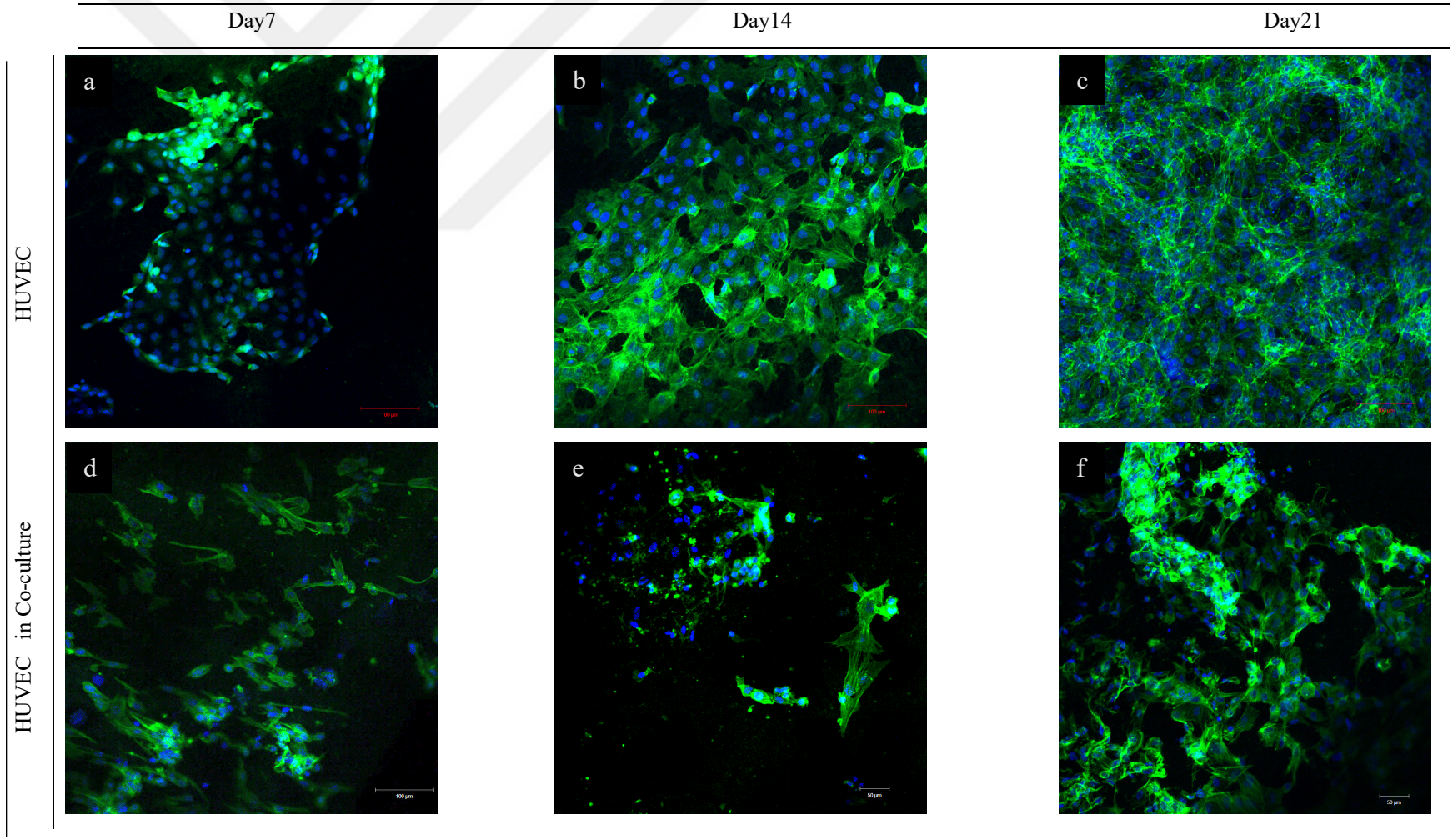

Figure 57. Confocal micrograph of Phalloidin (green)-DAPI(blue) stained HUVEC within the inner side of bilayered tubular scaffolds under (a,b,c) mono-cultured and (d,e,f) co-cultured conditions on day 7,14 and 21 of culture. Magnifications: X10 scale bar: 100 µm.

4.2.6 Formation of 3D multilayered vascular substitutes by incorporation of WJ MSC derived-SMCs and HUVECs

4.2.6.1 Proliferation of WJ MSC derived-SMCs and HUVECs in multilayered tubular scaffolds

In this study, a multilayered tubular scaffold with a 3 mm lumen size was fabricated to mimic the native muscular artery wall (in section 4.1.3). In this design, the circumferentially aligned fibers were deposited over the porous tubular film, and then random fibrous mat was wrapped over the bilayer scaffold as the third layer. The isolated WJ MSCs with a cell density of 7.5×10^4 cells/scaffold were seeded (P3) on the intermediate layer, the fibronectin coated circumferentially aligned electrospun mat part of the tubular scaffold (1 cm length x 3 mm diameter). Cells were cultured in their growth medium for 4 days to increase cell attachment and proliferation. After 4 days, medium of cells was replaced with the SMC induction medium 1 containing TGFβ1 (given in Section 3.2.2.4.1). Then, WJ MSCs were cultured in the induction medium for 24 days to differentiate into SMCs. After 24 days of induction, HUVECs with a cell density of 5×10^4 cell/scaffold were seeded onto the inner side of the scaffold, porous film surface, and then the random fibrous mat (1,5 cm x 1 cm), as an outermost layer, was rolled over the cell-seeded aligned fibrous mat. HUVECs and SMCs were co-cultured for 4 days in co-culture medium. At the end of 32 days of total incubation, the proliferation of SMCs and HUVECs was determined with MTS. In order to investigate the effect of rolling of the random fibrous mat over SMC-seeded bilayered tube, a set of samples were continued without rolling the random fibrous mat, and then both groups were mono-cultured.

MTS results showed that there was no significant decrease in number of SMCs upon rolling of the random fibrous mat over them when they were mono-cultured in induction medium (Figure 58) ($p > 0.05$). The slight decrease seen in the SMCs upon

rolling might be due to mechanical disruption of cells during the rolling process. Thus, it was revealed that the rolling of random fibrous mat over intermediate layer did not significantly affect SMCs, which were on it. Moreover, it was observed that both WJ MSC-derived SMCs and HUVECs were survived after rolling the outer layer and exposure to co-culture conditions (Figure 59). However, there was a decrease in SMC number in co-culture samples compared to mono-culture of SMCs (Figure 58 and 59). This decrease might be due to damaging of the induced cells because of mechanical force application during seeding HUVECs on day 28 of culture. It was observed that HUVEC number was close to seeding density within 4 days, which indicated that HUVEC lived in multilayered tubular scaffold under co-culture conditions. It was concluded that the vascular substitute could be obtained by incorporation and co-culture of both WJ MSC-derived SMCs and HUVECs in multilayered tubular scaffold.

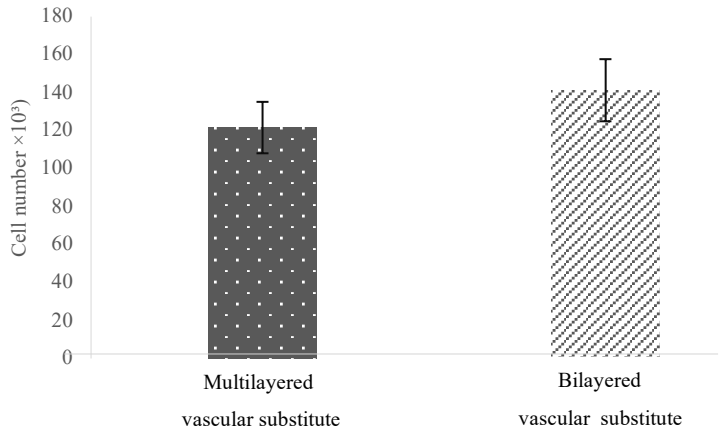

Figure 58. Cell number of SMCs on the scaffolds after 28 days of SMC culture .In multilayered vascular substitute group, the outer layer, random fibrous mat was rolled around cicumferentially aligned fibrous mat on which MSCs were differentiated into SMCs. The bilayered vascular substitute group did not contain the random fibrous mat, the outer layer (# $p > 0.05$).

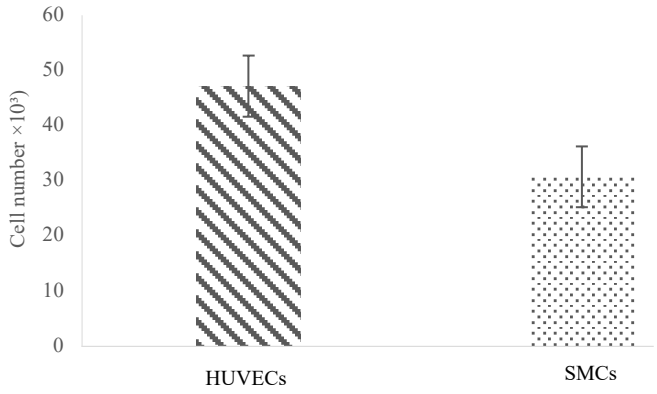

Figure 59. Cell number of HUVECs and and SMCs in the the multilayered vascular substitute after 32 days of culture including 24 days of SMC induction followed by 4 days of co-culture.

4.2.6.2 Immunocytochemistry and morphology analysis of WJ MSC-derived SMCs and HUVEC in multilayered tubular scaffolds

The morphology and organization of induced WJ MSCs on the scaffolds during formation of the multilayered vascular substitutes were investigated with Phalloidin-DAPI staining. Considering the steps of formation of vascular substitute, it was observed that WJ MSCs were attached to the circumferentially aligned intermediate layer of the scaffold, and organized parallel to each other along the fiber direction by sensing the topography on 3rd day of culture (Figure 60). Moreover, it was seen that the cells expanded and exhibited their specific spindle-like morphology with well-organized actin filaments on the scaffolds (Figure 60).

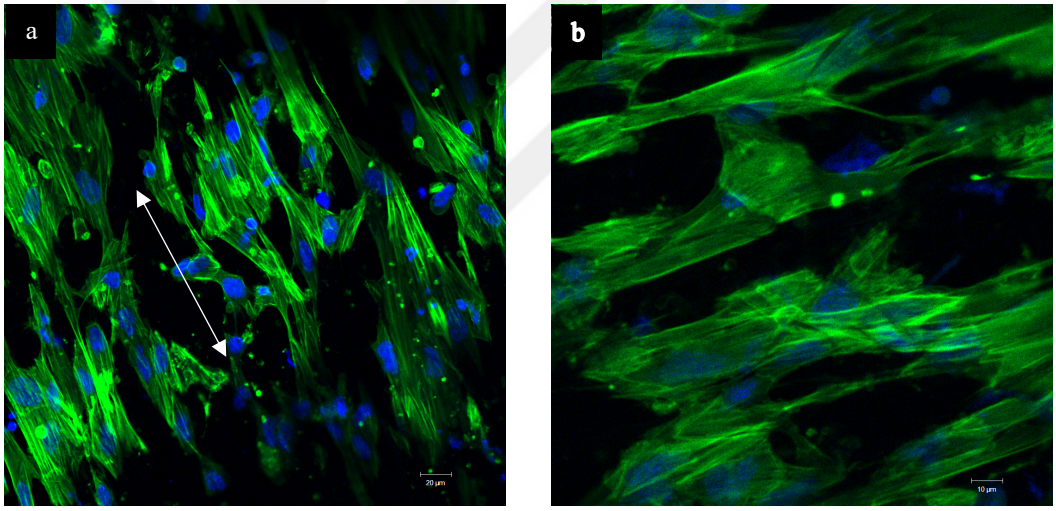

Figure 60. Confocal micrographs of Phalloidin (green)-DAPI(blue) stained WJ MSCs on the circumferentially aligned fibers of the tubular scaffold on the 3rd day of culture before SMC induction. Magnifications: (a) X20, scale bar 20 µm, (b) X40, scale bar 10 µm. (two sided arrows indicate the aligned fiber axis)

The medium of the cells were changed with SMC induction medium 1 at the 4th day of culture. After culturing WJ MSCs in the induction medium for 24 days, differentiation into SMCs was evaluated by immunostaining cells against α -SMA on day 17 (Figure 61). It was revealed that cells were spread and proliferated all over the circumferentially aligned fibrous layer of the tubular scaffold (Figure 61a). It was seen

that cells sensed the topography of aligned fibers, oriented along the fiber direction and kept this alignment even during differentiation (Figure 61b, c). It was observed that induced cells expressed α-SMA on the scaffolds like in the differentiation studies on TCPS (section 4.2.4), and this indicated the differentiation of WJ MSCs into SMCs on the scaffolds (Figur61b, c).

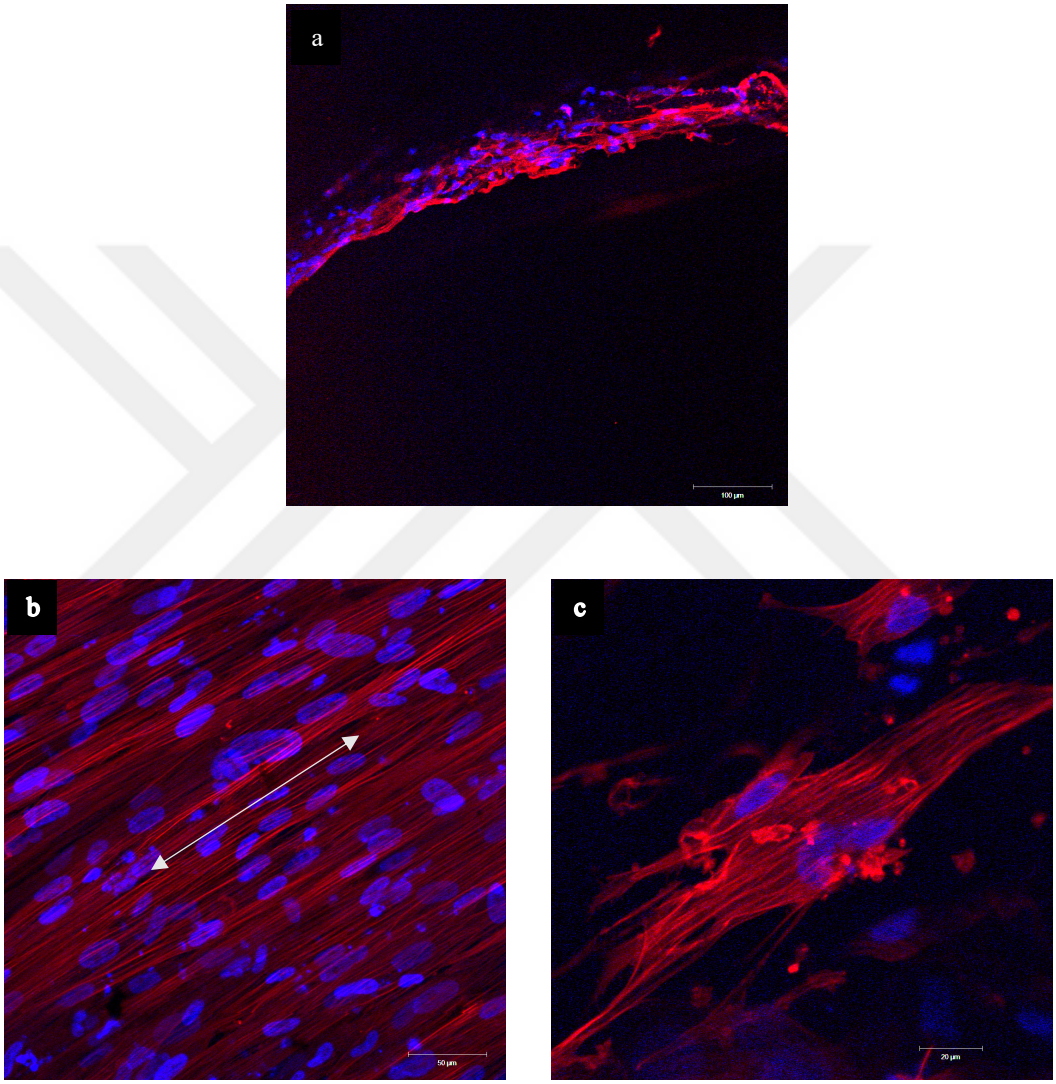

Figure 61. Confocal micrographs of WJ MSC-derived SMCs immunostained against α-SMA(red) on the circumferentially aligned fibrous mat layer of the tubular scaffold on 17th day of SMC differentation. Magnifications: (a) X10, scale bar: 100 µm, (b) X20, scale bar: 50 µm, (c) X40, scale bar: 20 µm. (two sided arrows indicate the aligned fiber axis

After 24 days of SMC induction, HUVECs were seeded onto the inner side of the tubular scaffold, and then it was rolled with random fibrous mat. Afterwards, WJ MSC-derived SMCs and HUVECs were co-cultured for 4 days in the tubular scaffolds. At the end of co-culture, immunostaining analysis was done for differentiated SMCs and HUVECs. It was observed that WJ MSC-derived SMCs expressed SMC specific markers, the early marker α-SMA and the late marker SMC-HC after formation of multilayered vascular substitute (Figure 62). In fact, the expression of α-SMA was slightly higher than the expression on 17^{th} day (Figure 61 and 62). The SMC specific markers expression did not reduced by differentiating cells on the scaffolds and by co-culturing them with HUVECs. Moreover, it was observed that the alignment was persisted after rolling of the outer layer and co-culture. It was revealed by the immunocytochemistry results that WJ MSCs were differentiated into SMC under applied culture conditions.

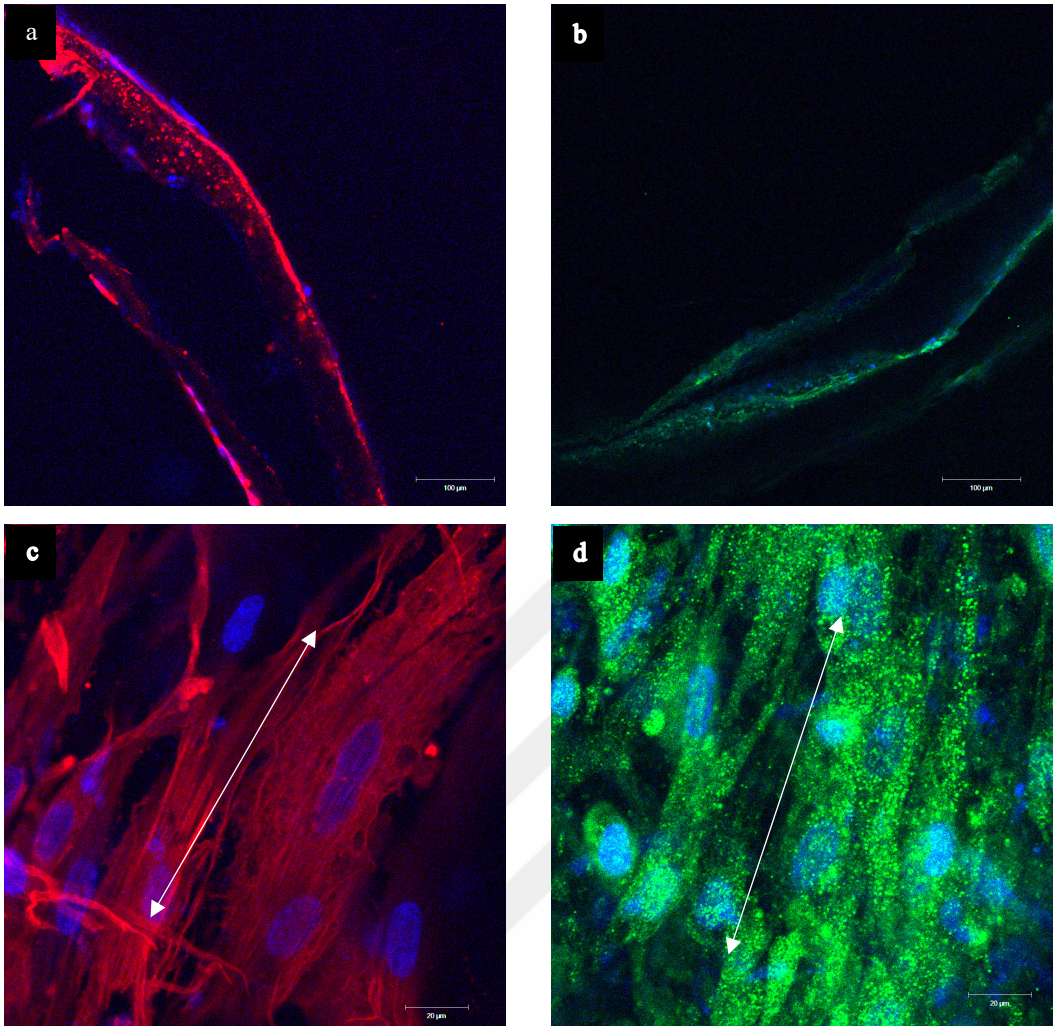

Figure 62. Confocal micrographs of WJ MSC-derived SMCs immunostained against α-SMA (a,c) and SMC-HC (b,d) on the cicumferentially aligned fibrous mat layer of the tubular scaffold at the end of the co-culture. Magnifications: (a,b) X10, scale bar: 100 µm, (c,d) X40, scale bar: 20 µm (two sided arrows indicate the aligned fiber axis).

After co-culture on the scaffolds for 4 days, HUVECs were immunostained against specific endothelial marker CD31. It was seen that HUVECs were attached and spread on the inner side of tubular scaffolds (Figure 63). The results showed that HUVECs preserved their immunotype characteristics by expressing CD31 on cell border after co-culture with SMCs (Figure 63b, c). Moreover, it was also seen that HUVECs exhibited their specific cobblestone morphology on the inner side of the scaffold (Figure 63b, c).

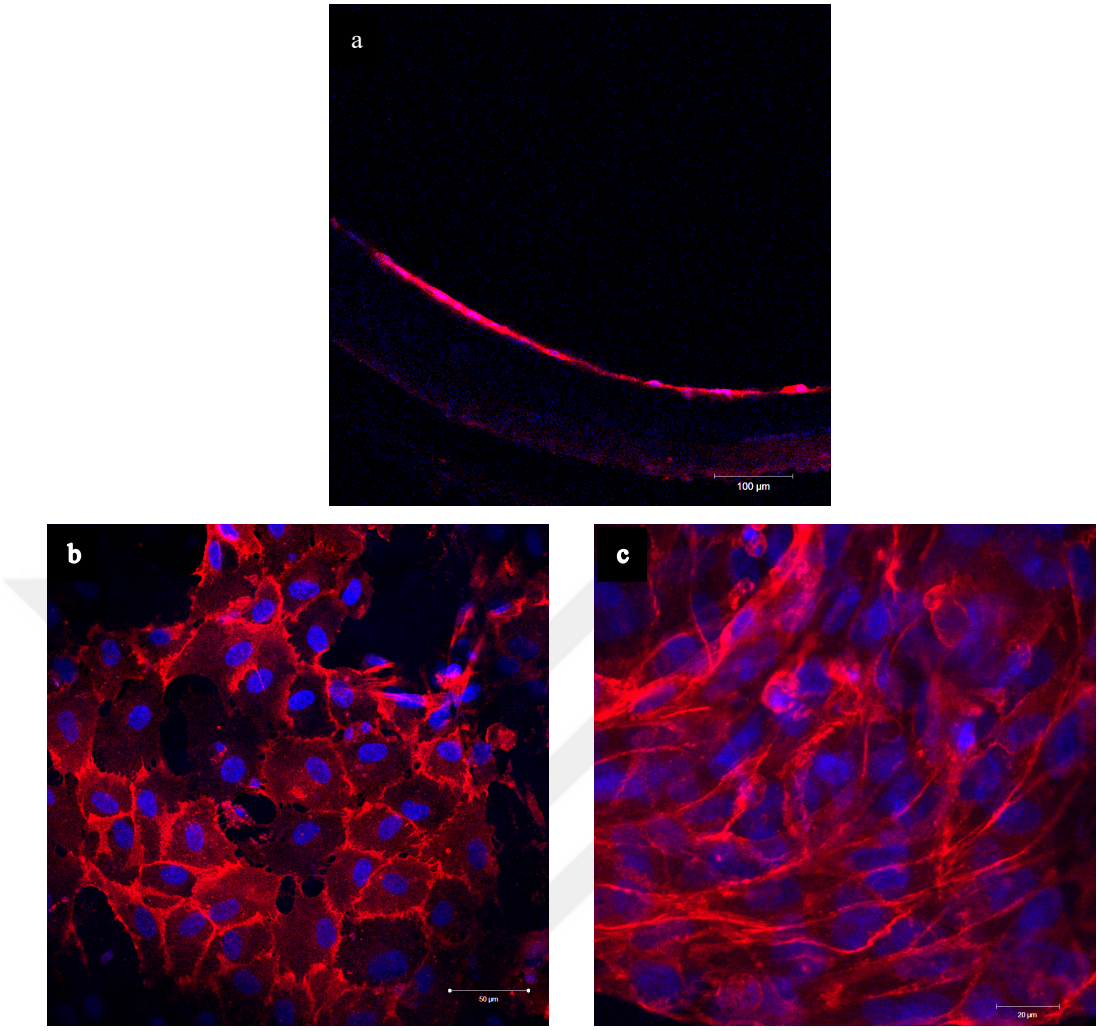

Figure 63. Confocal micrographs of HUVECs immunostained against (a,b) CD31 in the porous tubular film layer of the tubular scaffold at the end of the co-culture. Magnifications: (a) X10, scale bar: 100 µm, (b) X20, scale bar: 20 µm, (c) X40, scale bar: 20 µm.

In conclusion, HUVEC cells lined the lumen the multilayered vascular substitute like in native tunica intima. WJ MSCs were differentiated into SMCs and circumferentially aligned on the intermediate layer of the scaffolds as mimicking the tunica media of muscular artery. Moreover, the wrapped random electrospun mat as being the outermost layer imitated tunica adventitia of artery.

5. CONCLUSION and DISCUSSION

In vascular tissue engineering to achieve an ideal small-medium sized arterial substitute in terms of mimicking the native tissue architecture and function is still a challenge. There are various single or bilayered scaffolds used in tissue engineering; however, these scaffolds were far away to mimic the ECM properties of native blood vessels (56, 65, 81, 100-102, 108). In addition, multilayered vascular scaffolds were fabricated by applying different approaches and seeded with allogenic or xenogenic mature endothelial cells, smooth muscle cells or fibroblasts (56, 99-101, 108). Vacanti Et al. fabricated vascular scaffold with layers which were in sheet form in the beginning. The sheets were supported with mature xenogenic SMCs and fibroblast, separately. At the end, the tubular construct was formed by wrapping the sheets over silicon tubes which have a 6 mm diameter to mimic the native artery structure (56).

The layered scaffolds can be produced by electrospinning technique. There are various bilayered and multilayered tubular vascular scaffolds fabricated by electrospinning (99, 101, 106-108). However, the cells were cultured alone or separately in these studies. For instance, only HUVECs were seeded onto the lumen side of the scaffold (99, 101). In another study, mature SMCs and endothelial cells were seeded onto the corresponding layer separately to check cell proliferation on the layers, but they were not co-cultured (101). The layers of multilayered vascular scaffolds could also be obtained by sequential application of different techniques like electrospinning and freeze-drying using different synthetic or natural polymers or blends of these polymers. In one of the study, this type of scaffold was supported with endothelial cells and SMCs, and these cells were cultured separately like in most of vascular tissue engineering studies (101, 108). There are limited number of blood vessel tissue engineering studies which were conducted co-culturing of blood vessel cells using different solid scaffolds or hydrogels. In one of these studies, a natural polymer-based, three-layered, tubular substitute was obtained within the microfluidic platform, and it was supported with endothelial cells, SMCs, and fibroblasts. However,

it was indicated that the graft was not mechanically enough for the implantation since the graft was obtained from natural polymer (100).

In this study, small-medium sized, multilayered, tubular vascular substitute was constructed by considering the native ECM features of the blood vessel and tissue cell types to develop an alternative treatment approach for coronary artery disease. The scaffold with 3 mm diameter lumen size was composed of three layers: the innermost layer of the scaffold was porous tubular film which was produced by dip coating to mimic tunica intima of the native artery. The porosity of the film was achieved with the removal of PEG. The porosity of the film was appropriate to allow medium and gas diffusion but not to cell penetration. Considering the tunica media of native blood vessel, the intermediate layer of the scaffold was circumferentially aligned fibrous mat which was successfully deposited on the tubular film via electrospinning. The outermost layer, the random fibrous mat, was fabricated by electrospinning and was wrapped over the bilayered scaffold to mimic tunica adventitia. The multilayered scaffold composed of three layers including the tubular porous film, the circumferentially aligned fibrous mat, and the random fibrous mat was successfully constructed. The final vascular scaffold was 1 cm in length and 3 mm in diameter which is in the range of small-medium sized blood vessels.

HUVEC and WJ MSCs were isolated from the human umbilical cord to serve as a cell source in this study. WJ MSCs which exhibit low immunogenicity were differentiated into SMCs, cell type found in the tunica medium of the natural artery, in the presence of TGFβl. Differentiation of the WJ MSCs was evaluated at protein level with the immunocytochemistry. It was concluded that WJ MSCs were expressed the early and late SCMs specific markers.

In this study, WJ MSC were seeded on the intermediate layer of the tubular scaffold and differentiated into SMCs. After differentiation was achieved on the construct, HUVECs were seeded into the lumen side of the scaffold to provide endothelization which is one of the most important issues in vascular tissue engineering. SMCs and HUVECs were co-cultured on the tubular scaffold like in the native artery. Behavior, spreading and proliferation of both SMCs and HUVECs were examined with immunocytochemistry and cell proliferation assay. Immunocytochemistry results indicated that SMCs spread on the scaffold by time and were aligned circumferentially along the fibers like in the native artery. HUVECs were also lined the lumen of the tubular scaffold. Moreover, cell proliferation results revealed that both SMCs and HUVECs were attached and proliferated on the scaffolds after 32 days of culture. The results indicates that the multilayer blood vessel substitute developed via tissue engineering has a potential to be tested in *in vivo* studies

In vascular tissue engineering, the ideal blood vessel substitute should mimic histological properties of native blood vessel. The multilayered vascular substitute developed in this thesis study offers a promise to meet the desired properties with its native blood vessel ECM-like architecture and co-culture of MSC-derived SMCs and endothelial cells on the corresponding layers of the tubular construct. In addition, to obtain arterial substitutes with a diameter less than 6 mm is still a challenge in tissue engineering, and this developed vascular substitute could be a potential construct to meet this issue. In terms of vascular tissue engineering, endothelialized vascular substitute with altered mechanical properties is urgently needed in the clinic. This multilayered vascular substitute supported with MSC-derived SMCs and endothelial cells can be a promising alternative approach for the treatment of coronary artery disease to save millions of lives in the clinic.

REFERENCES

1. Cardiovascular diseases (CVDs): WHO; 23.03.2020
2. Michael H. Ross WP. Cardiovascular System. In: Taylor C, editor. Histology A Text and Atlas. Sixth Edition ed: Lippincott Williams & Wilkins, a Wolters Kluwer business. p. 400-39.
3. Seifu DG, Purnama A, Mequanint K, Mantovani D. Small-diameter vascular tissue engineering. Nat Rev Cardiol. 2013;10(7):410-21.
4. Langer R, Vacanti JP. Tissue engineering. Science. 1993;260(5110):920-6.
5. Virani SS, Alonso A, Benjamin EJ, Bittencourt MS, Callaway CW, Carson AP, et al. Heart Disease and Stroke Statistics-2020 Update: A Report From the American Heart Association. Circulation. 2020;141(9):e139-e596.
6. Criqui MH, Aboyans V. Epidemiology of peripheral artery disease. Circ Res. 2015;116(9):1509-26.
7. Anthony Y. Fung aJS. Epidemiology and Significance of Carotid Artery Stenosis. In: J. Saw JEE, D. S. Lee, and S. Yadav, editor. Contemporary Cardiology:. Totowa: Humana Press Inc.,; 2007.
8. Nerem RM. Blood vessel tissue engineering. In: Buddy D. Ratner ASH, Frederick J. Schoen,Jack E. Lemons,editor. Biomaterials Science. Third edition. Canada: Elsevier. p. 1237-46.
9. Hall JE. Guyton and Hall Textbook of Medical Physiology. 13th Edition ed. USA: Elsevier. p. 248-59.
10. Rhodin JAG. Architecture of the Vessel Wall. Comprehensive Physiology1980. p. 1-31.
11. Dejana E. Endothelial cell-cell junctions: happy together. Nat Rev Mol Cell Biol. 2004;5(4):261-70.
12. Eble JA, Niland S. The extracellular matrix of blood vessels. Curr Pharm Des. 2009;15(12):1385-400.
13. Hall JE. Guyton and Hall Textbook of Medical Physiology. 13th edition ed: Elseiver; 2016. p. 97-105.
14. Waller BF. The eccentric coronary atherosclerotic plaque: morphologic observations and clinical relevance. Clin Cardiol. 1989;12(1):14-20.
15. Burris A.C. SM. Basic Coronary Artery Anatomy and Histology. In: A. A, editor. Interventional Cardiology Imaging London: Springer; 2015.
16. Pashneh-Tala S, MacNeil S, Claeyssens F. The Tissue-Engineered Vascular Graft-Past, Present, and Future. Tissue Eng Part B Rev. 2016;22(1):68-100.
17. Nerem RM. Applications of Biomaterials. In: Buddy D. Ratner ASH, Frederick J. Schoen,Jack E. Lemons,, editor. Biomaterials Science. Third edition. Canada: Elsevier. p. 771-84.
18. Persidis A. Tissue engineering. Nature Biotechnology. 1999;17(5):508-10.
19. The Nobel Prize in Physiology or Medicine 1912: Alexis Carrel [online], [Internet]. [cited 27.03.2020]. Available from: http://www.nobelprize.org/nobel_prizes/medicine/laureates/1912/
20. Sabik JF. Understanding Saphenous Vein Graft Patency. Circulation. 2011;124(3):273-5.

21. Weintraub WS, Jones EL, Craver JM, Guyton RA. Frequency of repeat coronary bypass or coronary angioplasty after coronary artery bypass surgery using saphenous venous grafts. Am J Cardiol. 1994;73(2):103-12.
22. Maisel WH. A Device for Proximal Anastomosis of Autologous Coronary Vein Grafts. Circulation. 2005;112(10):1516-8.
23. Voorhees AB, Jr., Jaretzki A, 3rd, Blakemore AH. The use of tubes constructed from vinyon "N" cloth in bridging arterial defects. Ann Surg. 1952;135(3):332-6.
24. Institute NC. Physiology of Circulation [Available from: https://training.seer.cancer.gov/anatomy/cardiovascular/blood/physiology.html.
25. Abbott WM, Callow A, Moore W, Rutherford R, Veith F, Weinberg S. Evaluation and performance standards for arterial prostheses. J Vasc Surg. 1993;17(4):746-56.
26. Vascular Graft Market 2018| Industry Growth by Forecast to 2024 - GMI Analysis Merket Watch2019 [Available from: https://www.marketwatch.com/press-release/vascular-graft-market-2018-industry-growth-by-forecast-to-2024---gmi-analysis-2019-07-31.
27. Organ Procurement and Transplantation Network website. [
28. Hasırcı V., Hasırcı N. Tissue Engineering and Regenerative Medicine. Fundamentals of Biomaterials. New York, NY: Springer 2018. p. 281-302.
29. Balachandran K, Alford PW, Wylie-Sears J, Goss JA, Grosberg A, Bischoff J, et al. Cyclic strain induces dual-mode endothelial-mesenchymal transformation of the cardiac valve. Proc Natl Acad Sci U S A. 2011;108(50):19943-8.
30. Khetani SR, Bhatia SN. Microscale culture of human liver cells for drug development. Nature Biotechnology. 2008;26(1):120-6.
31. Hasırcı V., Hasırcı N. Fundamentals of Human Biology and Anatomy. Fundamentals of Biomaterials. New York, NY: Springer 2018.
32. Schoen FJ. Applications of Biomaterials in Functional Tissue Engineering. In: Buddy D. Ratner ASH, Frederick J. Schoen,Jack E. Lemons,, editor. Biomaterials Science. Third edition. Canada: Elsevier. p. 1119-37.
33. Mitchell FJSaRN. Tissues, The Extracellular Matrix, and Cell-Biomateriasl Interactions. In: Buddy D. Ratner ASH, Frederick J. Schoen,Jack E. Lemons,, editor. Biomaterials Science. Third edition. Canada: Elsevier. p. 452-63.
34. Atzet GDPaS. Engineered Natural Materials. In: Buddy D. Ratner ASH, Frederick J. Schoen,Jack E. Lemons,, editor. Biomaterials Science. Third edition. Canada: Elsevier. p. 195-209.
35. MacDevitt TC. Stem Cells: Key Concept. In: Buddy D. Ratner ASH, Frederick J. Schoen,Jack E. Lemons,editor. Biomaterials Science. Third edition. Canada: Elsevier. p. 487-95.
36. Hasırcı V., Hasırcı N. Blood Interfacing Applictions. Fundamentals of Biomaterials. New York, NY: Springer 2018. p. 233-56.
37. Stekelenburg M, Rutten MC, Snoeckx LH, Baaijens FP. Dynamic straining combined with fibrin gel cell seeding improves strength of tissue-engineered small-diameter vascular grafts. Tissue Eng Part A. 2009;15(5):1081-9.

38. Rabkin E, Schoen FJ. Cardiovascular tissue engineering. Cardiovasc Pathol. 2002;11(6):305-17.
39. Bajpai VK, Andreadis ST. Stem cell sources for vascular tissue engineering and regeneration. Tissue Eng Part B Rev. 2012;18(5):405-25.
40. Patel A, Fine B, Sandig M, Mequanint K. Elastin biosynthesis: The missing link in tissue-engineered blood vessels. Cardiovasc Res. 2006;71(1):40-9.
41. Tranquillo RT. The tissue-engineered small-diameter artery. Ann N Y Acad Sci. 2002;961:251-4.
42. Kim BS, Mooney DJ. Development of biocompatible synthetic extracellular matrices for tissue engineering. Trends Biotechnol. 1998;16(5):224-30.
43. Zhang WJ, Liu W, Cui L, Cao Y. Tissue engineering of blood vessel. J Cell Mol Med. 2007;11(5):945-57.
44. Vats A, Tolley NS, Polak JM, Gough JE. Scaffolds and biomaterials for tissue engineering: a review of clinical applications. Clin Otolaryngol Allied Sci. 2003;28(3):165-72.
45. Berglund JD, Galis ZS. Designer blood vessels and therapeutic revascularization. Br J Pharmacol. 2003;140(4):627-36.
46. Quint C, Arief M, Muto A, Dardik A, Niklason LE. Allogeneic human tissue-engineered blood vessel. J Vasc Surg. 2012;55(3):790-8.
47. Conklin BS, Richter ER, Kreutziger KL, Zhong DS, Chen C. Development and evaluation of a novel decellularized vascular xenograft. Med Eng Phys. 2002;24(3):173-83.
48. Badylak SF, Freytes DO, Gilbert TW. Extracellular matrix as a biological scaffold material: Structure and function. Acta Biomater. 2009;5(1):1-13.
49. Scott EC, Glickman MH. Conduits for hemodialysis access. Semin Vasc Surg. 2007;20(3):158-63.
50. Madden RL, Lipkowitz GS, Browne BJ, Kurbanov A. Experience with cryopreserved cadaveric femoral vein allografts used for hemodialysis access. Ann Vasc Surg. 2004;18(4):453-8.
51. Weinberg C, Bell E. A blood vessel model constructed from collagen and cultured vascular cells. Science. 1986;231(4736):397-400.
52. Yow KH, Ingram J, Korossis SA, Ingham E, Homer-Vanniasinkam S. Tissue engineering of vascular conduits. Br J Surg. 2006;93(6):652-61.
53. Hubbell JA. Bioactive biomaterials. Curr Opin Biotechnol. 1999;10(2):123-9.
54. Higgins SP, Solan AK, Niklason LE. Effects of polyglycolic acid on porcine smooth muscle cell growth and differentiation. J Biomed Mater Res A. 2003;67(1):295-302.
55. Nair LSaL, C.T. . Biodegradable Polymers as Biomaterials. . Progress in Polymer Science, . 2007;32, :762- 98
56. Iwasaki K, Kojima K, Kodama S, Paz AC, Chambers M, Umezu M, et al. Bioengineered Three-Layered Robust and Elastic Artery Using Hemodynamically-Equivalent Pulsatile Bioreactor. Circulation. 2008;118(14_suppl_1):S52-S7.
57. Zhao J, Qiu H, Chen DL, Zhang WX, Zhang DC, Li M. Development of nanofibrous scaffolds for vascular tissue engineering. Int J Biol Macromol. 2013;56:106-13.
58. Vroman I, Tighzert L. Biodegradable Polymers. Materials (Basel). 2009;2(2):307-44.

59. Gentile P, Chiono V, Carmagnola I, Hatton PV. An overview of poly(lactic-co-glycolic) acid (PLGA)-based biomaterials for bone tissue engineering. Int J Mol Sci. 2014;15(3):3640-59.
60. Jeong SI, Kim SY, Cho SK, Chong MS, Kim KS, Kim H, et al. Tissue-engineered vascular grafts composed of marine collagen and PLGA fibers using pulsatile perfusion bioreactors. Biomaterials. 2007;28(6):1115-22.
61. Rodrigues Coimbra ME GBM, Nelson Elias C, Coelho PG. . In Vitro Degradation of Poly-L-DL-Lactic Acid (PLDLLA) after Two Processing Methods. . Journal of Biomimetics, Biomaterials and Biomedical Engineering 2014(20):45–64. .
62. M. A. T. Duarte ACM, and E. A. d. R. Duek,. Mechanical properties of membranes of poly (L-co-DL-lactic acid) with Poly (caprolactone triol) and study in vivo. International Journal of Polymer Science. 2014.
63. Bergström JS, Hayman D. An Overview of Mechanical Properties and Material Modeling of Polylactide (PLA) for Medical Applications. Annals of Biomedical Engineering. 2016;44(2):330-40.
64. Maluf-Meiken LC, Silva DR, Duek EA, Alberto-Rincon MC. Morphometrical analysis of multinucleated giant cells in subdermal implants of poly-lactic acid in rats. J Mater Sci Mater Med. 2006;17(5):481-5.
65. Koch S, Flanagan TC, Sachweh JS, Tanios F, Schnoering H, Deichmann T, et al. Fibrin-polylactide-based tissue-engineered vascular graft in the arterial circulation. Biomaterials. 2010;31(17):4731-9.
66. Lam CXF, Olkowski R, Swieszkowski W, Tan KC, Gibson I, Hutmacher DW. Composite PLDLLA/TCP Scaffolds for Bone Engineering: Mechanical and In Vitro Evaluations. 2009.
67. Veiranto M, Törmälä P, Suokas E. In vitro mechanical and drug release properties of bioabsorbable ciprofloxacin containing and neat self-reinforced P(L/DL)LA 70/30 fixation screws. Journal of Materials Science: Materials in Medicine. 2002;13(12):1259-64.
68. Khan I, Mansha M, Mazumder MAJ. Polymer Blends. In: Jafar Mazumder MA, Sheardown H, Al-Ahmed A, editors. Functional Polymers. Cham: Springer International Publishing; 2018. p. 1-38.
69. Gunn J, Zhang M. Polyblend nanofibers for biomedical applications: perspectives and challenges. Trends Biotechnol. 2010;28(4):189-97.
70. Dubey G, Mequanint K. Conjugation of fibronectin onto three-dimensional porous scaffolds for vascular tissue engineering applications. Acta Biomater. 2011;7(3):1114-25.
71. A. Sionkowska. Current research on the blends of natural and synthetic polymers as new biomaterials: Review. Progress in Polymer Science 2011;36 (9):1254–76.
72. Landau L, & Levich, B. . Dragging of a Liquid by a Moving Plate. . Dynamics of Curved Fronts. 1988:141–53.
73. Neacşu IA, Nicoară, A. I., Vasile, O. R., & Vasile, B. Ş. . Inorganic micro- and nanostructured implants for tissue engineering. Nanobiomaterials in Hard Tissue Engineering, . (2016). ;4:271–95.
74. Niu Y, Chen KC, He T, Yu W, Huang S, Xu K. Scaffolds from block polyurethanes based on poly(varepsilon-caprolactone) (PCL) and poly(ethylene glycol) (PEG) for peripheral nerve regeneration. Biomaterials. 2014;35(14):4266-77.

75. Motealleh A, Eqtesadi S, Perera FH, Pajares A, Guiberteau F, Miranda P. Understanding the role of dip-coating process parameters in the mechanical performance of polymer-coated bioglass robocast scaffolds. Journal of the Mechanical Behavior of Biomedical Materials. 2016;64:253-61.
76. Mouw JK, Ou G, Weaver VM. Extracellular matrix assembly: a multiscale deconstruction. Nat Rev Mol Cell Biol. 2014;15(12):771-85.
77. Jun I, Han H-S, Edwards JR, Jeon H. Electrospun Fibrous Scaffolds for Tissue Engineering: Viewpoints on Architecture and Fabrication. Int J Mol Sci. 2018;19(3):745.
78. Seeram Ramakrishna KF, Wee-Eong Teo,Teik-Cheng,Lim & Zuwei Ma. Basics Relevant to Electrospinning. An Introduction to Electrospinning and Nanofibers. **Singapore**: World Scientific Publishing Co. Pte. Ltd.; 2005. p. 22-89.
79. Huidong Jia MC, and Mohamed T Ghorbe. Stem cells in vascular graft tissue engineering for congenital heart surgery. Interventional Cardiology. 2013;5(6):647–62.
80. Vacanti JP, Langer R. Tissue engineering: the design and fabrication of living replacement devices for surgical reconstruction and transplantation. Lancet. 1999;354 Suppl 1:Si32-4.
81. Niklason LE, Gao J, Abbott WM, Hirschi KK, Houser S, Marini R, et al. Functional arteries grown in vitro. Science. 1999;284(5413):489-93.
82. De Los Angeles A, Ferrari F, Xi R, Fujiwara Y, Benvenisty N, Deng H, et al. Hallmarks of pluripotency. Nature. 2015;525(7570):469-78.
83. Lo B, Parham L. Ethical issues in stem cell research. Endocr Rev. 2009;30(3):204-13.
84. Owen M, Friedenstein AJ. Stromal stem cells: marrow-derived osteogenic precursors. Ciba Found Symp. 1988;136:42-60.
85. Dominici M, Le Blanc K, Mueller I, Slaper-Cortenbach I, Marini F, Krause D, et al. Minimal criteria for defining multipotent mesenchymal stromal cells. The International Society for Cellular Therapy position statement. Cytotherapy. 2006;8(4):315-7.
86. Li H, Shen S, Fu H, Wang Z, Li X, Sui X, et al. Immunomodulatory Functions of Mesenchymal Stem Cells in Tissue Engineering. Stem Cells Int. 2019;2019:9671206-.
87. Caplan Al. Cell Sources for Tissue Engineering: Mesenchymal Stem Cells. In: Buddy D. Ratner ASH, Frederick J. Schoen,Jack E. Lemons,, editor. Biomaterials Science. Third edition. Canada: Elsevier. p. 1159-64.
88. Pappa KI, Anagnou NP. Novel sources of fetal stem cells: where do they fit on the developmental continuum? Regen Med. 2009;4(3):423-33.
89. Oleg S. Mesenchymal Stem Cells Derived from Wharton's Jelly and their Potential for Cardio-Vascular Tissue Engineering. The Open Tissue Engineering and Regenerative Medicine Journal. 2011;4:64-71.
90. Weiss ML, Medicetty S, Bledsoe AR, Rachakatla RS, Choi M, Merchav S, et al. Human umbilical cord matrix stem cells: preliminary characterization and effect of transplantation in a rodent model of Parkinson's disease. Stem Cells. 2006;24(3):781-92.

91. Leopold B, Strutz J, Weiss E, Gindlhuber J, Birner-Gruenberger R, Hackl H, et al. Outgrowth, proliferation, viability, angiogenesis and phenotype of primary human endothelial cells in different purchasable endothelial culture media: feed wisely. Histochem Cell Biol. 2019;152(5):377-90.
92. Gu W. Smooth Muscle Differentiation from Human Umbilical Cord Derived Mesenchymal Stem Cells:
miRNA-involved Mechanism and Potential Application for Vascular Tissue Engineering [PhD]: King's College London; 2017.
93. Tang Y, Yang X, Friesel RE, Vary CP, Liaw L. Mechanisms of TGF-beta-induced differentiation in human vascular smooth muscle cells. J Vasc Res. 2011;48(6):485-94.
94. Murakami M. Signaling Required for Blood Vessel Maintenance: Molecular Basis and Pathological Manifestations. International journal of vascular medicine. 2012;2012:293641.
95. Huber B, Czaja A, Kluger P. Influence of epidermal growth factor (EGF) and hydrocortisone on the co-culture of mature adipocytes and endothelial cells for vascularized adipose tissue engineering. Cell biology international. 2016;40.
96. Schutte SC, Chen Z, Brockbank KG, Nerem RM. Cyclic strain improves strength and function of a collagen-based tissue-engineered vascular media. Tissue Eng Part A. 2010;16(10):3149-57.
97. Cummings CL, Gawlitta D, Nerem RM, Stegemann JP. Properties of engineered vascular constructs made from collagen, fibrin, and collagen-fibrin mixtures. Biomaterials. 2004;25(17):3699-706.
98. Matsumura G, Isayama N, Matsuda S, Taki K, Sakamoto Y, Ikada Y, et al. Long-term results of cell-free biodegradable scaffolds for in situ tissue engineering of pulmonary artery in a canine model. Biomaterials. 2013;34(27):6422-8.
99. Wise SG, Byrom MJ, Waterhouse A, Bannon PG, Weiss AS, Ng MK. A multilayered synthetic human elastin/polycaprolactone hybrid vascular graft with tailored mechanical properties. Acta Biomater. 2011;7(1):295-303.
100. Hasan A, Paul A, Memic A, Khademhosseini A. A multilayered microfluidic blood vessel-like structure. Biomed Microdevices. 2015;17(5):88.
101. Jia W, Li M, Weng H, Gu G, Chen Z. Design and comprehensive assessment of a biomimetic tri-layer tubular scaffold via biodegradable polymers for vascular tissue engineering applications. Materials Science and Engineering: C. 2020;110:110717.
102. Zorlutuna P, Vadgama P, Hasirci V. Both sides nanopatterned tubular collagen scaffolds as tissue-engineered vascular grafts. J Tissue Eng Regen Med. 2010;4(8):628-37.
103. Yucel D, Kose GT, Hasirci V. Polyester based nerve guidance conduit design. Biomaterials. 2010;31(7):1596-603.
104. Yucel D, Kose GT, Hasirci V. Tissue engineered, guided nerve tube consisting of aligned neural stem cells and astrocytes. Biomacromolecules. 2010;11(12):3584-91.
105. Zorlutuna P, Vadgama P, Hasirci V. Both sides nanopatterned tubular collagen scaffolds as tissue-engeered vascular grafts. Journal of tissue engineering and regenerative medicine. 2010;4:628-37.

106. Wu H, Fan J, Chu C, Wu J. Electrospinning of small diameter 3-D nanofibrous tubular scaffolds with controllable nanofiber orientations for vascular grafts. Journal of materials science Materials in medicine. 2010;21:3207-15.
107. Zhang X, Thomas V, Xu Y, Bellis SL, Vohra YK. An in vitro regenerated functional human endothelium on a nanofibrous electrospun scaffold. Biomaterials. 2010;31(15):4376-81.
108. Wu T, Zhang J, Wang Y, Li D, Sun B, El-Hamshary H, et al. Fabrication and preliminary study of a biomimetic tri-layer tubular graft based on fibers and fiber yarns for vascular tissue engineering. Mater Sci Eng C Mater Biol Appl. 2018;82:121-9.
109. Chan BP, Leong KW. Scaffolding in tissue engineering: general approaches and tissue-specific considerations. Eur Spine J. 2008;17 Suppl 4(Suppl 4):467-79.
110. Gao J, Chen S, Tang D, Jiang L, Shi J, Wang S. Mechanical Properties and Degradability of Electrospun PCL/PLGA Blended Scaffolds as Vascular Grafts. Transactions of Tianjin University. 2018;25.
111. Panseri S, Cunha C, Lowery J, Del Carro U, Taraballi F, Amadio S, et al. Electrospun micro- and nanofiber tubes for functional nervous regeneration in sciatic nerve transections. BMC Biotechnol. 2008;8:39-.
112. Qin X, Wu D. Effect of different solvents on poly(caprolactone) (PCL) electrospun nonwoven membranes. Journal of Thermal Analysis and Calorimetry. 2012;107(3):1007-13.
113. Liu X, Baldursdottir SG, Aho J, Qu H, Christensen LP, Rantanen J, et al. Electrospinnability of Poly Lactic-co-glycolic Acid (PLGA): the Role of Solvent Type and Solvent Composition. Pharm Res. 2017;34(4):738-49.
114. Vaughan DW. Circulatory System. A Learning System in Histology. Oxford. New York: Oxford University Press Inc.,; 2002. p. 99-114.
115. Seeram Ramakrishna KF, Wee-Eong Teo,Teik-Cheng,Lim & Zuwei Ma. Electrospinning Process. An Introduction to Electrospinning and Nanofibers. **Singapore**: World Scientific Publishing Co. Pte. Ltd.; 2005. p. 90-154.
116. Chen Y-P, Liu H-Y, Liu Y-W, Lee T-Y, Liu S-J. Determination of Electrospinning Parameters' Strength in Poly(D,L)-lactide-co-glycolide Micro/Nanofiber Diameter Tailoring. Journal of Nanomaterials. 2019;2019:1-8.
117. Fong H, Chun I, Reneker DH. Beaded nanofibers formed during electrospinning. Polymer. 1999;40(16):4585-92.
118. Theocharis AD, Skandalis SS, Gialeli C, Karamanos NK. Extracellular matrix structure. Adv Drug Deliv Rev. 2016;97:4-27.
119. Guidoin R, King M, Marceau D, Cardou A, de la Faye D, Legendre JM, et al. Textile arterial prostheses: is water permeability equivalent to porosity? J Biomed Mater Res. 1987;21(1):65-87.
120. Wang X, Lin P, Yao Q, Chen C. Development of small-diameter vascular grafts. World J Surg. 2007;31(4):682-9.
121. Kim S, von Recum H. Endothelial stem cells and precursors for tissue engineering: cell source, differentiation, selection, and application. Tissue Eng Part B Rev. 2008;14(1):133-47.

122. Patrick Wuchter WW, and Anthony D. Ho. Mesenchymal Stromal Cells (MSC). In: Steinhoff G, editor. Regenerative Medicine -from Protocol to Patient. Third Edition ed. Switzerland Springer International Publishing 2016. p. 295-315.
123. Rojewski MT, Weber BM, Schrezenmeier H. Phenotypic Characterization of Mesenchymal Stem Cells from Various Tissues. Transfus Med Hemother. 2008;35(3):168-84.
124. Troyer DL, Weiss ML. Wharton's jelly-derived cells are a primitive stromal cell population. Stem cells (Dayton, Ohio). 2008;26(3):591-9.
125. Michael H. Ross WP. Bone. In: Taylor C, editor. Histology A Text and Atlas. Sixth Edition ed: Lippincott Williams & Wilkins, a Wolters Kluwer business. p. 218-54.
126. Kim YH, Yoon DS, Kim HO, Lee JW. Characterization of different subpopulations from bone marrow-derived mesenchymal stromal cells by alkaline phosphatase expression. Stem Cells Dev. 2012;21(16):2958-68.
127. Robert Fitridge MT. Endothelium. Mechanisms of Vascular Disease. Australia: Barr Smith Press; 2011. p. 1-13.
128. Trávníčková M, Filová E, Matějka R, Stepanovska J, Musílková J, Zarubova J, et al. Vascular Smooth Muscle Cells (VSMCs) in Blood Vessel Tissue Engineering: The Use of Differentiated Cells or Stem Cells as VSMC Precursors. 2018.
129. Narita Y, Yamawaki A, Kagami H, Ueda M, Ueda Y. Effects of transforming growth factor-beta 1 and ascorbic acid on differentiation of human bone-marrow-derived mesenchymal stem cells into smooth muscle cell lineage. Cell Tissue Res. 2008;333(3):449-59.
130. Arakawa E, Hasegawa K, Irie J, Ide S, Ushiki J, Yamaguchi K, et al. L-ascorbic acid stimulates expression of smooth muscle-specific markers in smooth muscle cells both in vitro and in vivo. J Cardiovasc Pharmacol. 2003;42(6):745-51.
131. Arakawa E, Hasegawa K, Yanai N, Obinata M, Matsuda Y. A mouse bone marrow stromal cell line, TBR-B, shows inducible expression of smooth muscle-specific genes. FEBS Lett. 2000;481(2):193-6.
132. Liu Y, Deng B, Zhao Y, Xie S, Nie R. Differentiated markers in undifferentiated cells: expression of smooth muscle contractile proteins in multipotent bone marrow mesenchymal stem cells. Dev Growth Differ. 2013;55(5):591-605.
133. Wilson D. Vascular Smooth Muscel Cells and Function. Mechanisms of Vascular Disease. Australia: Barr Smith Press; 2011. p. 13-42.
134. Li M, Mills D, Cui T, McShane M. Cellular Response to Gelatin- and Fibronectin-Coated Multilayer Polyelectrolyte Nanofilms. IEEE transactions on nanobioscience. 2005;4:170-9.
135. Ayyob M. And Kim Y.J Effect of Chemical Composition Variant and Oxygen Plasma Treatments on the Wettability of PLGA Thin Films, Synthesized by Direct Copolycondensation. Polymers 2018, 10(10), 1132
136. Martins K.*F.,* Messias *A.D.,* Leite *F.L., and* Duek *E.A.R.* Preparation and Characterization of Paclitaxel-loaded PLDLA Microspheres. Materials Research. 2014; 17(3): 650-656.

APPENDICIES

A. Calibration Curves for Cell Number Determination of WJ MSC

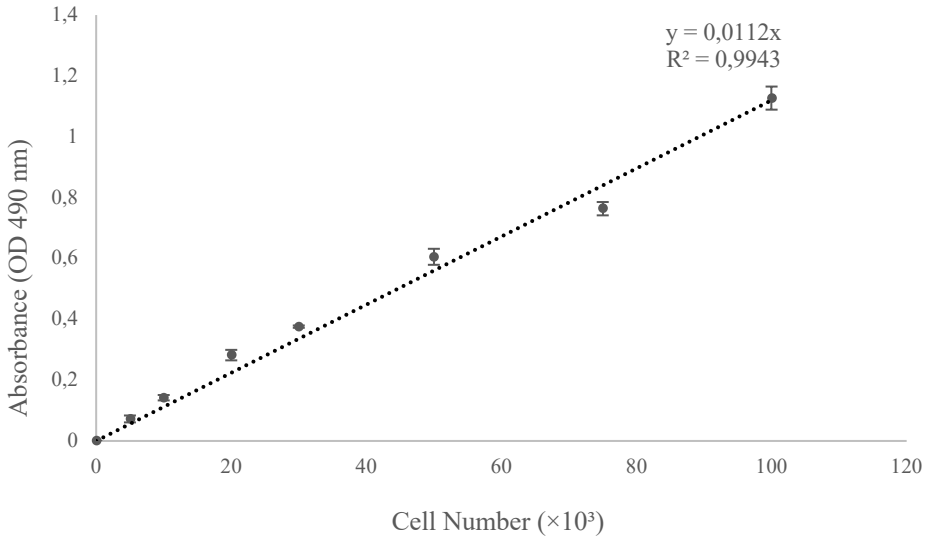

Figure A. 1. The calibration curve obtained by MTS assay using WJ MSC.

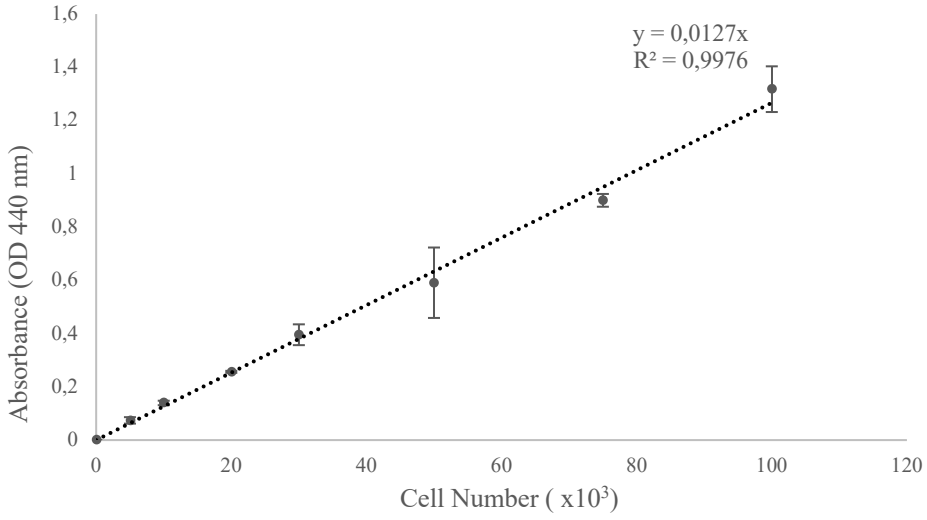

Figure A. 2 .The calibration curve obtained by WST-1 assay using WJ MSC.

B. Calibration Curves for Cell Number Determination of HUVEC

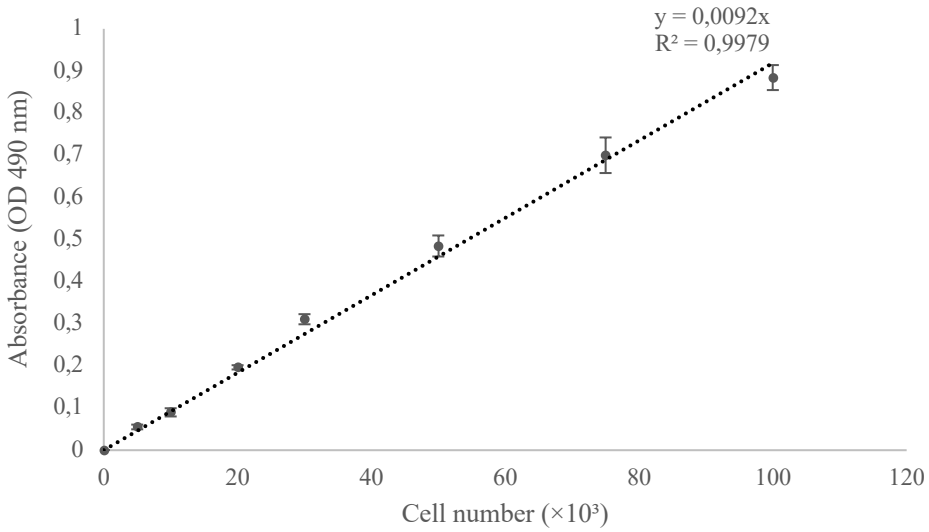

Figure A. 3. The calibration curve obtained by MTS assay using HUVEC.

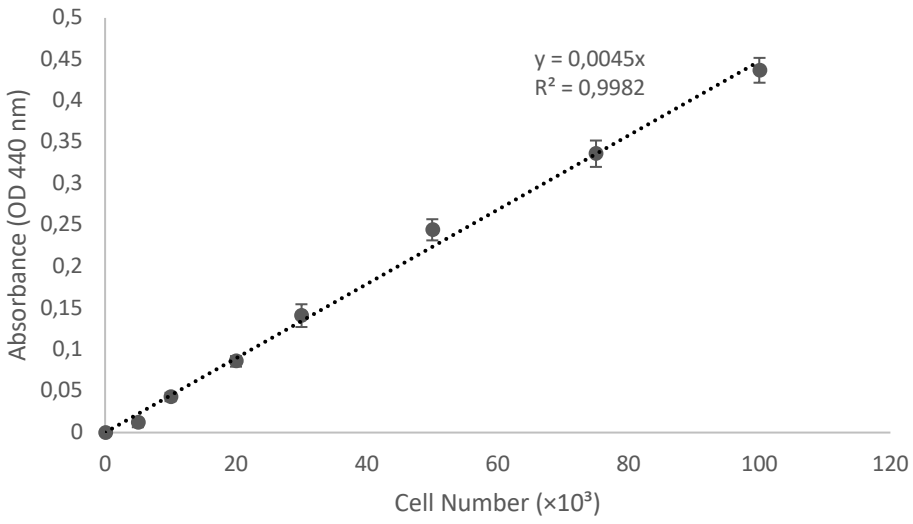

Figure A. 4. The calibration curve obtained by WST-1 assay using HUVEC.

C. Calibration Curves for ALP Activity

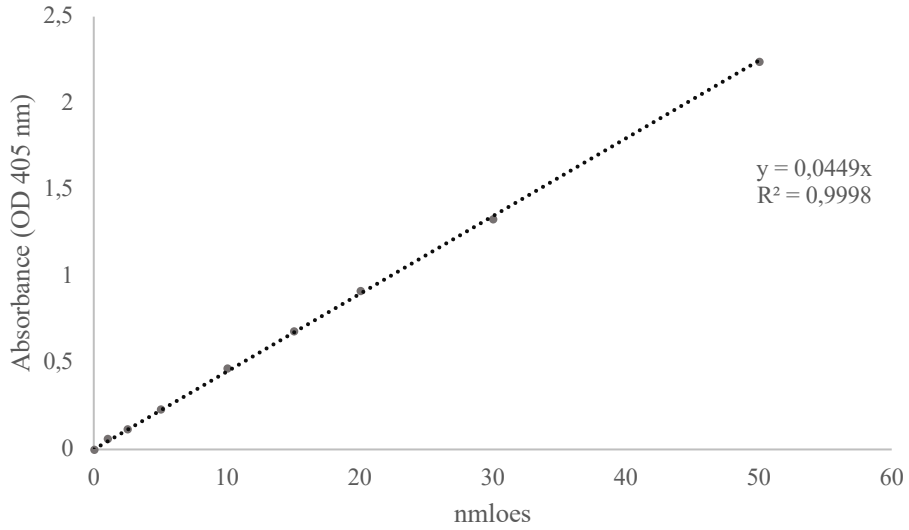

Figure A. 5. The calibration curve for ALP activity prepared by p-nitrophenol at different concentrations.

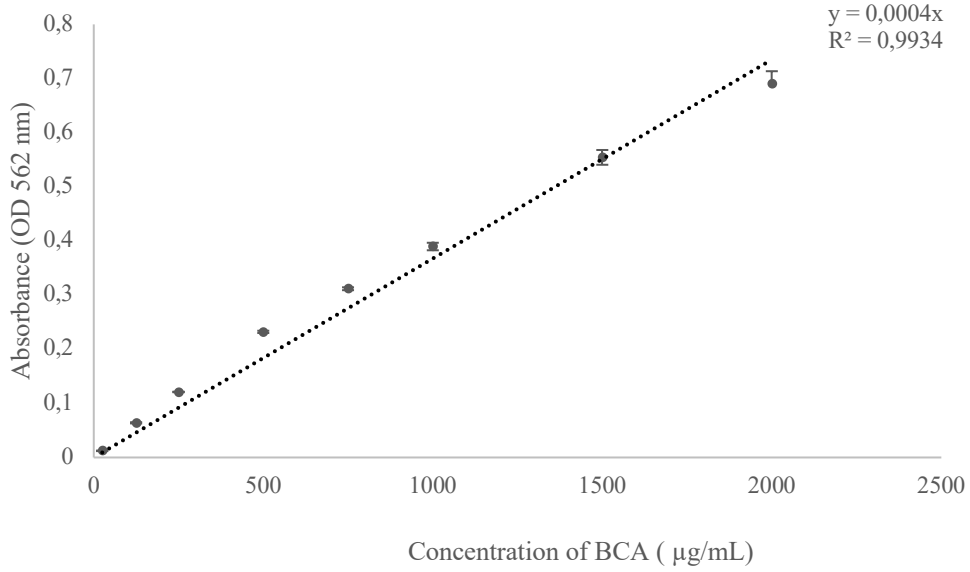

Figure A. 6. The calibration curve for the quantification of total protein using BCA at different concentrations

D. Ethical Approval

ACIBADEM
ÜNİVERSİTESİ

SAYI: ATADEK-2018/2
KONU: Etik Kurul Kararı

Sayın Yrd. Doç. Dr. Deniz Yücel,

Sorumluluğunu yürüttüğünüz **"Doku Mühendisliği Yöntemleriyle Katmanlı, Tübüler, Küçük-Orta Çaplı Damar Dokusu Geliştirilmesi"** başlıklı proje 15.02.2018 tarih 2018/2 Sayılı Atadek Toplantısında görüşülmüş olup 2018-2/64 karar numarası ile tıbbi etik yönden uygun bulunmuştur.

Prof.Dr. İsmail Hakkı ULUS
ATADEK Başkanı

D. (continued)

ACIBADEM MEHMET ALİ AYDINLAR ÜNİVERSİTESİ
TIBBİ ARAŞTIRMALAR DEĞERLENDİRME KURULU (ATADEK)

Etik onay istenen tıbbi araştırmanın başlığı:

Doku Mühendisliği Yöntemleriyle Katmanlı, Tübüler, Küçük-Orta Çaplı Damar Dokusu Geliştirilmesi

Etik onay istenen tıbbi araştırmanın yürütücüsü (sorumlusu):

Yrd. Doç. Dr. Deniz Yücel

Karar:

Kabul (Etik olarak uygun) (X) **Revizyon** ( )* **Etik olarak uygun değil** ( )**

Toplantı Tarihi: 15.02.2018 **Karar Numarası:** 2018-2/64

		Karara	Karara
Kurul Üyesi-Unvan Ad-Soyad	**İmza**	**Katılıyorum**	**Katılmıyorum*** **
Prof. Dr. İsmail Hakkı Ulus (Başkan)		(X)	( )
Prof. Dr. Güldal Süyen (Başkan Yrd)		(X)	( )
Prof.Dr. Mert Ülgen		(X)	( )
Doç.Dr. Ükke Karabacak		(X)	( )
Doç.Dr. A.Elif Eroğlu Büyüköner		( )	( )
Doç.Dr. Berrin Karadağ		(X)	( )
Yrd.Doç.Dr. Fatih Artvinli		(X)	( )
Yrd.Doç.Dr. Günseli Bozdoğan		(X)	( )

CURRICULUM VITAE

Personal Information

Name	Gözde Ervin	**Surname**	Köle
Birth Place	Istanbul	**Birth Date**	16/12/1994
Nationality	Turkish	**Phone Number**	+90534 453 8287
E-mail	gozdeervin@gmail.com		

Education

	Institution	**Graduation Year**
BSc	Istanbul University Molecular Biology and Genetics	2017
High School	Bakirköy Medical Vocational High School	2012

Experience

Job Title	**Institution**	**Duration**
Visiting fellow	Middle East Technical University- Center of Excellence in Biomaterials and Tissue Engineering	August, 2018

Languages	**Reading**	**Speaking**	**Writing**
English	Advanced	Advanced	Advanced

	Foreign Language Examination Grade								
KPDS	ÜDS	IELTS	TOEFL IBT	TOEFL PBT	TOEFL CBT	FCE	CAE	CPE	YOKDIL
									90

	Quantitative	Equally Weighted	Verbal
ALES Note	87,76272	87,36146	85,84566

Computer Skills

Program	Skill Degree
Microsoft Office	Very Good

Presentations

Köle E. G., Kenar H., Hasırcı V., Yucel D. Construction of a Bilayer Tissue Engineered Blood Vessel. 23th Biomedical Science and Technology Symposium. 2019 (Poster Presentation).

Köle E. G., Dursun Usal T.,Hasırcı V., Yucel D. Development of tubular vascular graft with tissue engineering techniques. 23th Biomedical Science and Technology Symposium. 2018 (Poster Presentation).

Kaya Z., Köle E. G., Gülmez O. A. Comparison of blood counts in bone marrow and peripheral blood samples from healthy bone marrow donors. 2017 ASPHO Annual Meeting. Poster 242.